

Figure 27. Peach-Koehler Force (Hirth and Lothe (1982): $d\mathbf{F} = [\mathbf{b} \bullet \boldsymbol{\sigma}] \times d\mathbf{l}$; $d\mathbf{F}/dl$ is the "force"/length on a dislocation with Burgers vector \mathbf{b} , $\boldsymbol{\sigma}$ is the stress tensor and $d\mathbf{l}$ is an incremental distance along a dislocation loop with tangent vector $\xi = d\mathbf{l}/dl$, $dl \equiv \|d\mathbf{l}\| = [d\mathbf{l} \bullet d\mathbf{l}]^{1/2}$. **a)** A dislocation loop; beginning with the front segment of the dislocation line and moving clockwise: the right-hand screw segment is denoted ' \mathbf{S} ', positive edge segment \perp , left-hand screw segment backwards ' \mathbf{S} ', and negative edge segment \top . The loop with $\mathbf{b} = (b_x, b_y, b_z) = (0, -b, 0)$ expands under the influence of stress $\sigma^{ij} = \sigma^{yy} = -\tau$, so that $\mathbf{b} \bullet \boldsymbol{\sigma} = (0, 0, b\tau)$, as follows: For the \pm edge segments, $d\mathbf{l} = (\mp dl, 0, 0)$ and $[\mathbf{b} \bullet \boldsymbol{\sigma}] \times d\mathbf{l} = (0, \mp b\tau, 0)dl$; for the right/left-hand screw segments, $d\mathbf{l} = (0, \mp dl, 0)$ and $[\mathbf{b} \bullet \boldsymbol{\sigma}] \times d\mathbf{l} = (\pm b\tau, 0, 0)dl$. **b)** After expanding throughout the slip plane the crystal is offset distance b , $\dot{\varepsilon}_{ji} \equiv \frac{1}{2}(\Delta u_i/\Delta x^j + \Delta u_j/\Delta x^i) = \dot{\varepsilon}_{yz} = \frac{1}{2}(\Delta u_z/\Delta y + \Delta u_y/\Delta z) = \frac{1}{2}\Delta u_y/\Delta z = \frac{1}{2}\dot{\gamma}_{yz} = \frac{1}{2}b/h$.

Figure 27 (Continued).

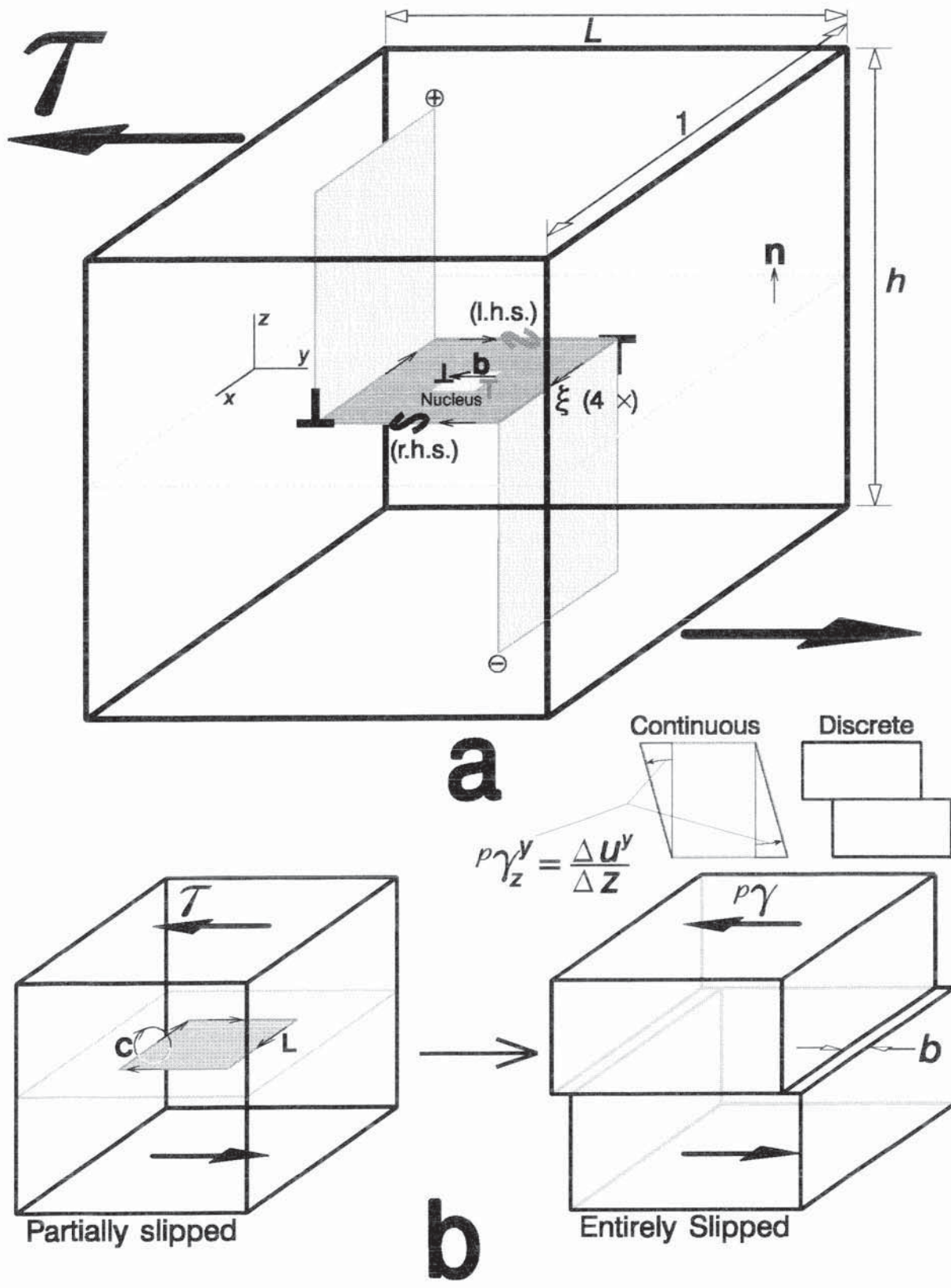
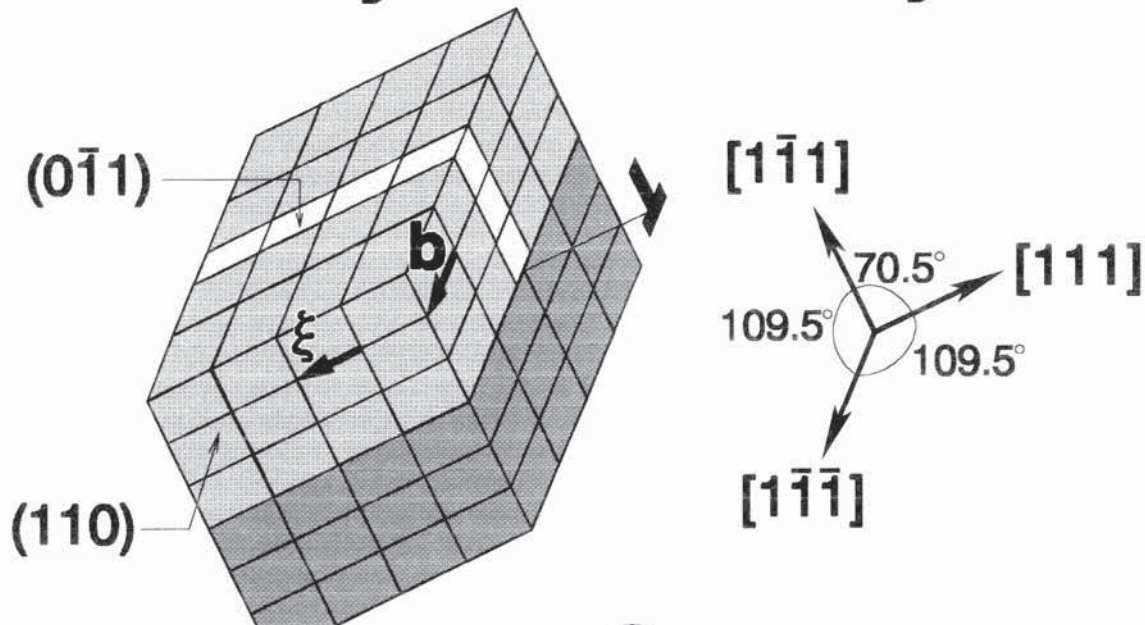


Figure 28. *Crystal plasticity* is illustrated for the BCC lattice. A single edge dislocation is shown; its Burgers vector is $\mathbf{b} = \frac{1}{2}a[1\bar{1}\bar{1}]$. The extra half plane is shown lightly shaded.

b) For a compressive stress in the $-\mathbf{b}$ -direction the dislocation climbs up and the atoms in the extra half plane "plate-out" on top of the crystal (Hirth and Lothe 1982). **c)** For a shear stress in the \mathbf{b} -direction the dislocation glides in this direction and the atoms in the upper-half crystal are translated relative to those in the lower half by \mathbf{b} ; a shear strain of $\gamma = 1/6$ results. **d)** A schematic rendering of the dislocation core in a BCC lattice. Two $(0\bar{1}1)$ planes are shown; lightly shaded atoms are on top. The top plane has an extra row of atoms. The dislocation axis runs in the direction $\xi = -[111]/\sqrt{3}$.

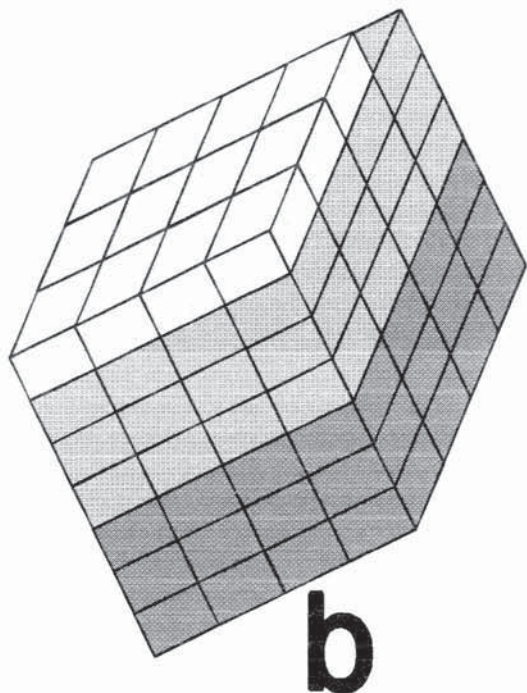
Figure 28 (Continued).

Crystal Plasticity



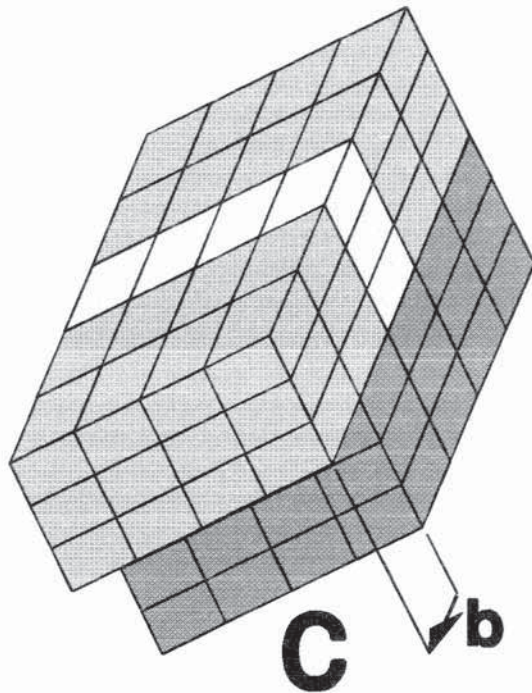
a

Climb



b

Glide



c

Figure 28 (Continued).

Dislocation Core

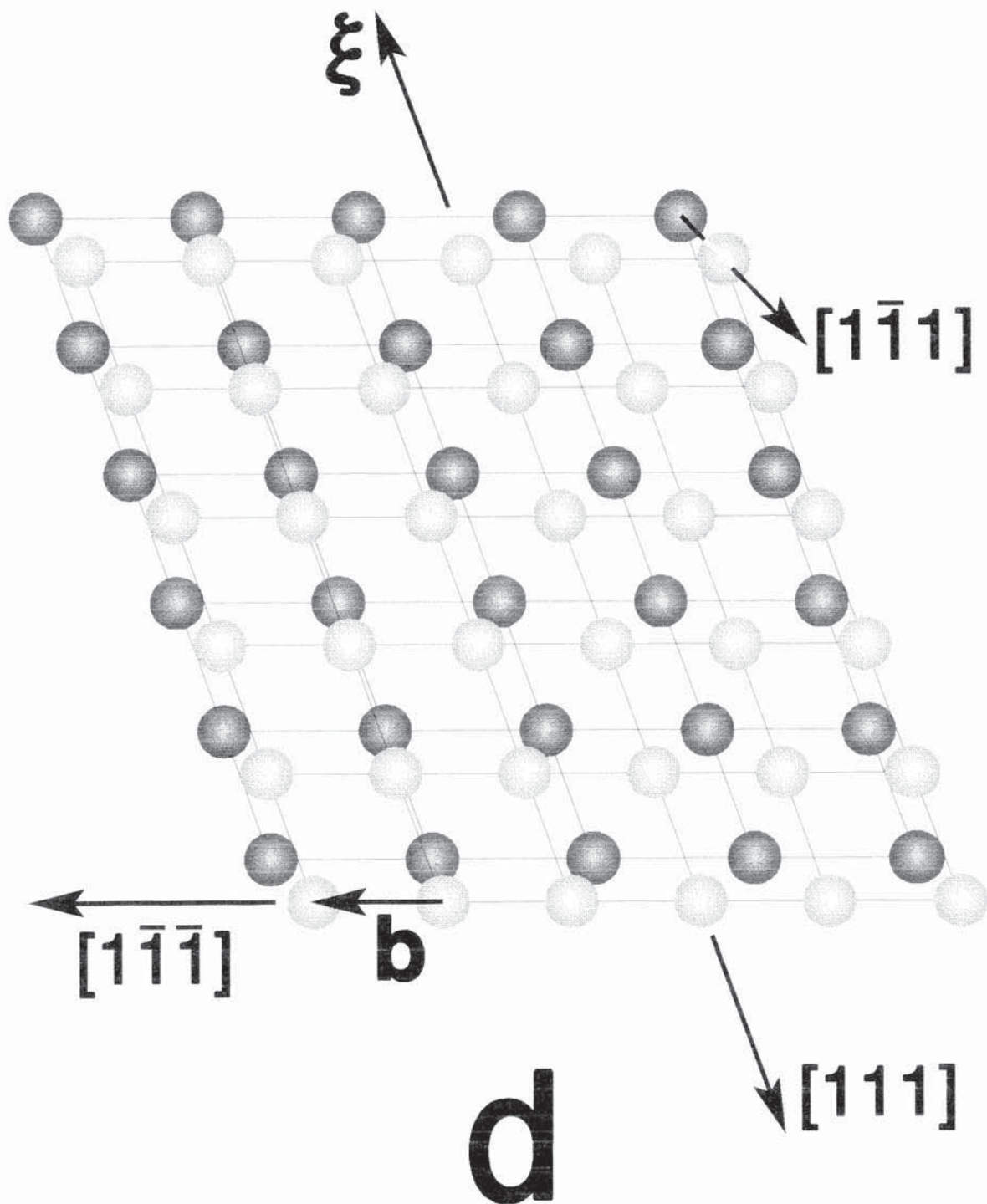


Figure 29. Elastic and plastic deformations in a lattice with sixfold symmetry are compared.

Plastic Deformation: Two types are shown, (1) top and bottom atoms each move $\frac{1}{2}b$ in opposing directions, and (2) the four atoms rotate 60° about the center of the array (Kröner and Anthony 1975). Both processes look like a mirror transformation about the center of the array, but only the translational motion is an actual *mirror transformation*. Initial and final states are both equilibrium lattice sites; consequently the action responsible for the relative motions can be released and the atoms will maintain the final state. Type (1) is associated with dislocation glide while type (2) is from disclination motion. For dislocation glide (1): In the initial state atoms B and C are nearest neighbors while atoms A and D are not; after the mirror transformation atoms A and D become nearest neighbors while atoms B and C are separated. Thus:

Dislocation glide corresponds to core-atoms switching neighbors.



Elastic Deformation: The shear distorts both the atomic bonds and moves the atoms and after the bonds have relaxed only the atoms are moved by the shear. There are no relative atomic movements, and since the atoms are displaced from equilibrium sites, if the shear stress is removed the reaction will occur in reverse. **d)** An extreme elastic shear strain $\gamma = u/a = \tan 30^\circ = 0.58$ is shown. Further elastic strain is not possible. (The area of the unit cell is $\mathbf{b}_1 \wedge \mathbf{b}_2$ before deformation and $\mathbf{b}_1 \wedge \mathbf{a} = \mathbf{b}_1 \wedge (\mathbf{b}_2 + \mathbf{u}) = \mathbf{b}_1 \wedge \mathbf{b}_2$ after deformation since $\mathbf{u} = \text{const.} \mathbf{b}_1$ and $\mathbf{b}_1 \wedge \text{const.} \mathbf{b}_1 = \mathbf{0}$ (Burke (1985).) **e)** If further strain occurs top and bottom atoms suffer the relative displacements $\pm \frac{1}{2}b$, $b = \|\mathbf{b}_1\| = \|\mathbf{b}_2\| = 2\|\mathbf{u}_+\| = 2\|\mathbf{u}_-\|$.

Figure 29 (Continued).

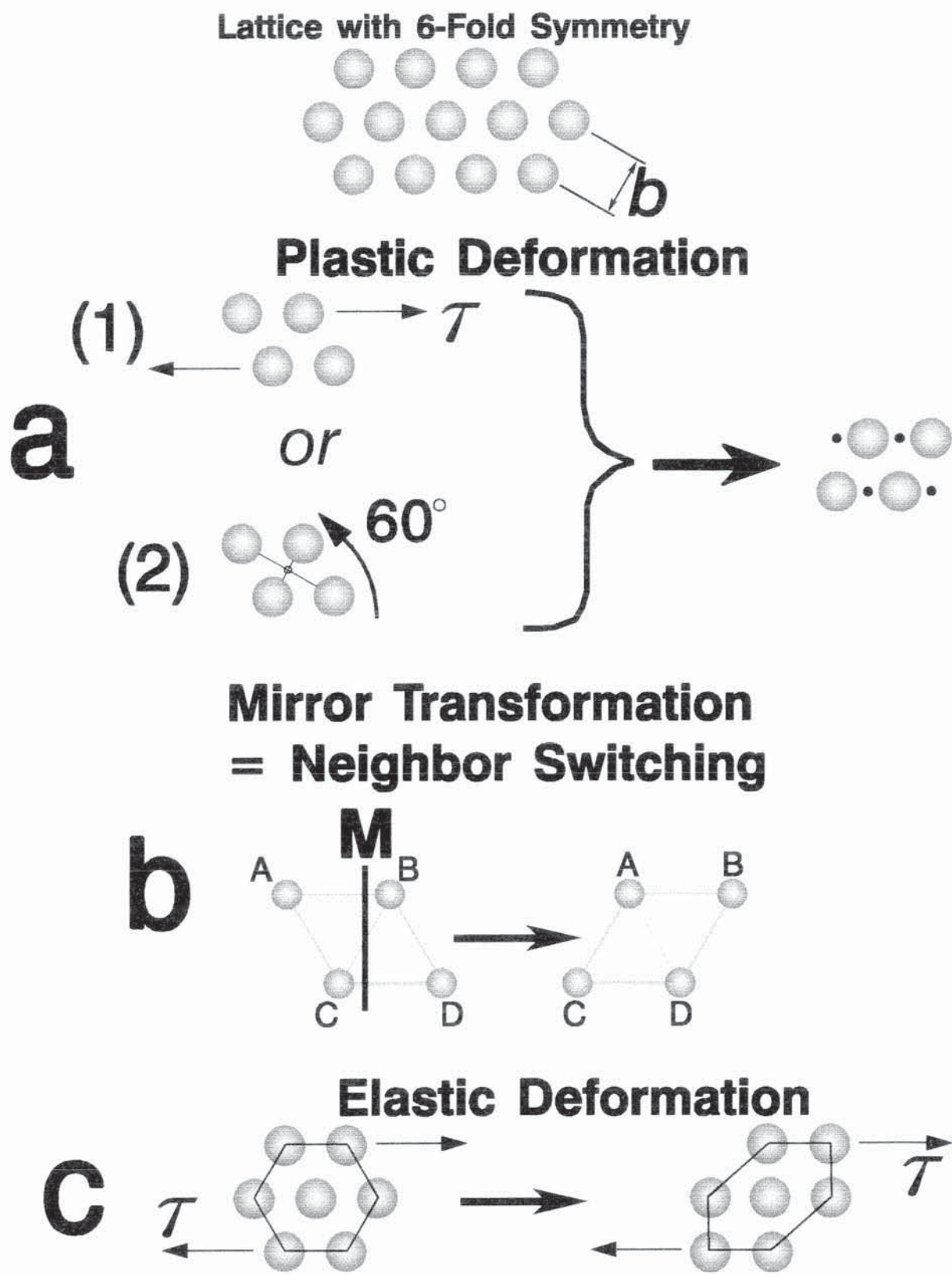
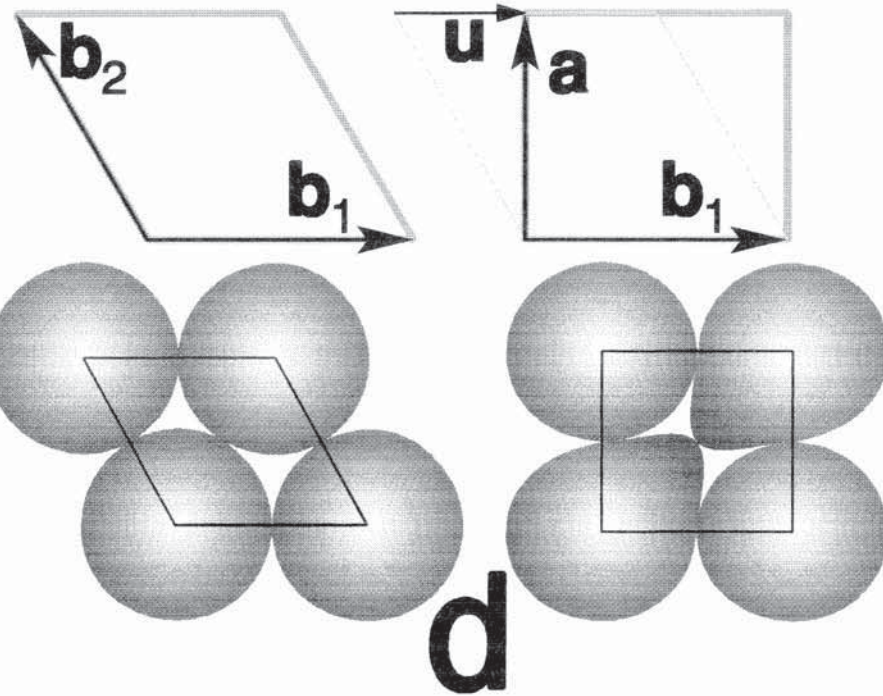


Figure 29 (Continued).

Elastic Deformation



Plastic Deformation

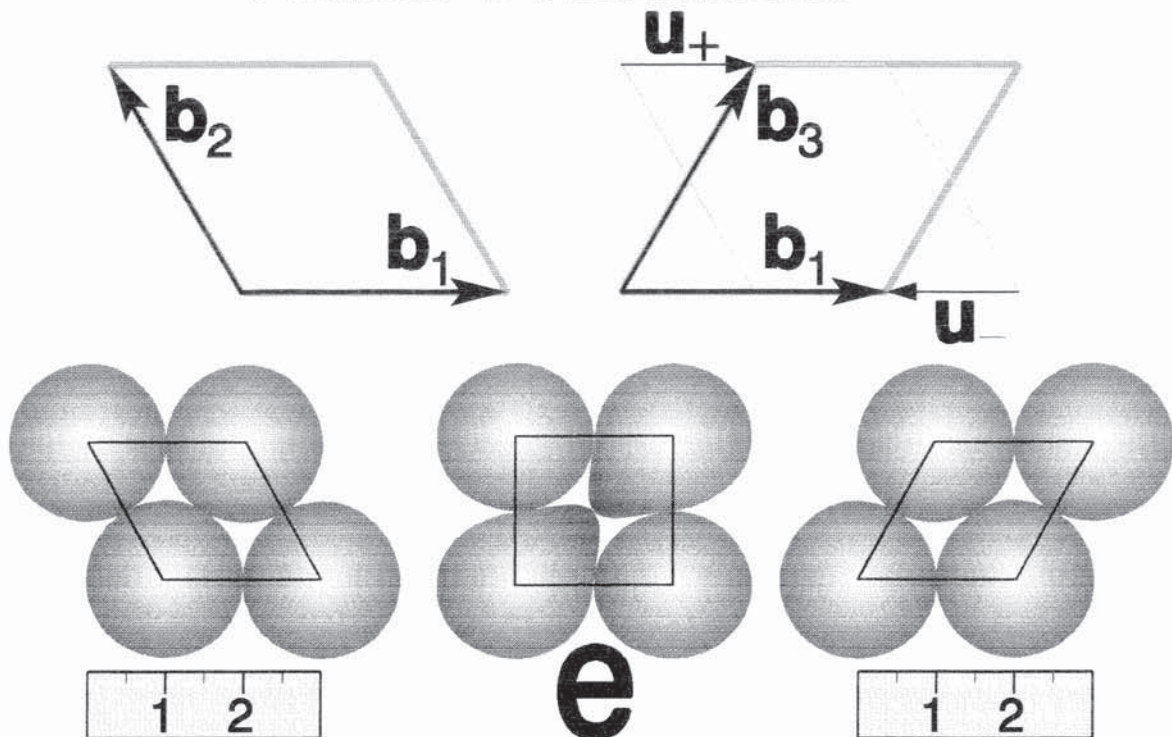


Figure 30. Diagonal Dislocation Lattice Taylor (1934). **a)** Positive (\perp) and negative (τ) edge dislocations form a stable array in which the dislocation spacing is $d_{\perp} = d_{\tau} = 2a$, where a (not the lattice constant) is the spacing of the grid lines scribed onto the material. The spacing of the slip planes is d_{slip} : shaded blocks do not move while un-shaded blocks suffer slip. A relative displacement of the positive and negative dislocation lattices through $\frac{1}{2}d_{\perp} = a$ brings the configuration to 'b': the shear stress \mathcal{T} moves negative dislocations $\frac{1}{2}a$ right and positive dislocations $\frac{1}{2}a$ left. **b)** Another stable array of dislocations results from the aforementioned movements. Relative motions of the material may be noted by comparing the blocks with those of the prior configuration: Shaded blocks have not moved; blocks for the positive defects have moved $\frac{1}{2}a$ left while blocks for the negative defects have moved $\frac{1}{2}a$ right; the relative displacement of the positive and negative dislocations is therefore a . **c)** Interpretation of the prior two configurations in terms of two *interpenetrating dislocation lattices*: the *initial state* corresponds to configuration 'a' and the *final state* to 'b'. Positive dislocations experience the resolved shear stress \mathcal{T}_{\perp} to the left and negative dislocations the resolved shear stress \mathcal{T}_{τ} to the right.

Figure 30 (Continued).

Taylor's Dislocation "Lattice"

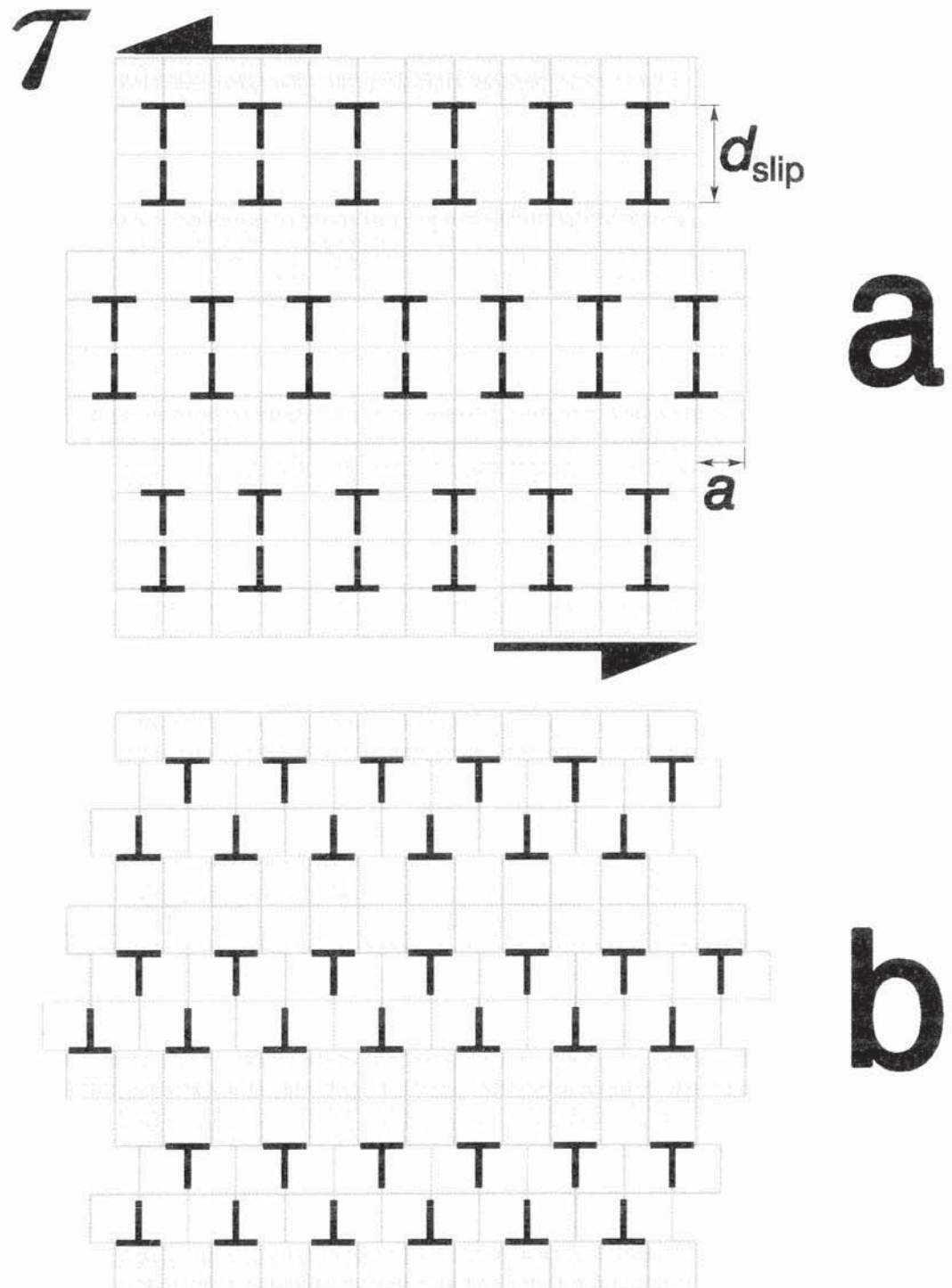


Figure 30 (Continued).

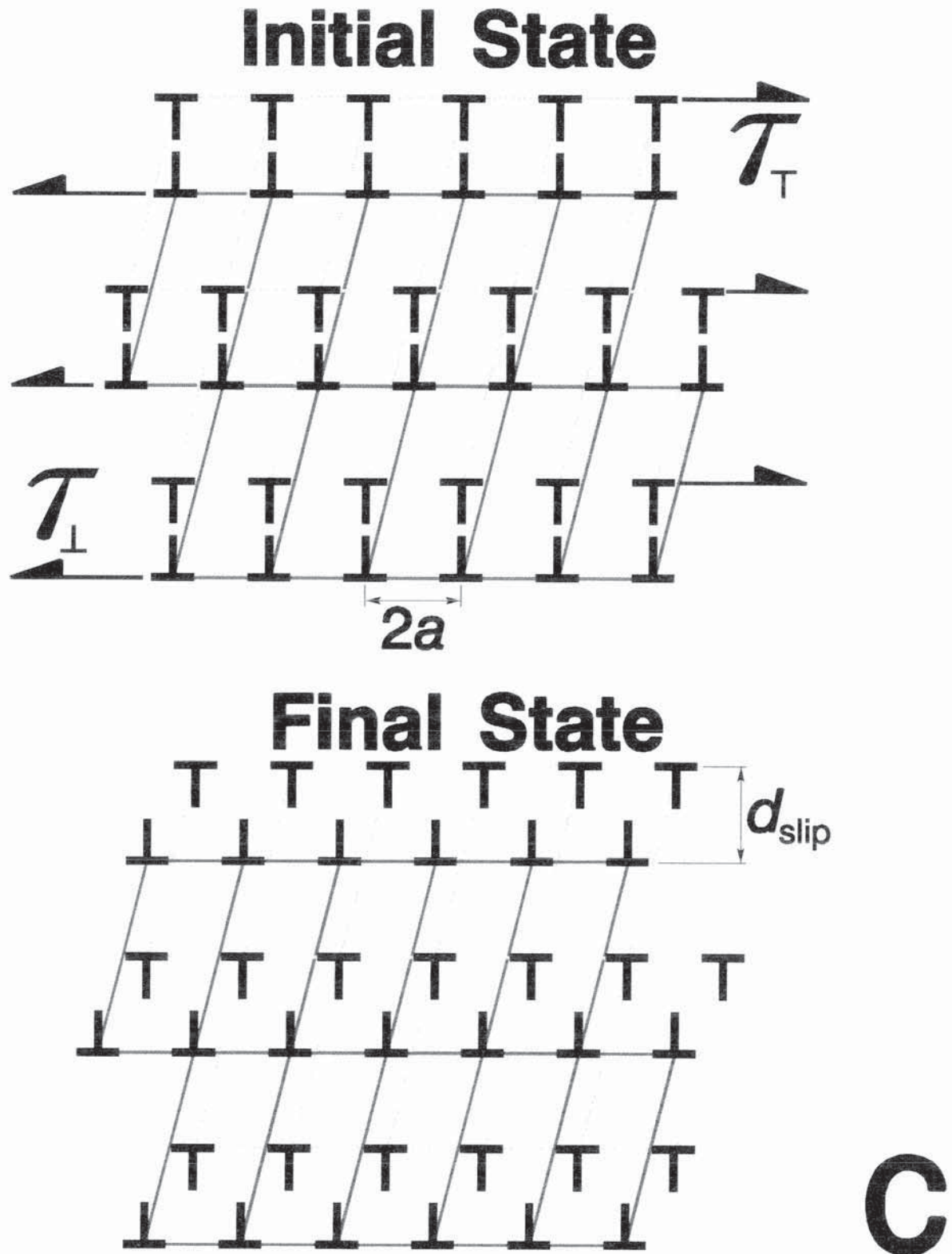


Figure 31. *"Geometrization" of Slip.* **a)** "Geometrization" of tensile specimen. Complexions comprised of many corpuscles (*i.e.* atoms or grains) are bundled together to model the gauge length of a tensile specimen. **b)** Geometry of a BCC lattice assuming plasticity by slip. **c)** Geometry of slip. **d)** The dislocation current 1-form J^m defines how much of a slip plane has been covered by a mobile dislocation. Its dual, $*J^m$, is similar but represents the part of a *slip band* which has slipped.

Figure 31 (Continued).

"Geometrization" of Tensile Specimen

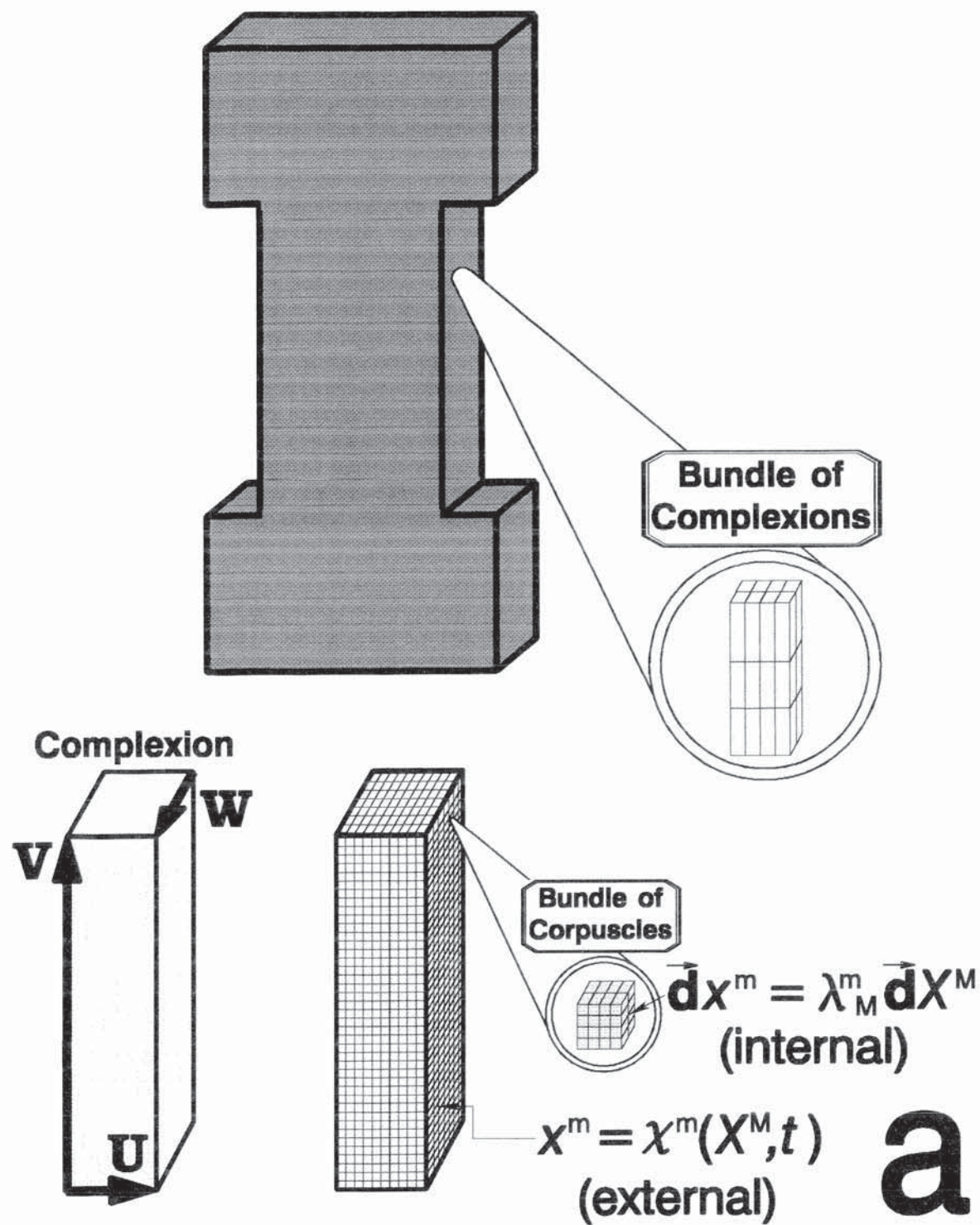


Figure 31 (Continued).

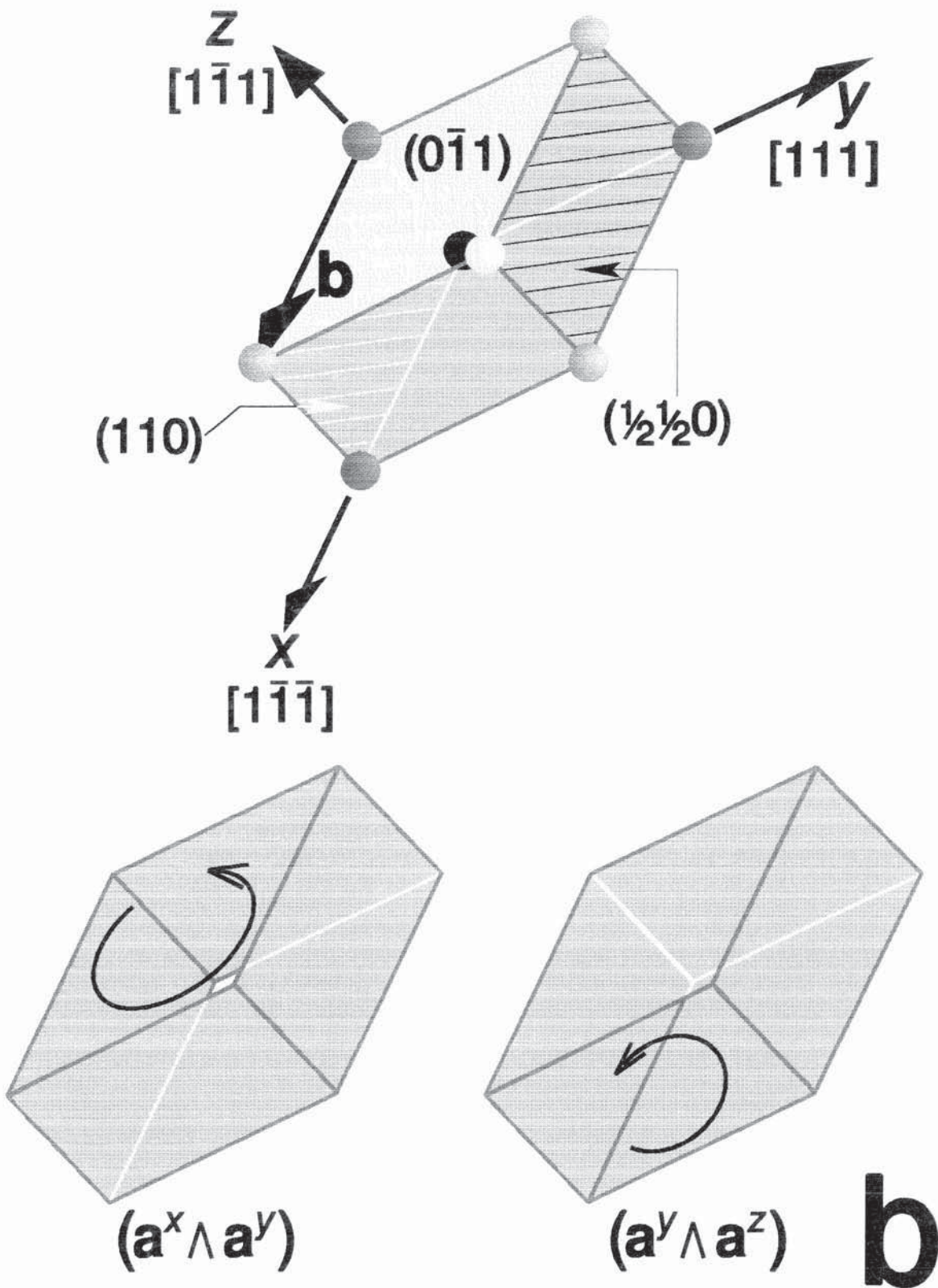


Figure 31 (Continued).

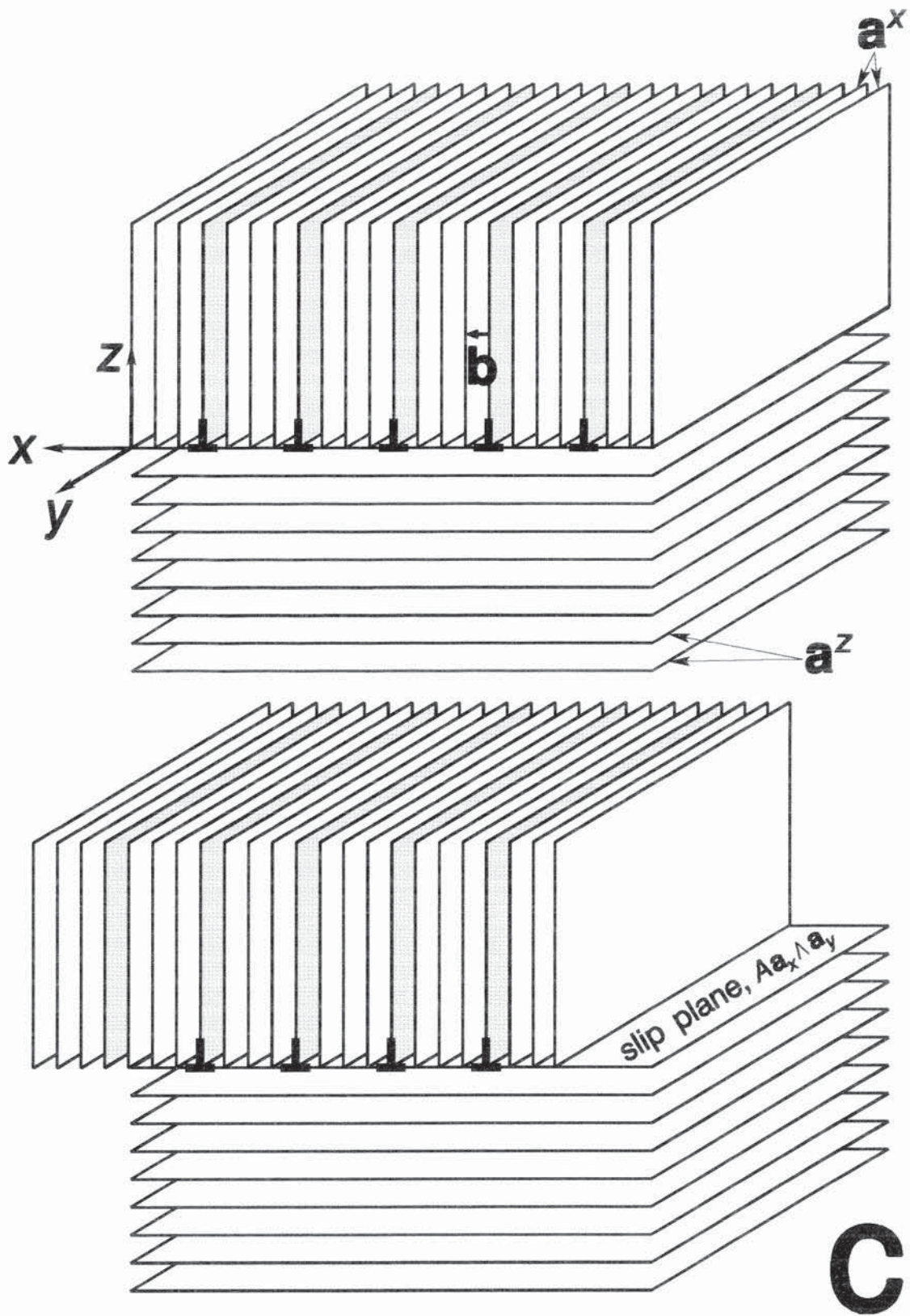
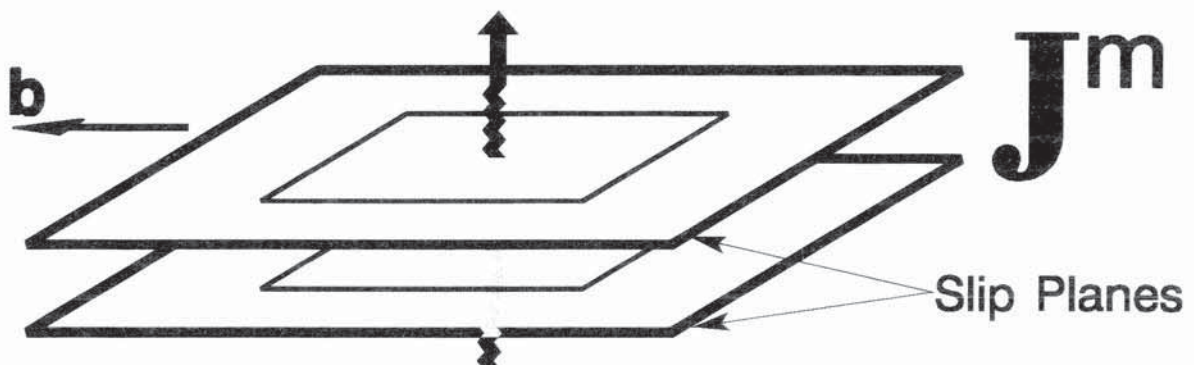


Figure 31 (Continued).

Dislocation Current 1-Form



Dual Representation

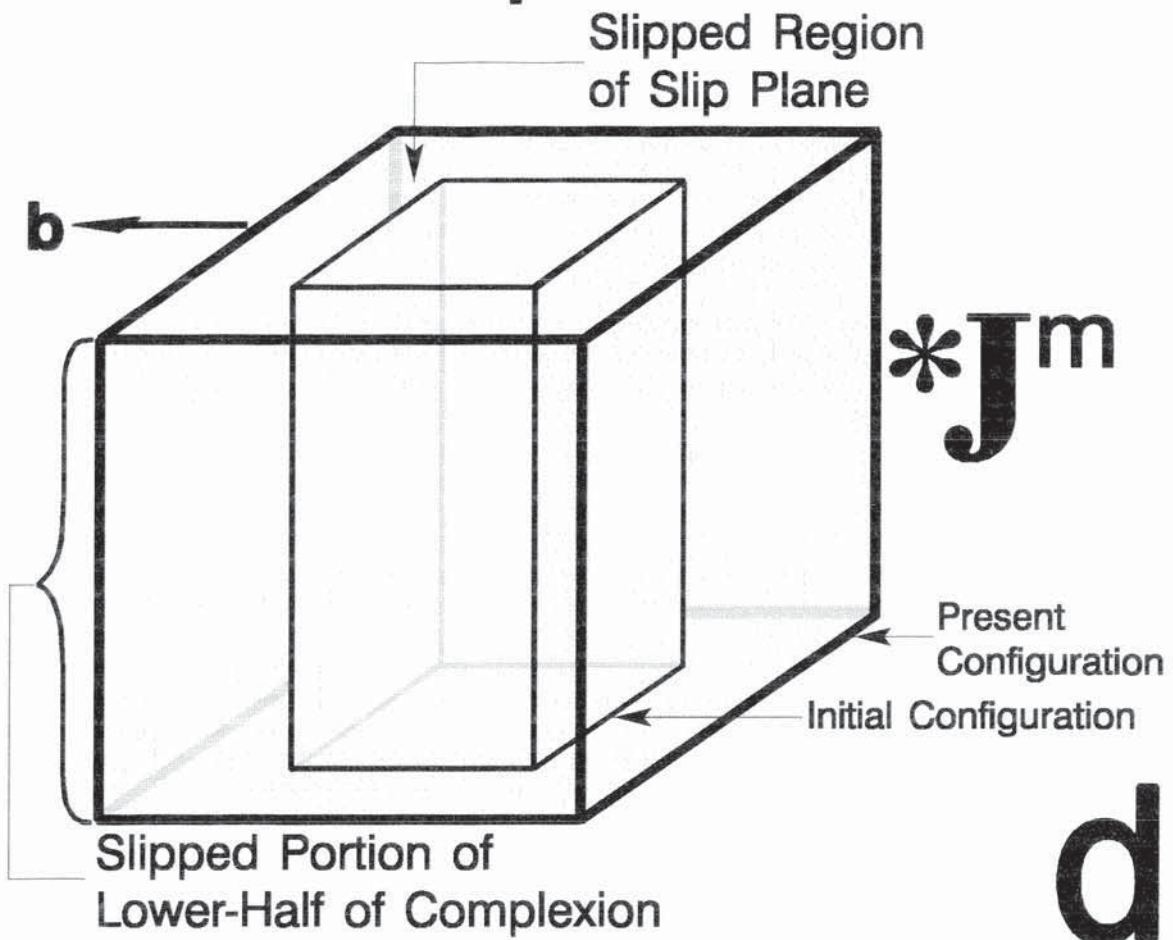
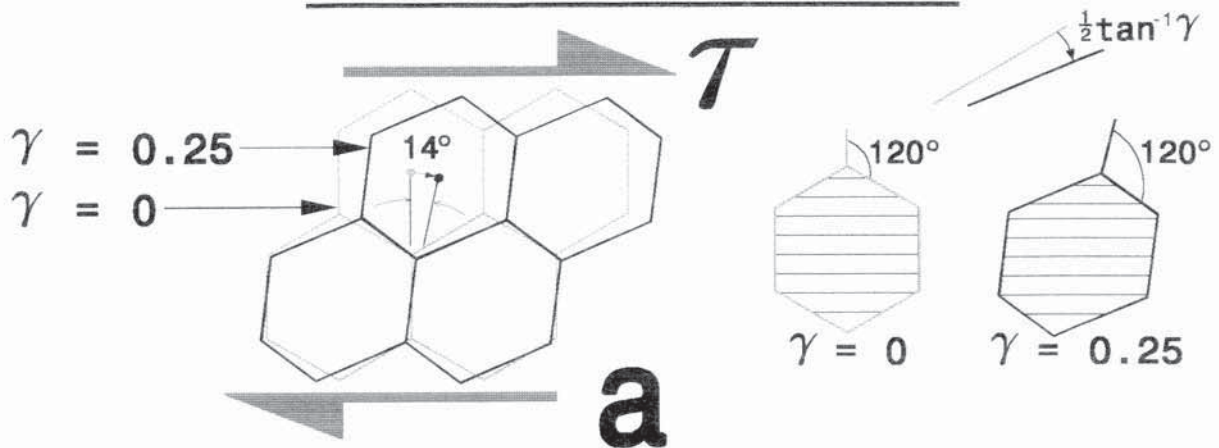


Figure 32. *Grain Rearrangements During Creep, or "Superplastic Creep"* (Beeré 1978): **a)** The shear stress τ produces shear strain $\gamma = 0.25$, cell centroids rotate by $\tan^{-1} \gamma = 14^\circ$ and, to maintain *surface tension equilibrium* = 120° angles at triple points, grain boundary rotations (a type of grain rearrangement, produced by sliding/migration) are required. Lattice rotations are assumed to not occur here. **b)** For a tensile stress such grain boundary rotations are not required to maintain surface tension equilibrium if cells deform as shown by configurations **i** and **ii**; but after large strains cell boundary length, and thus free energy is reduced by *neighbor switching*, configuration **iii**. **iii.** In the state $\epsilon = 0.5$, cells 1 and 3 are not neighbors while cells 2 and 4 are; but following neighbor switching, cells 1 and 3 become neighbors and cells 2 and 4 separate. Note also that the switched configuration is rotated by 30° from the unswitched configuration. This neighbor switching mechanism is examined further in part 'c'.

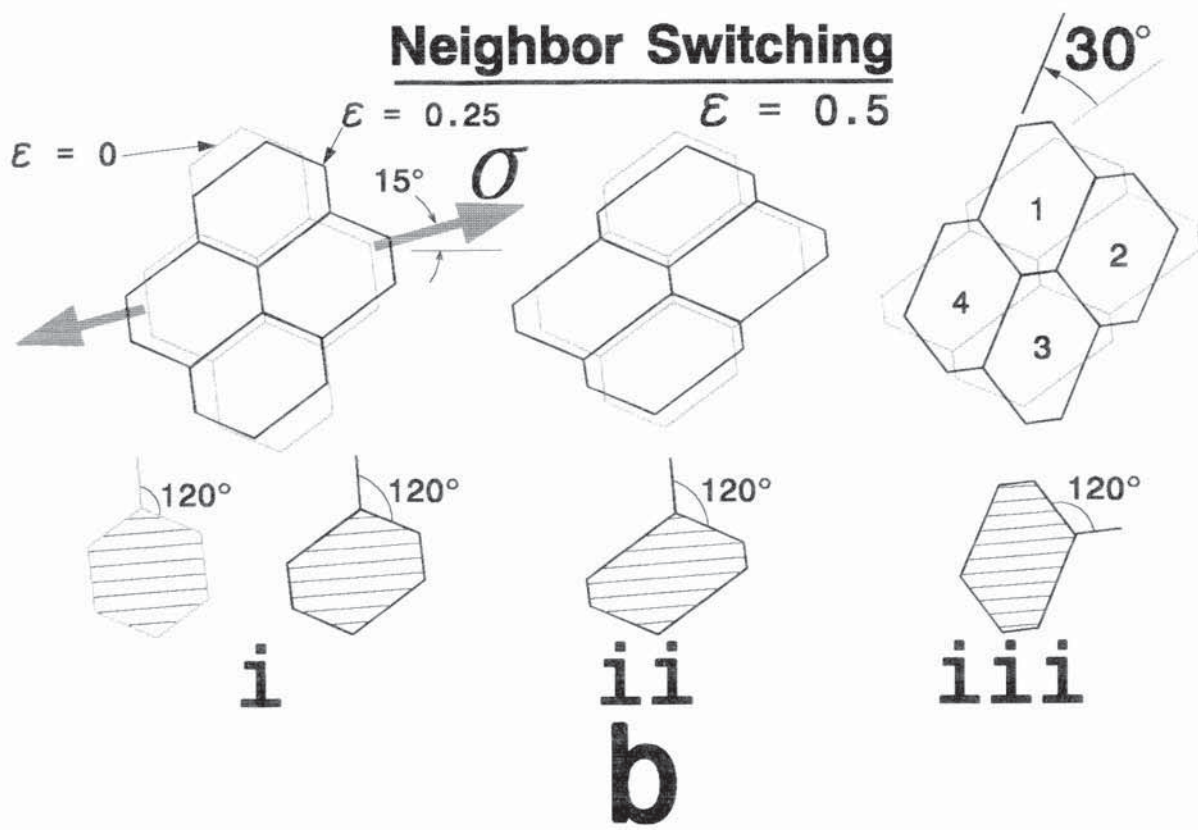
Figure 32 (Continued).

Grain Boundary Rotations



a

Neighbor Switching



b

- Grain Boundary
- Grain Boundary in Prior Configuration
- Lattice Planes

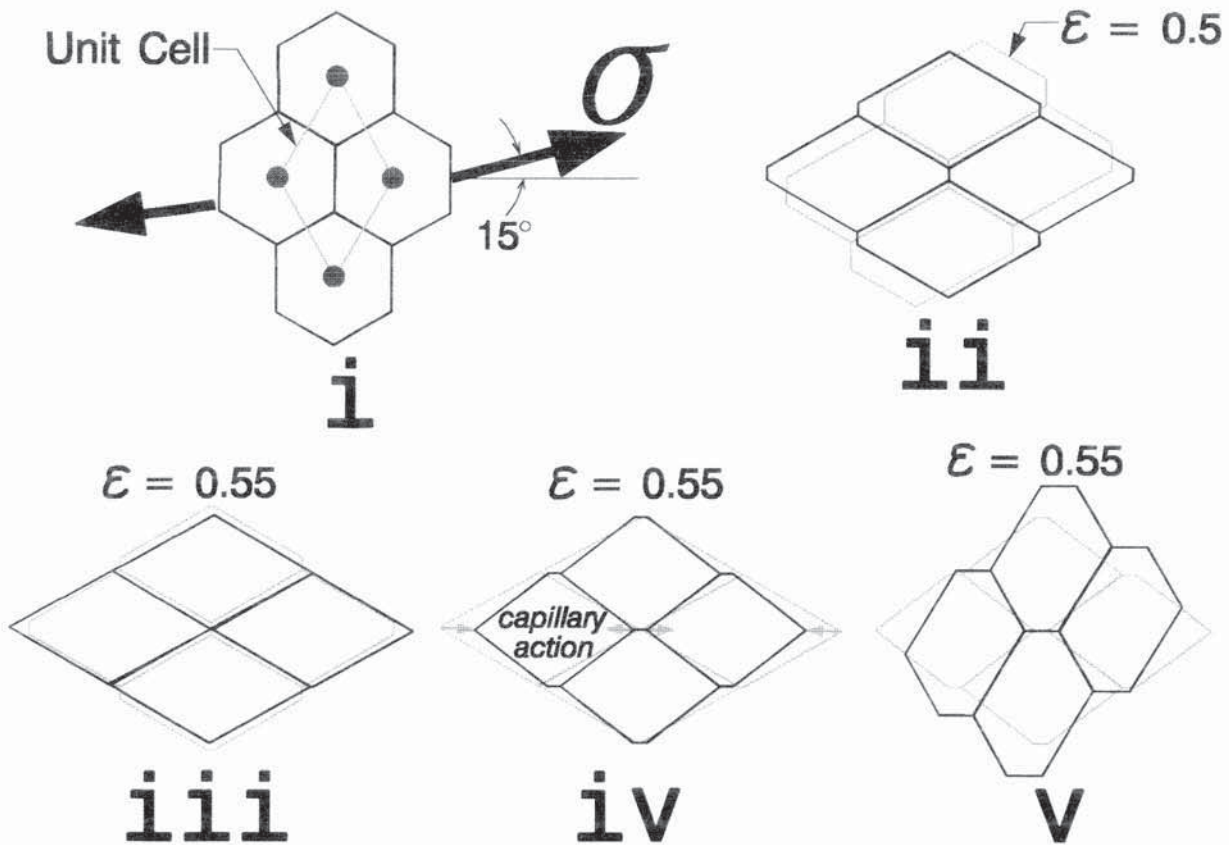


Figure 32 (Continued). c) Beeré's (1978) neighbor switching reaction. Tensile stress σ produces grain boundary sliding/migration until $\epsilon = 0.55$, at which point triple points converge. Subsequent grain boundary migration is driven by capillarity until dihedral angles again become 120° (Springarn and Nix 1978). **i.** The initial condition. The "unit cell" is constructed from the centroids of four hexagons and has the same area as one hexagon, but a larger perimeter. **ii.** The array is deformed beyond $\epsilon = 0.5$ by the applied stress. **iii.** The array is strained to $\epsilon = 0.55 \equiv \epsilon_0$ until triple points collapse; an unstable configuration which decomposes by capillarity. **iv.** Capillary action causes grain boundary migration which reorients the grain boundaries so that surface tension equilibrium is attained, configuration **v.** **v.** The final, switched state; the strain is still $\epsilon_0 = 0.55$.

Figure 32 (Continued). **d) Capillary Action.** **i.** Here, L denotes perimeter and A denotes area. **ii.** Forces at a triple point from capillarity are balanced if the following relationship between the dihedral angles, θ_i , and surface tensions, Γ_i , is obeyed:

$$\Gamma_1/\sin\theta_1 = \Gamma_2/\sin\theta_2 = \Gamma_3/\sin\theta_3.$$

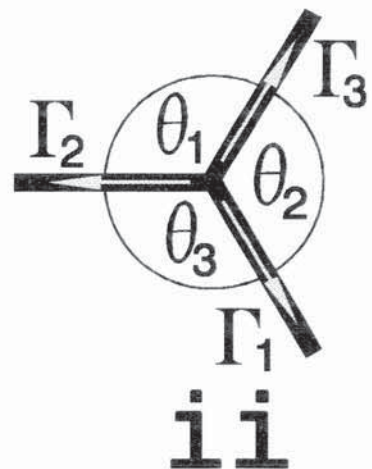
If $\Gamma_1 = \Gamma_2 = \Gamma_3$, then $\theta_1 = \theta_2 = \theta_3 = 120^\circ$. **iii.** A group of diamond-shaped "grains," or cells. Diamond cells decompose to hexagons when the boundaries shown in bold migrate to reduce free energy at the most rapid rate possible (Fortes and Ferro 1985): the tetravalent vertex has a larger energy than two trivalent vertices, or triple points; the perimeter of the diamond-shaped cells is greater than the hexagonal cells, and *free energy \propto surface tension \times cell perimeter*. **iv.** The unstable, tetravalent vertex decays into two trivalent vertices along the bisectors of the original 60° angles. This is the definition of capillary action for neighbor switching.

Figure 32 (Continued).

Capillary Action

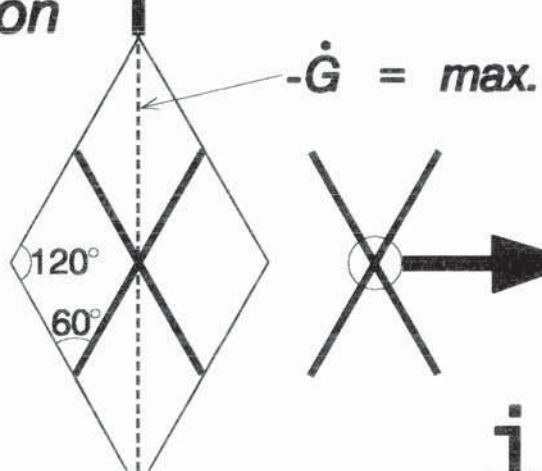
$$P_{\text{unit cell}} = 2\sqrt{3}d \quad P_{\text{hex.}} = 3d$$

$$A_{\text{unit cell}} = A_{\text{hex.}} = \frac{1}{2}\sqrt{3}(d/2)^2$$

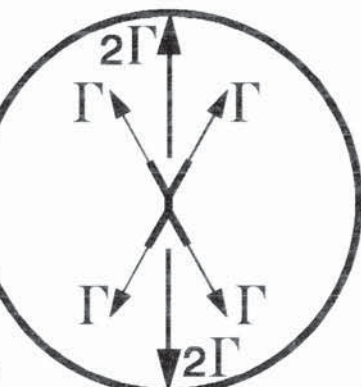


i

capillary action

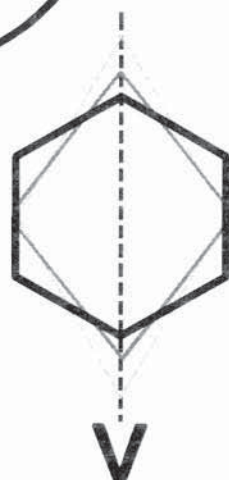


iv



iii

d



Aggregate Behavior

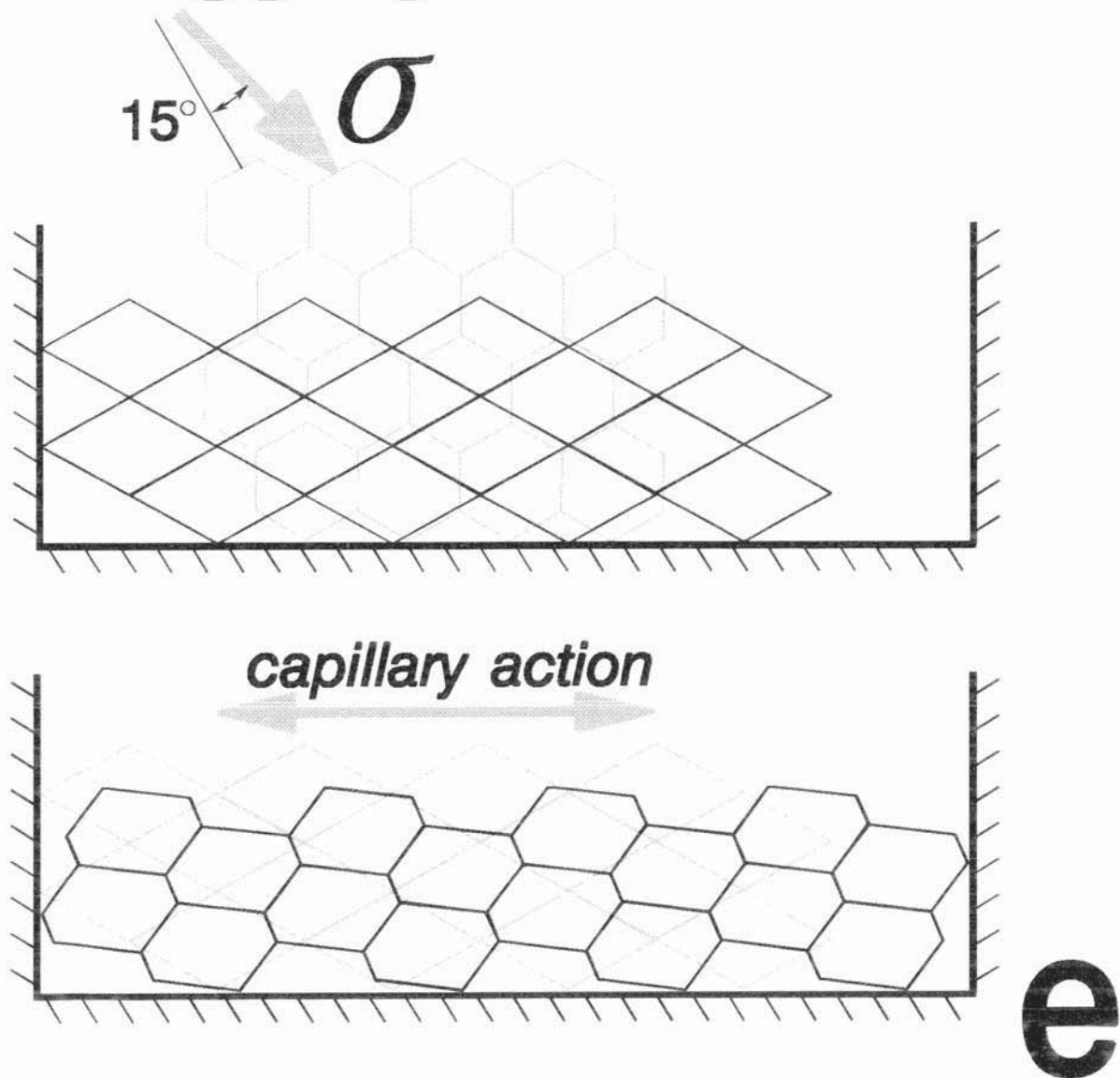


Figure 32 (Continued). e) *Metal Forming from "Superplastic Creep"*. The behavior of an aggregate of grains that deform as in part 'c' is shown. Top: the stress σ applied to the initial state produces the intermediate diamond configuration with strain $\varepsilon_0 = 0.55$. Bottom: capillary action changes the intermediate configuration to the final state.

Figure 33. After Morral and Ashby (1974): *Lattice graphs* are shown here; "points" on these graphs are the *duals* to the cells of a hexagonal array which has one 5-7 combination (pentagon adjacent to heptagon is a cellular dislocation). **a) Cellular dislocation climb:** i. The initial state. ii. An intermediate state after two neighbor switching reactions have redistributed the nearest neighbors of "points" on the graph. iii. The final state. **b) Cellular dislocation glide** (or T1 reaction).

Figure 33 (Continued).

Cellular Dislocation Climb

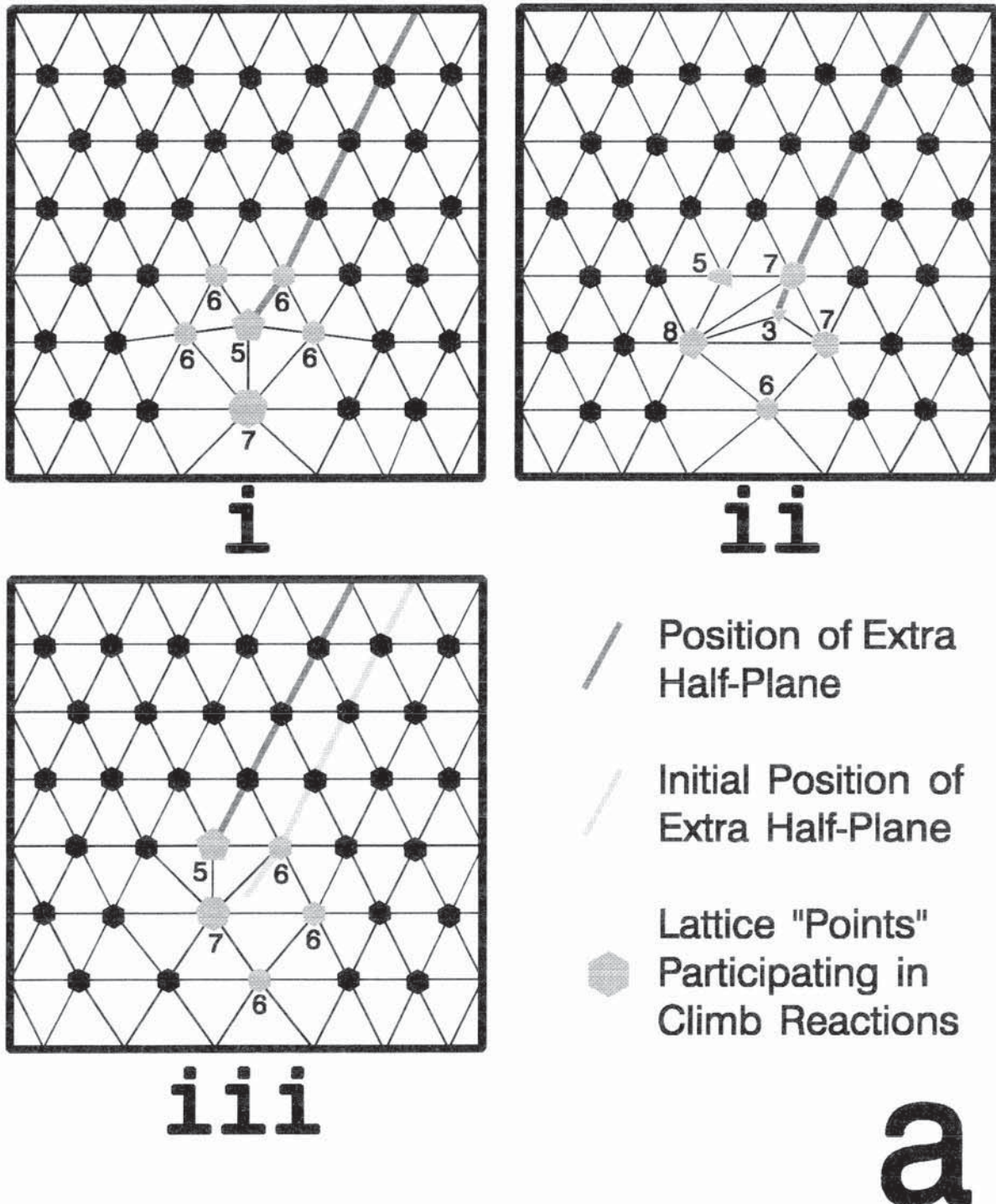
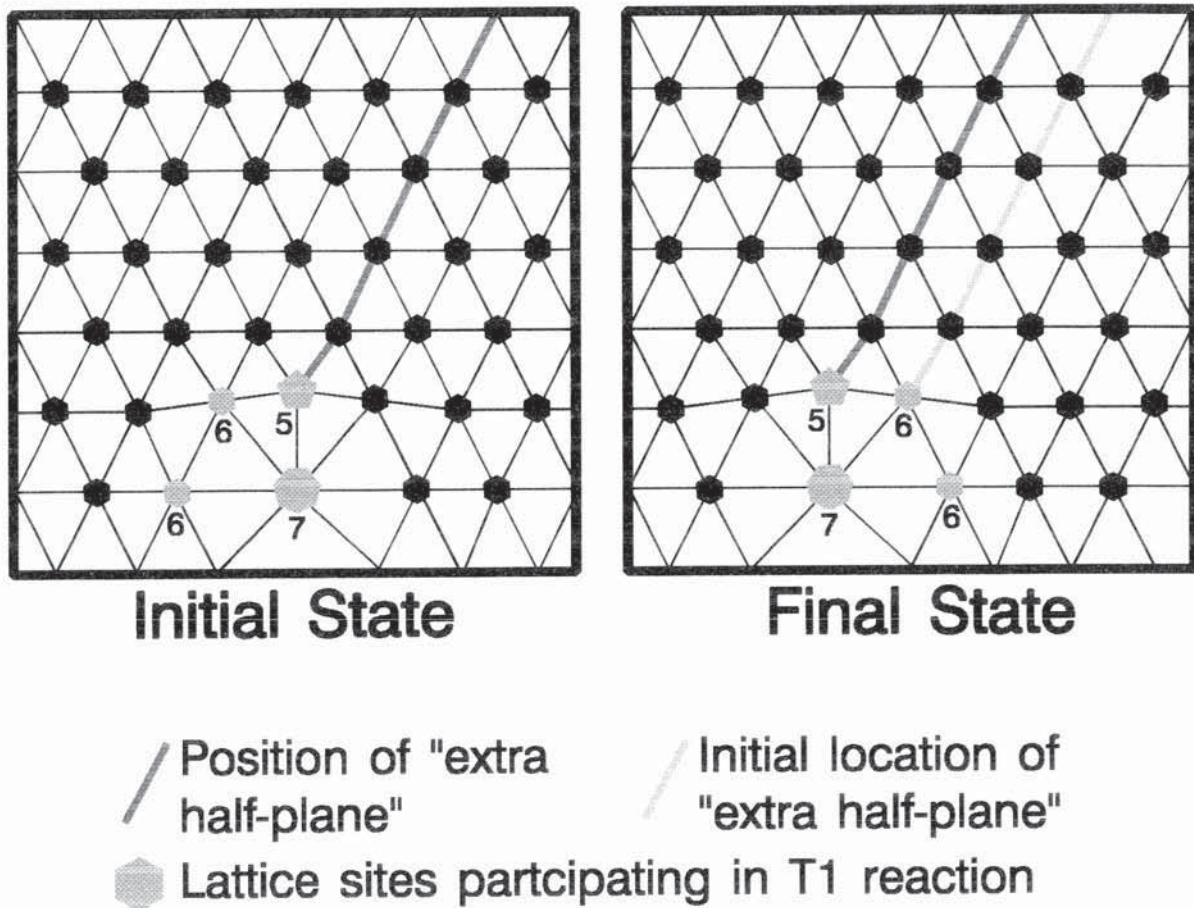


Figure 33 (Continued).

Cellular Dislocation Glide



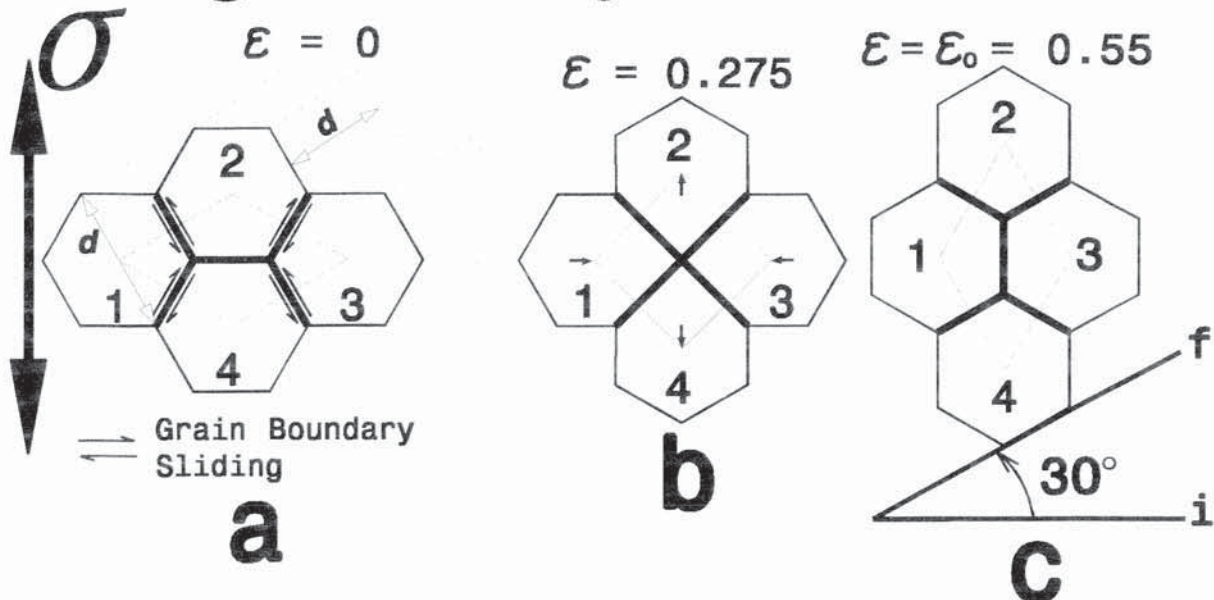
b
(Corrected)

Figure 34. Ashby-Verrall Neighbor Switching Mechanism. **a)** The initial condition, $\varepsilon = 0$. Grain boundary sliding occurs as indicated, which, with grain boundary migration, results in configuration 'b'. **b)** The unstable intermediate state, $\varepsilon = 0.275$. Grain boundary migration and grain rotations from this configuration produce the final state. Capillary action provides the driving force for the decomposition of this unstable configuration to the final state (Spingarn and Nix 1978). **c)** The final state, the group of "grains" attains the strain $\varepsilon = \varepsilon_0 = 0.55$. **d)** The Ashby-Verrall mechanism requires less matter transport per unit strain and has more available paths for atomic transport than "conventional" diffusion creep.

- i.** An exploded view overlaying configurations 'a' and 'b', showing atomic transport requirements for producing the strain $\varepsilon = 0.275$ from the initial configuration.
- ii.** Atomic transport requirements for diffusional creep; "grains" at $\varepsilon = 0$ and $\varepsilon = 0.275$ are overlaid.
- e)** Ashby *et al.* (1978) provide this diagram to defend their position on the intermediate, *square grain* configuration. The square "grain" configuration may require accommodation by both atomic dislocation and diffusive processes (Nix 1985).

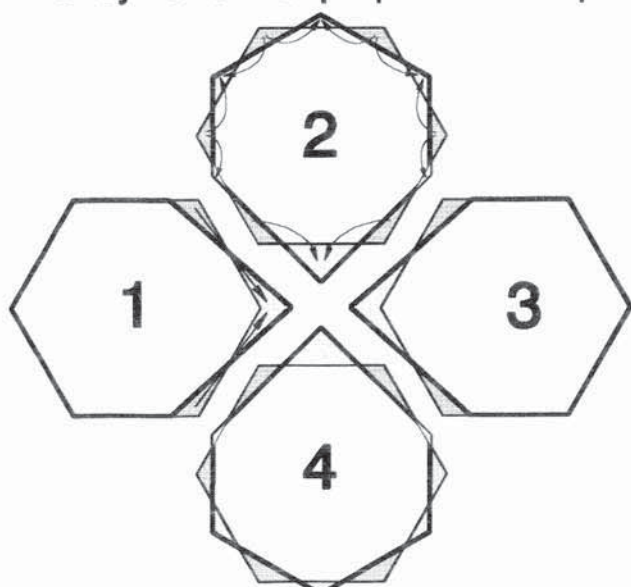
Figure 34 (Continued).

Original Ashby-Verrall Model



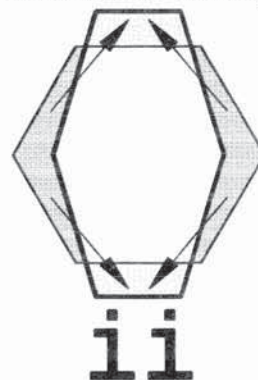
$$\epsilon = 0.275$$

Ashby-Verrall "Superplastic Creep"



i d

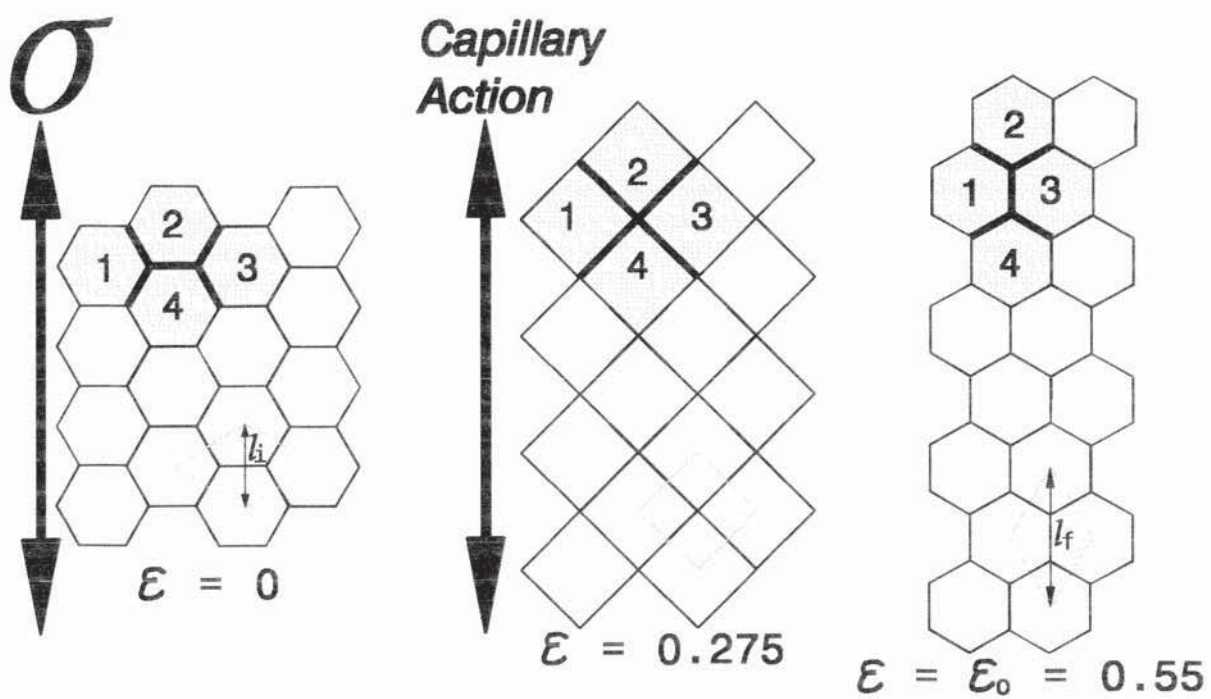
Diffusional Creep



—	$\epsilon = 0$
—	$\epsilon = 0.275$
→	Mass Transport
[hatched]	Grain Volume Involved in Mass Transport
[white]	Transports

Figure 34 (Continued).

Square Grain Model



e

Figure 35. **a)** Beeré's (1976) neighbor switching mechanism is "*grain rolling*". The lack of a 30° rotation of the cell group, in contrast to the Ashby-Verrall neighbor switching mechanism, should be noted. **i.** The initial condition. Grain boundary sliding and migration produce configurations ii through iii. **ii.** Intermediate configuration. **iii.** The unstable intermediate configuration. Unlike the Ashby-Verrall neighbor switching mechanism, here the strain is $\varepsilon = \varepsilon_0 = 0.55$. This configuration decomposes to iv by grain boundary migration from capillarity. In changing from configuration iii to configuration iv, the length of each "grain" boundary is reduced by a factor of 1.15. **iv.** The final state, $\varepsilon = \varepsilon_0 = 0.55$. **b)** Deformation of the "unit cell" can be viewed as resulting from a shear stress, τ , which produces a shear strain, γ . **c)** Mass transport required to produce configuration iii from the initial state. Note that atomic motion is more clearly stress-directed here than in the Ashby-Verrall mechanism (Figure 34d). **d)** Aggregate behavior for the grain rolling mechanism. **e)** The final state is a *mirror transformation* from the initial state for each group of four cells involved in Beeré's neighbor switching reaction (grain rolling).

Figure 35 (Continued).

Beeré's (1976) Neighbor Switching Reaction

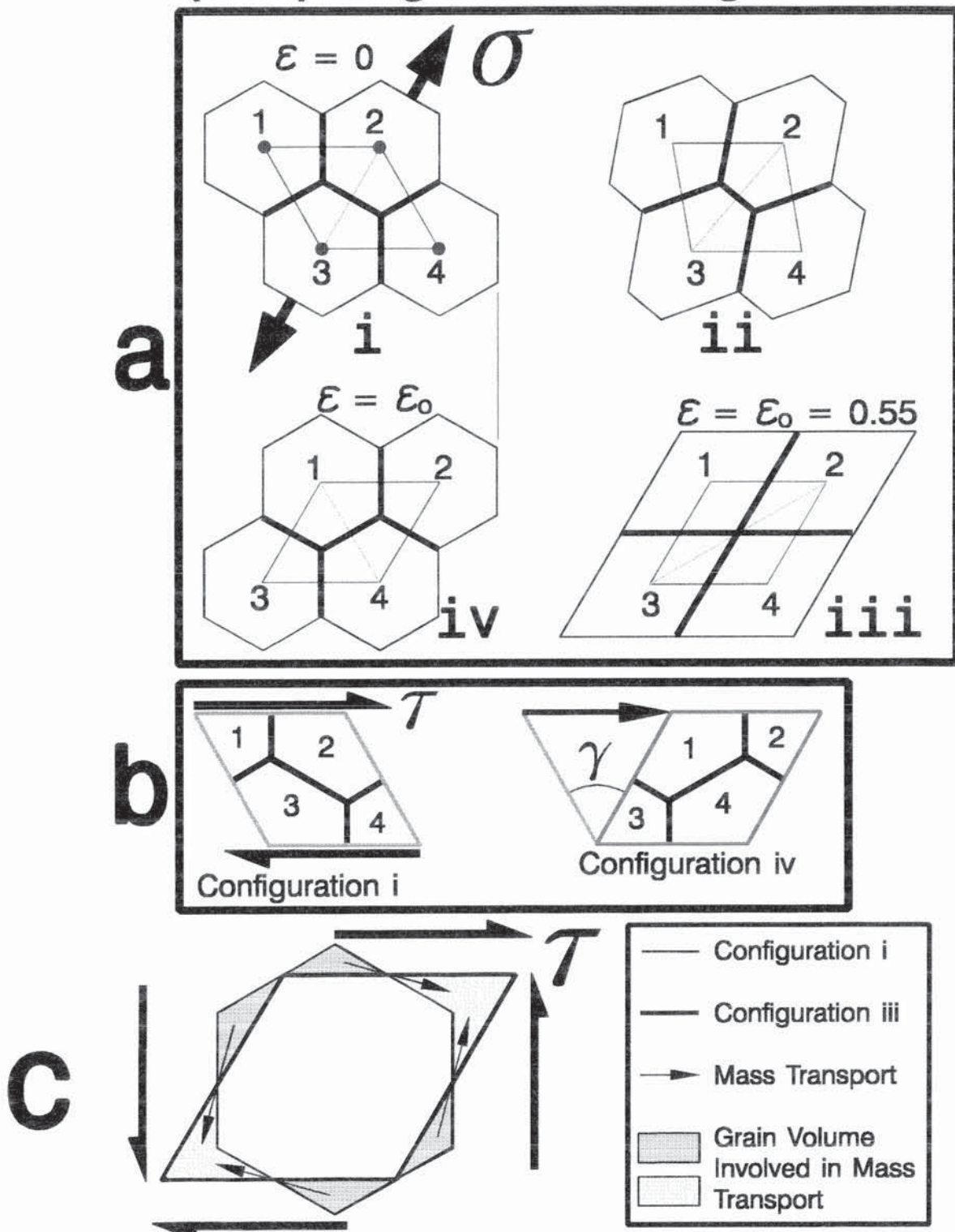
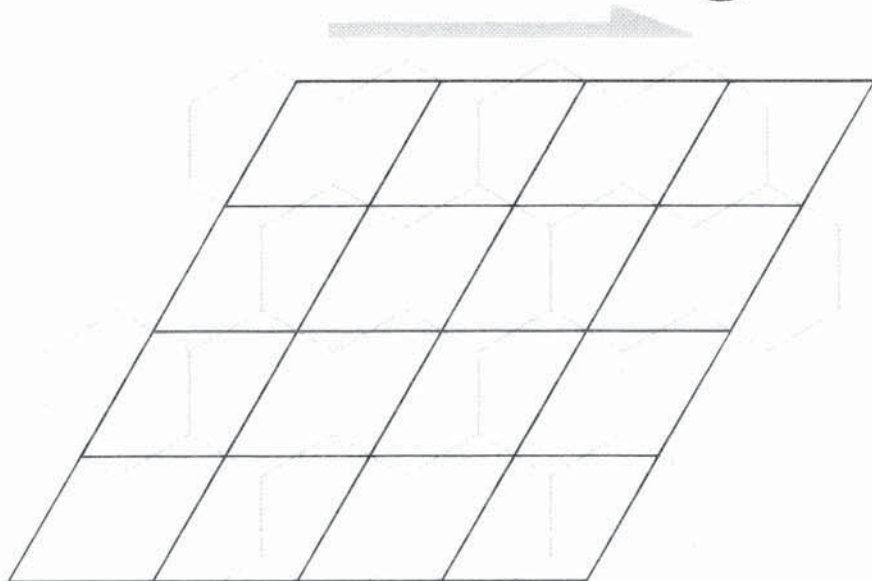
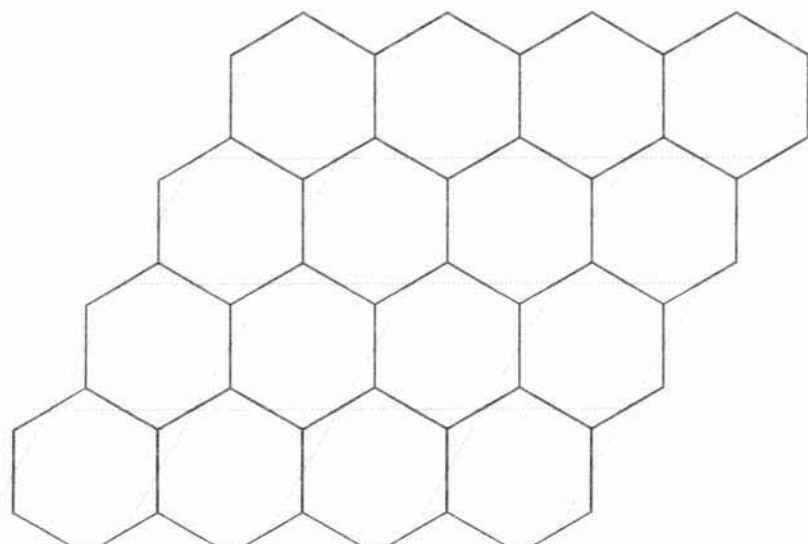


Figure 35 (Continued).

Grain Rolling



τ_i

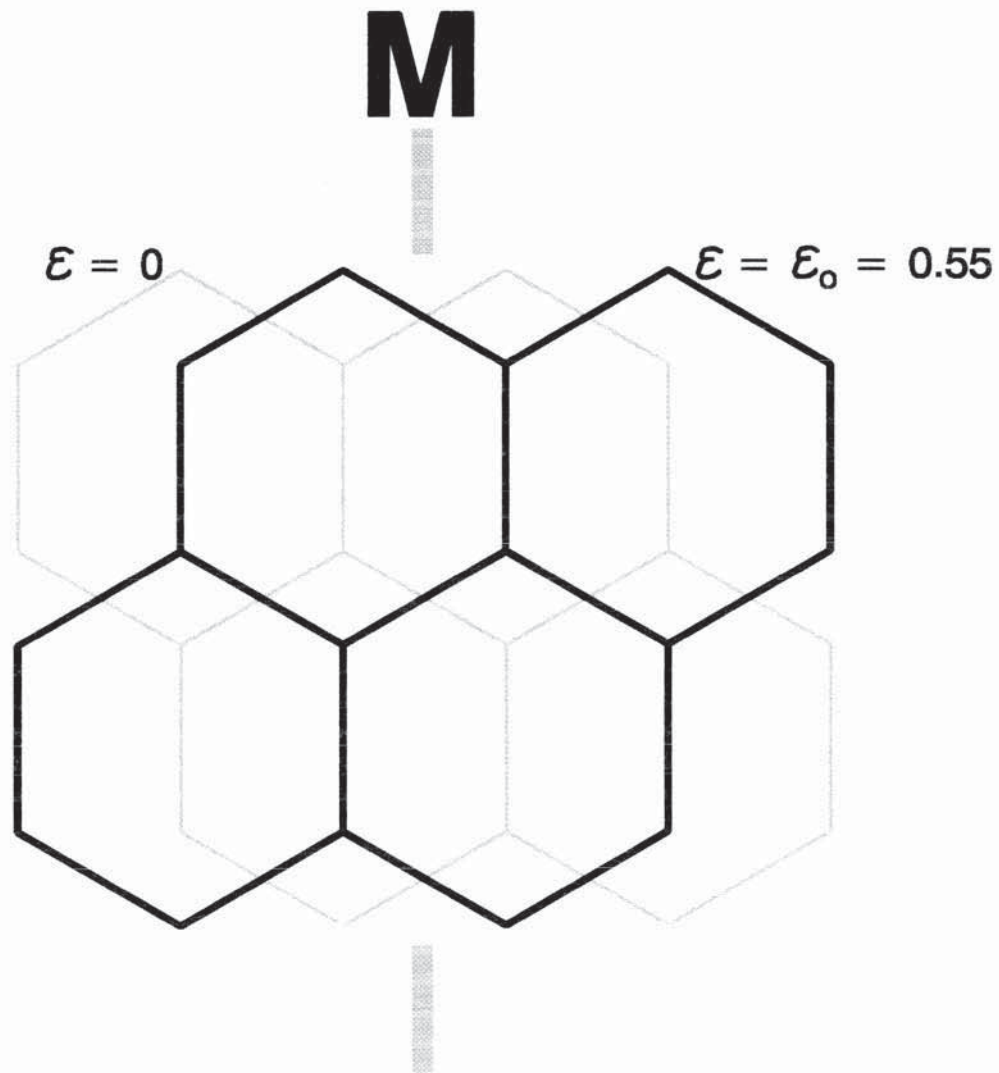


i_i

d

Figure 35 (Continued).

Mirror Transformation



e

Figure 36. **a)** Comparison of neighbor switching mechanisms for the plastic deformation of a cellular array: Ashby-Verrall (1973), Spingarn-Nix (Lee 1970, Spingarn and Nix 1978) and Beeré (1976); see also Ashby *et al.* (1978). These mechanisms model superplastic deformation of a polycrystalline material. **b)** Beeré's (1976) final state is the only one that does not involve a 30° rotation from the intermediate state and is therefore the most "slip-like." **c)** The Ashby-Verrall intermediate state and Beeré's (1976) final state are used to produce a "*slip-like*" *neighbor switching reaction* to model superplastic deformation with cellular dislocation glide. The Ashby-Verrall square grain intermediate state is the most slip-like; see Ashby *et al.* (1978). **d)** *Cellular dislocation glide*, after Sato *et al.* (1990), is neighbor switching involving non-hexagonal cells.

Presumably, because the 5-sided cell has a shorter edge length, mechanisms

for neighbor switching proceed more rapidly here than elsewhere.



Figure 36 (Continued).

Comparison of Neighbor Switching Mechanisms for Cellular Deformation

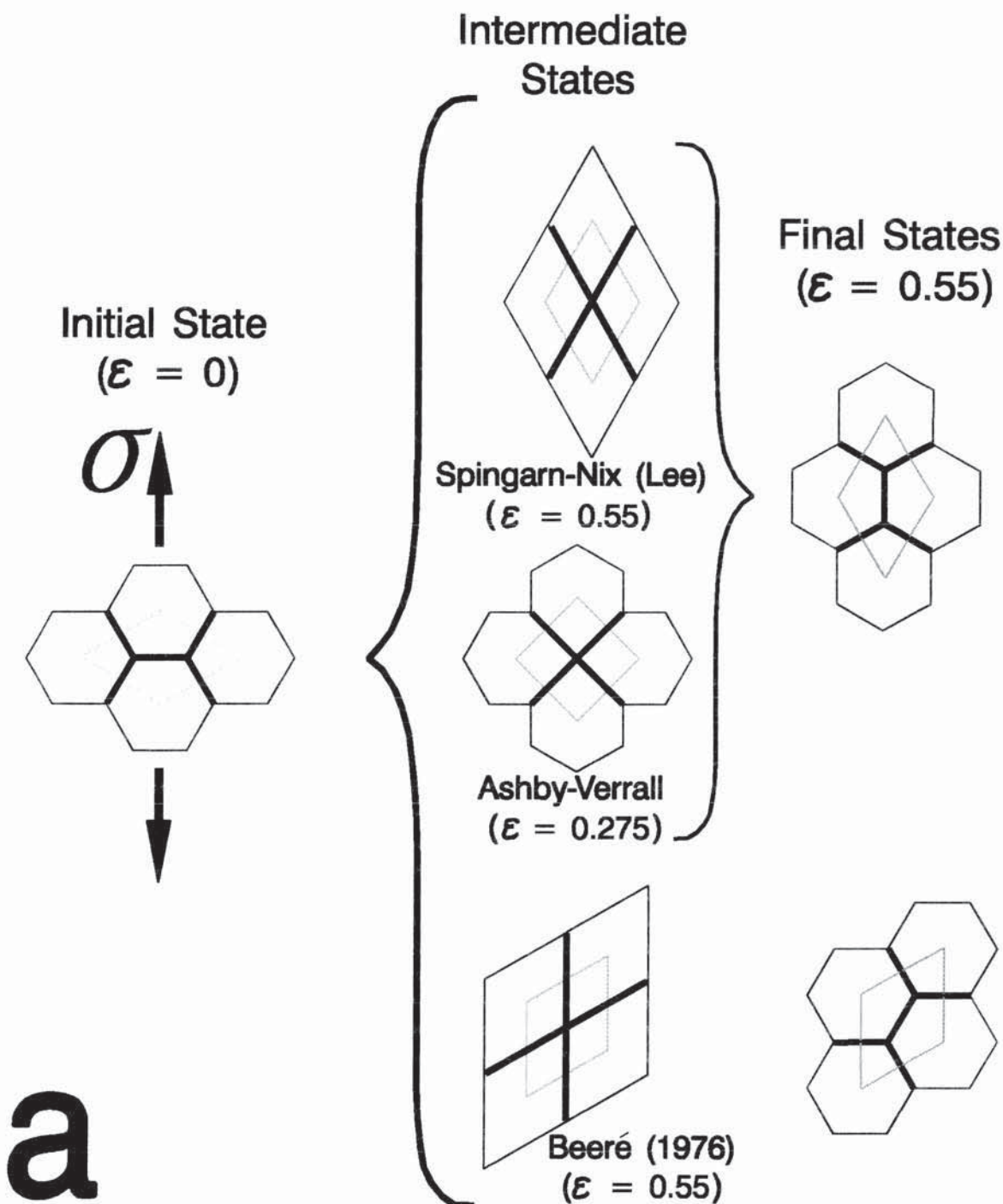
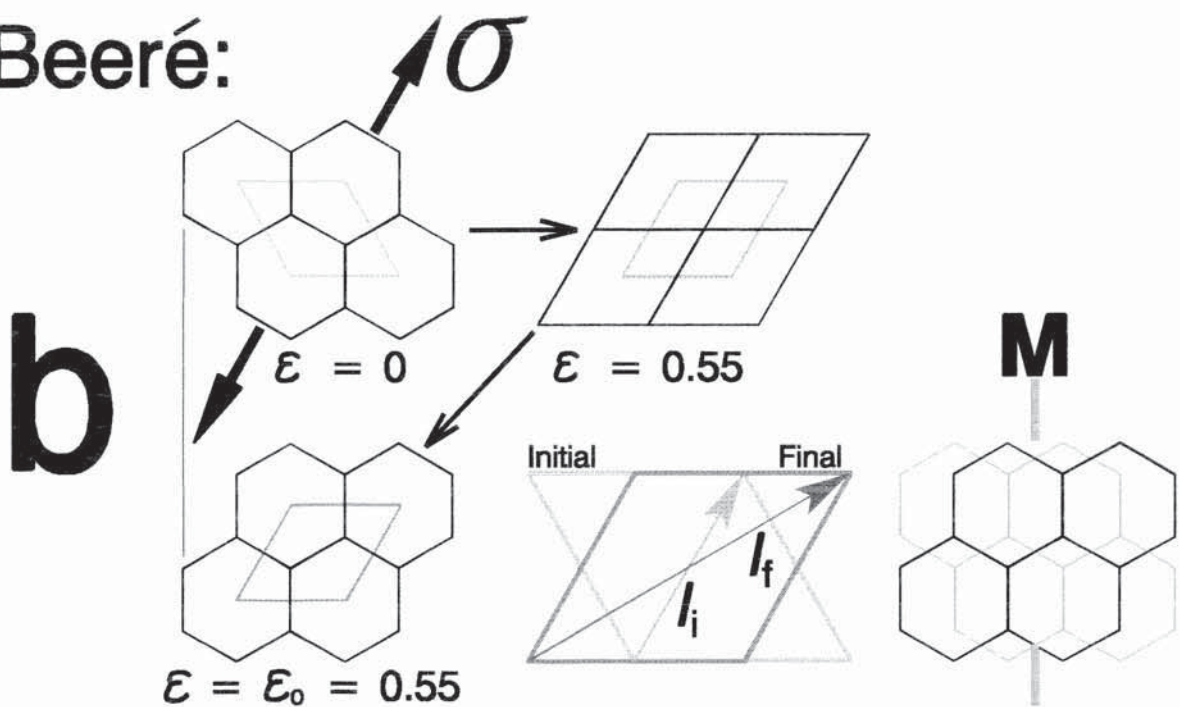


Figure 36 (Continued).

Beeré:



Slip-Like:

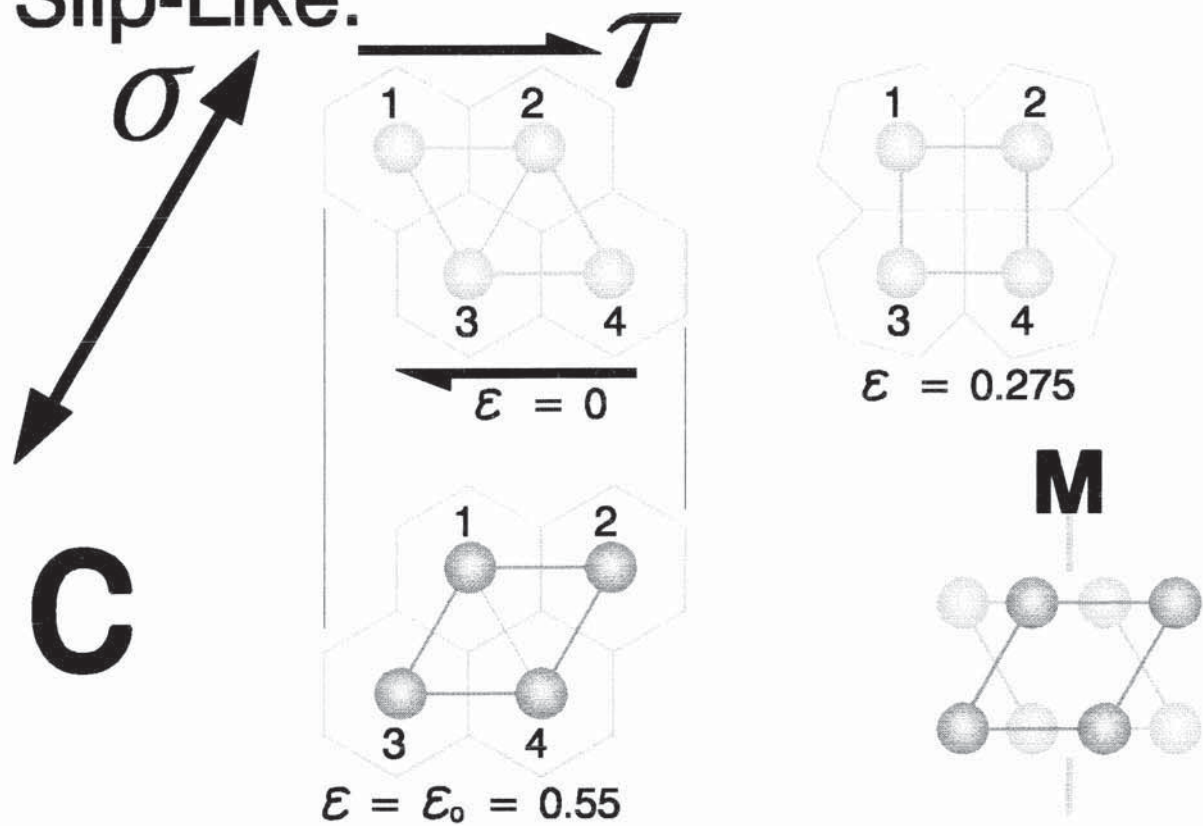
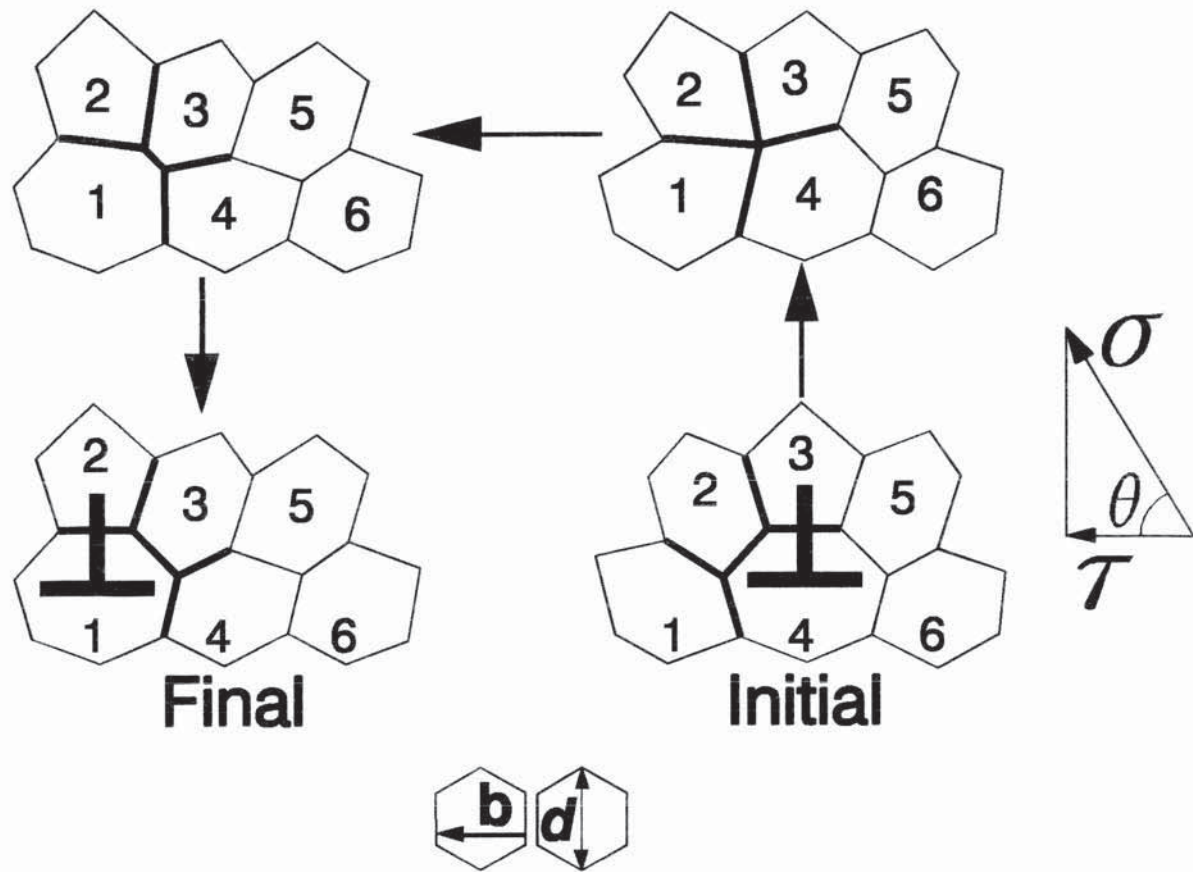


Figure 36 (Continued).

Cellular Dislocation Glide = Neighbor Switching



d

Figure 37. A cellular dislocation pair glide under an applied stress σ (Sherwood and Hamilton 1994). The dislocations are shown before and after each neighbor switching (T1) reaction, 'I' and 'F' denoting the initial and final states, respectively. Deformation results entirely from T1 reactions, but deformation is inhomogeneous, as in crystal slip. **a)** The first T1 reaction. **b)** The second T1 reaction (the initial state is the same as the final state from the prior configuration). **c)** The defects annihilate with image dislocations, leaving behind an array of uniform hexagons, thereby producing a plastic shear strain of $\gamma = 1/7$. **d)** The topological rule shown here (Carnal and Mocellin 1981), originally communicated to Burke and Turnbull (1952) by C. S. Smith, is obeyed for cellular dislocation glide. It is not obeyed for neighbor switching as in Figure 36a-c since all cells in that figure are hexagons.

Figure 37 (Continued).

"Slip" from Cellular Dislocation Glide

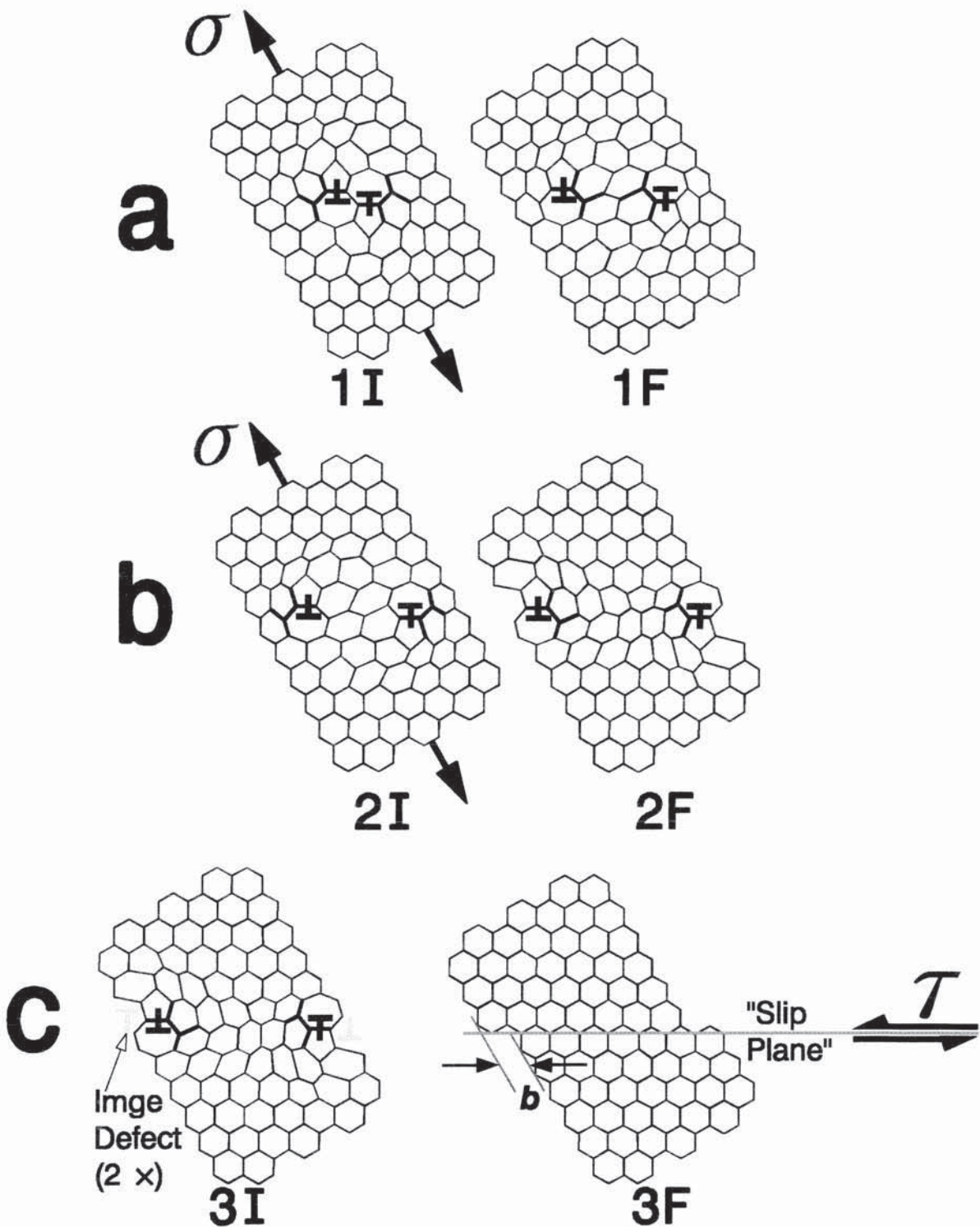


Figure 37 (Continued).

Topological Rule

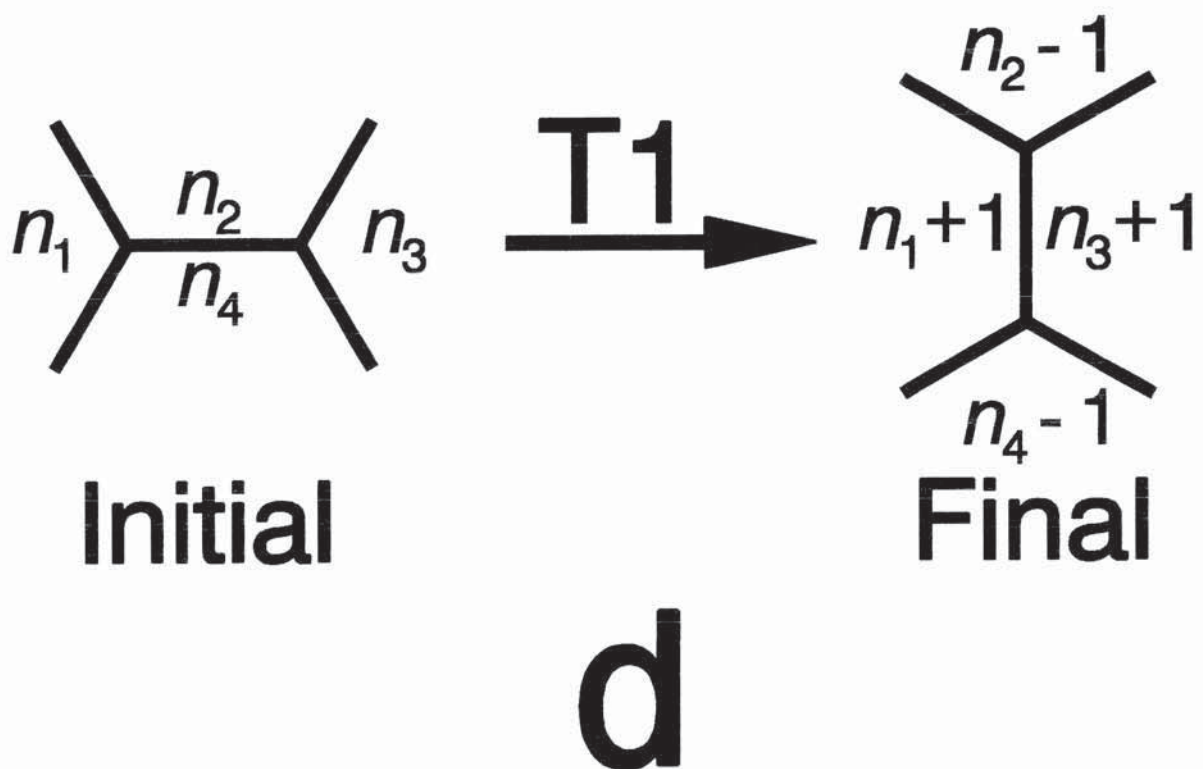


Figure 38. **a)** Model of superplastic flow via cellular dislocation glide (Sherwood and Hamilton 1994)—a *complexion*. "Slip planes" are a distance $3d/2$ apart. The array contains one dislocation (two non-hexagonal cells) for every 4 cells, $X_d = 1/2$; it is somewhat analogous to Taylor's (1934) Fig. 11 (Figure 30). In changing from the initial to the final state, dislocations pass through an unstable configuration (see Taylor's (1934) Fig. 11b): dislocations are separated by the applied stress, and then "attracted" to one another.

b) Analysis of neighbor switching reaction used in part 'a'. Here, there is no rotation of cell groups: the initial and final states are mirror images of each other (see Taylor (1934) too), as is also the case for Beeré's (1976) neighbor switching reaction, Figure 35. **i.** Cellular dislocation glide, left; Beeré's (1976) neighbor switching reaction, right. Initial and final states of both neighbor switching reactions shown here are mirror images of one another. **iii.** Analysis of the "unit cells" indicates that the cellular array has suffered a plastic strain of $\epsilon = \epsilon_0 = 0.55$.

Figure 38 (Continued).

Superplastic Flow from Cellular Dislocation Glide

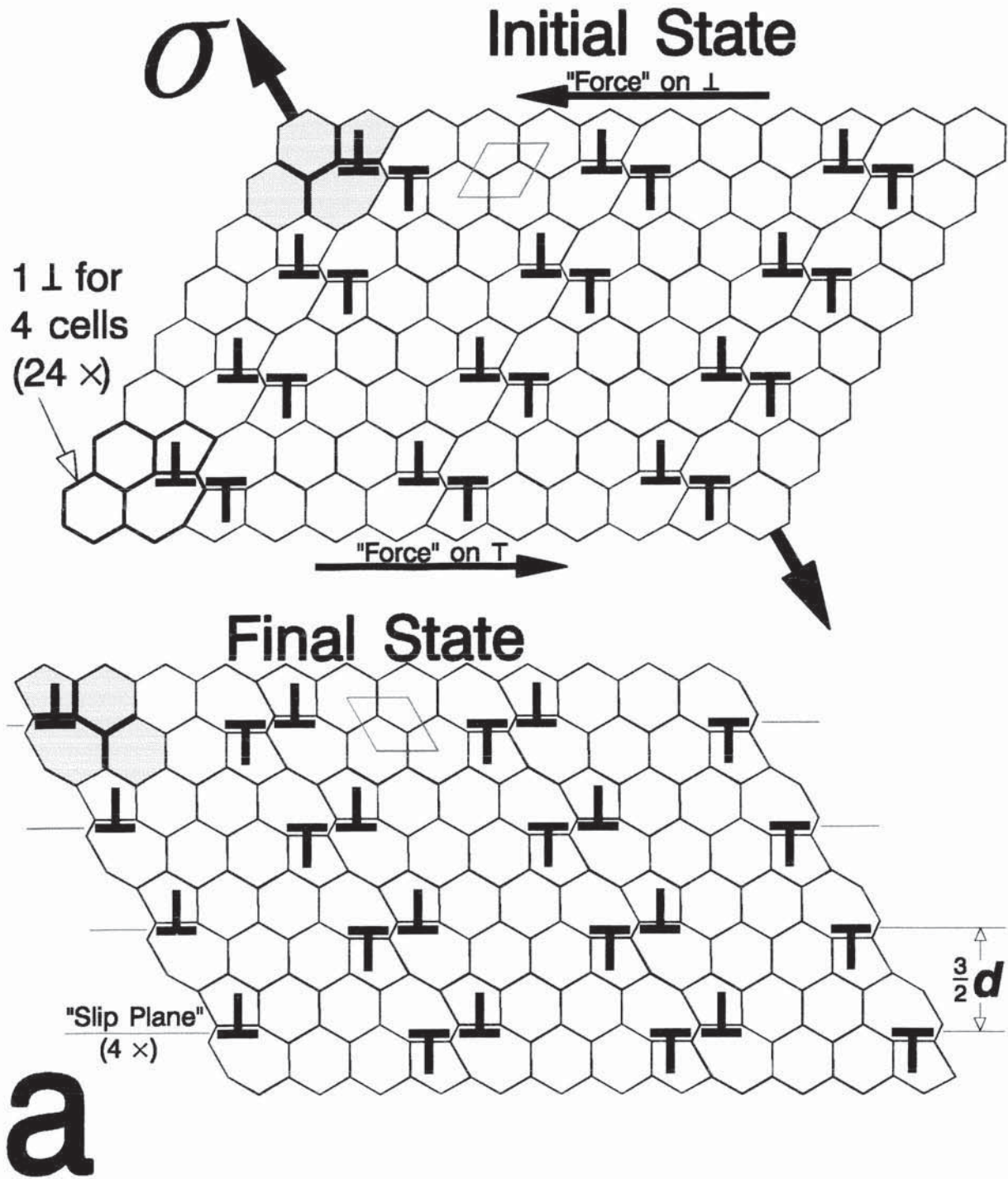


Figure 38 (Continued).

Analysis of Cellular Dislocation Glide as Mirror Transformation

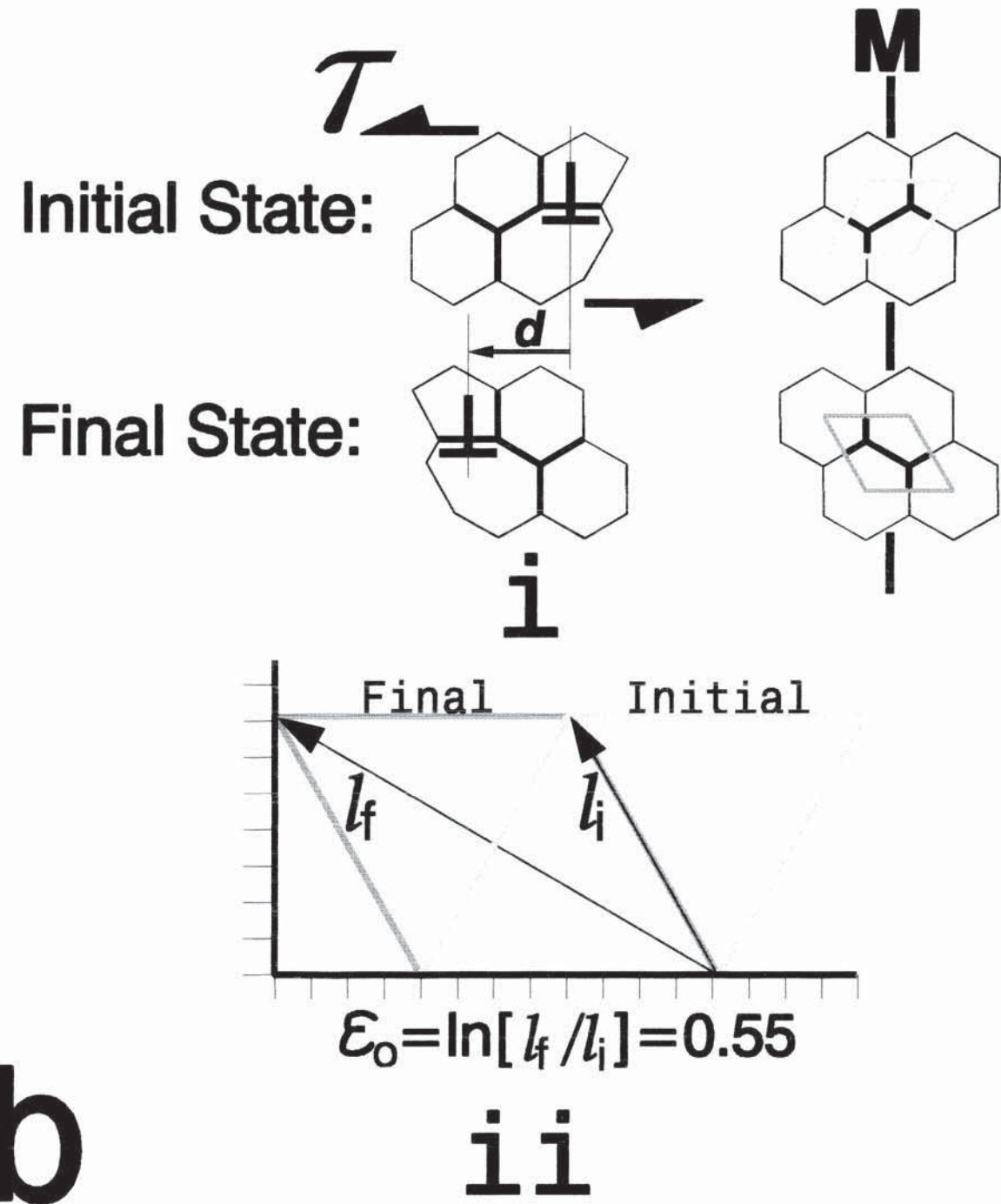


Figure 39. Grain growth follows *topological transformations* between grains which redistribute boundaries such that small grains with fewer than average neighbors are periodically produced and eliminated (Christian 1965). In a two-dimensional honeycomb array these are *neighbor switching* and *cell disappearance* (Morral and Ashby 1974). Dihedral angles for a two-dimensional cell with n -sides, ϕ_n ($n \geq 3$), are $\phi_n = \pi - 2\pi/n$. Thus, for constant surface tensions between cells, only an array of hexagons can be in *metastable equilibrium* with all dihedral angles equal to $\phi_6 = \frac{2}{3}\pi = 120^\circ$. If cells in a two-dimensional array have "defects" \equiv non-hexagonal cells (Hillert 1965), dihedral angles will not equal 120° unless boundaries are curved: $\phi_n > 120^\circ$ or boundary curvature both produce a "driving force" for migration, proportional to the *capillary "pressure"*, $p = \Gamma/\varrho$, Γ denoting the surface tension and ϱ the boundary radius of curvature (Verhoeven 1975).

Hillert's (1965) *grain growth "reaction"*, or *thermally-activated cellular dislocation climb* (Cahn and Padawer 1965, Morral and Ashby 1974). Three elementary reactions are involved: two neighbor switching (T1) reactions and one cell disappearance (T2) reaction. These reactions are all assumed to result from capillarity. **a)** The initial state: bold cell edges migrate via capillarity until the two triple points converge. This unstable configuration decomposes under further capillary action (Fortes and Ferro 1985), denoted with the arrows, causing cells 1-4 to switch neighbors, producing configuration 'b'. **b)** The final state from the first T1 reaction. **c)** Same as configuration 'b'; the initial state for the second T1 reaction. **d)** The final state from the second T1 reaction; cell 3 becomes 3-sided. **e)** Same as configuration 'd'; the initial state for the T2 reaction. **f)** The final state from the T2 reaction; cell 3 has disappeared and the cellular dislocation has reappeared.

Figure 39 (Continued).

Grain Growth "Reaction"

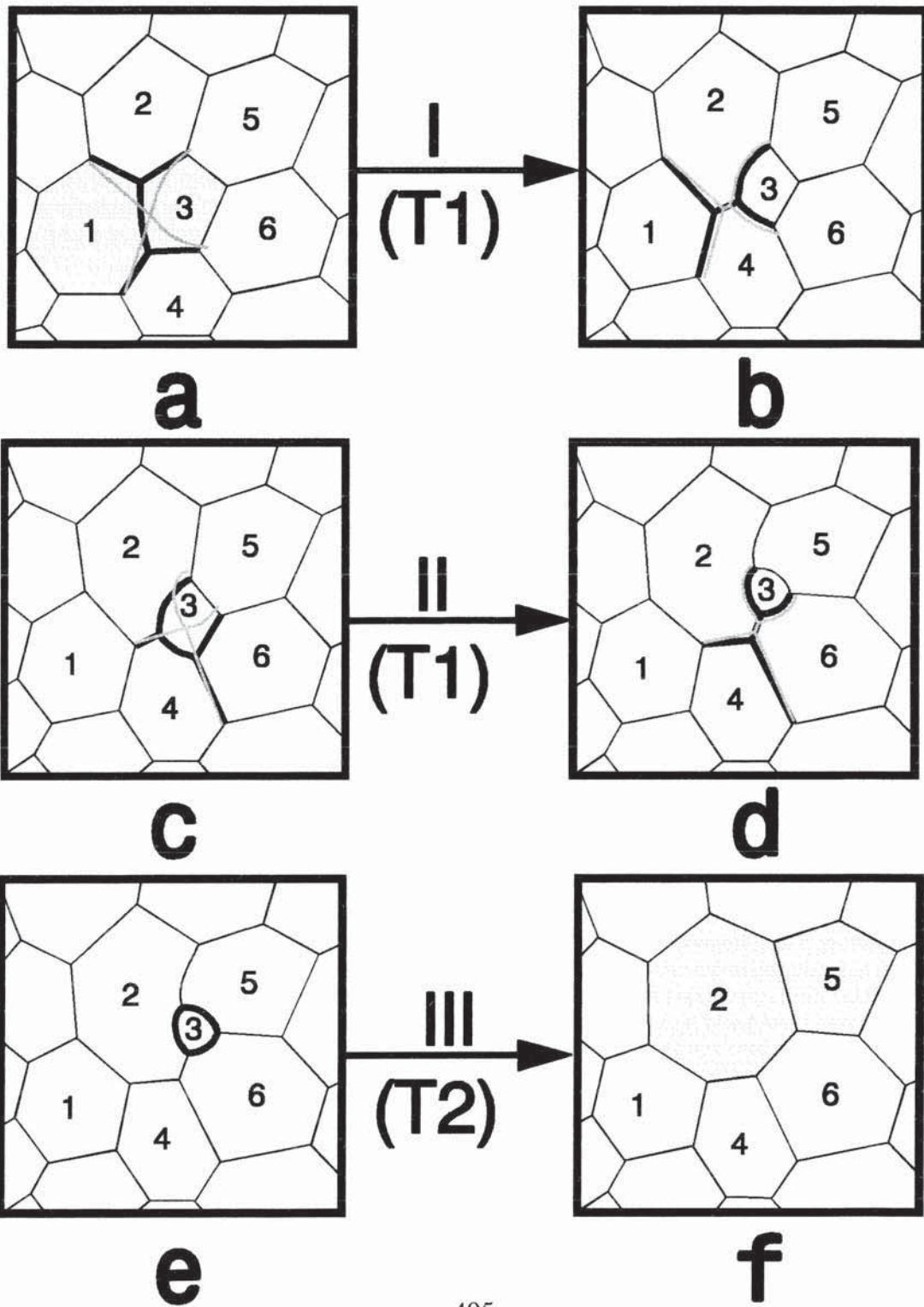


Figure 40. Two-dimensional model microstructures for superplastic materials; see Arieli and Mukherjee (1980) for discussion. **a)** *Single phase*: grain boundaries are modelled as a hexagonal array. **b)** *Quasi-single phase* materials have a fine dispersion of second phase particles which tend to pin the grain boundaries (Zener 1948). **c)** Microduplex materials are comprised of two distinct phases, designated α and β . The phases are separated from each other, phase coarsening (or grain growth) consequently requires long range atomic diffusion.
i. Typical microduplex microstructure; the β -phase has a volume fraction approaching that of the α -phase. ii. As the volume fraction of the β -phase decreases this type of microstructure is expected, where the β -phase is associated with the corners of the α -phase. This is a model for Holm *et al.*'s (1977) superplastic Zr-2.5% Nb alloy.

Figure 40 (Continued).

Model Microstructures for Superplastic Materials

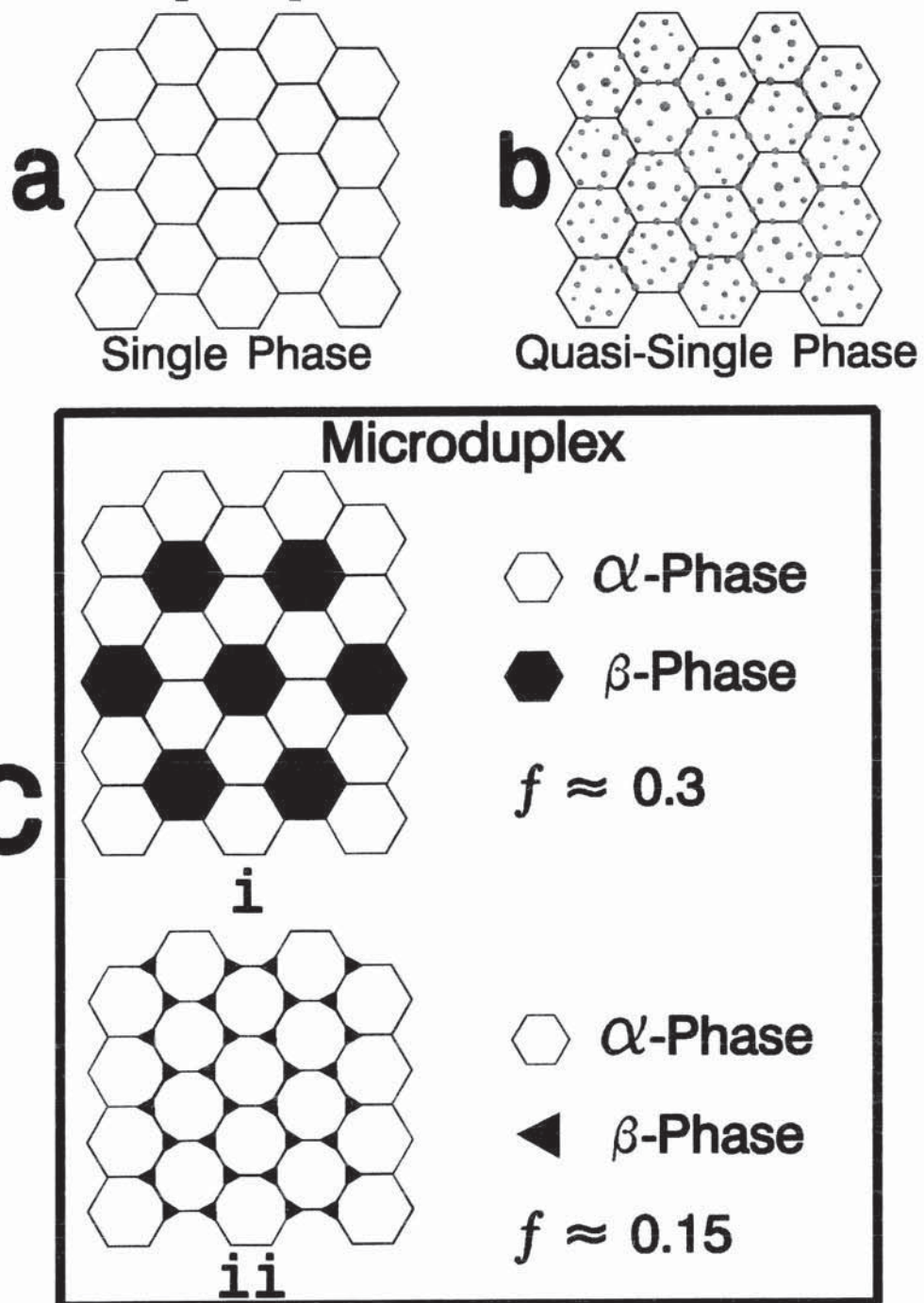
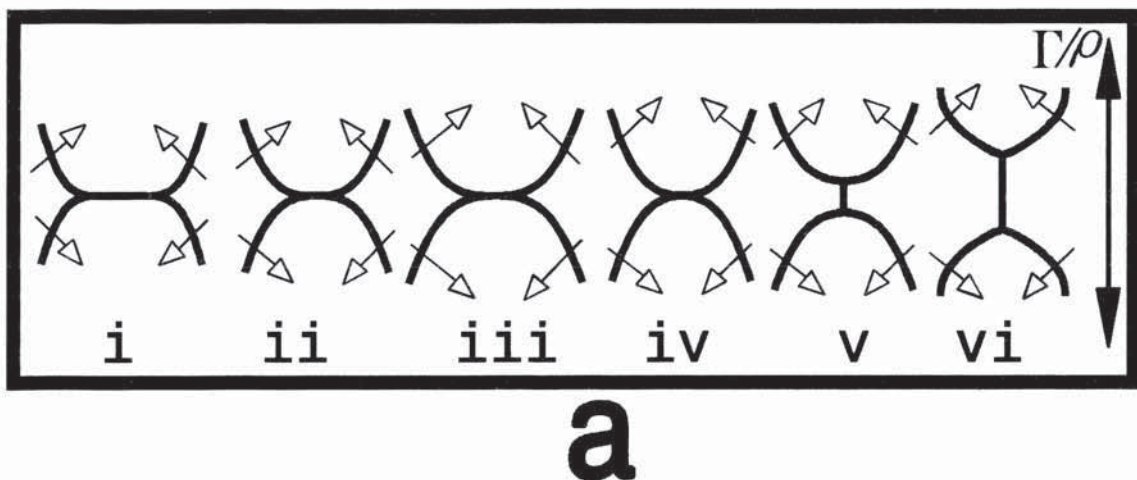


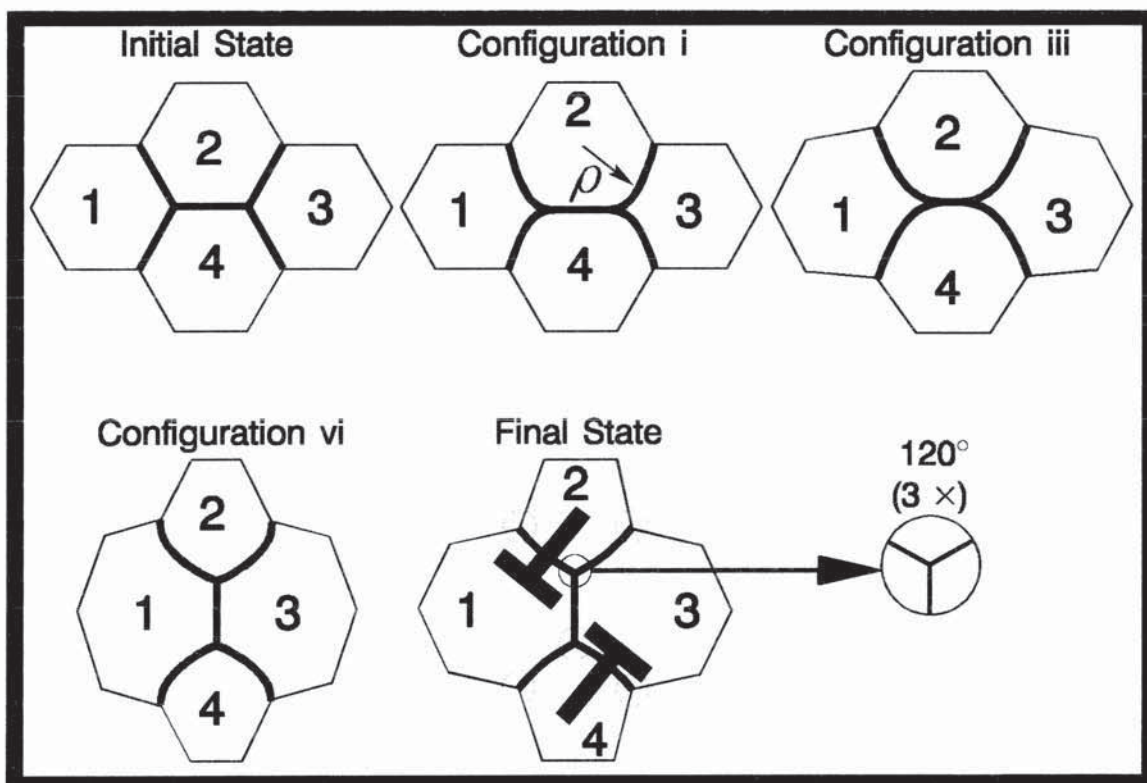
Figure 41. Cellular dislocations are also produced during annealing (Hillert 1965). Burke and Turnbull's (1952) discussion indicates that capillarity as in box 'a' produces a pair of 5-7 combinations as in box 'b'. Here, neighbor switching defines the topological rule shown by Figure 37d. **a)** *Capillary action* $\equiv \Gamma/\varrho$, where Γ is the surface tension and ϱ the boundary radius of curvature. **b)** The initial state is a metastable hexagonal array with $\varrho = \infty$. A thermal fluctuation produces curvature $1/\varrho$ in configuration i, where $\varrho = \frac{1}{2}\mathbf{b}$, with \mathbf{b} denoting the cell width. The final state follows neighbor switching when cell edges minimize their lengths. A cellular dislocation pair is produced. Free energy is increased by this reaction; but since the defects created here can participate in the grain growth "reaction," the free energy of the whole array of cells will eventually decrease.

Figure 41 (Continued).

Production of Cellular Dislocation Pair During Annealing



a



b

Figure 42. A mechanism for the production of a cellular dislocation pair in an array of hexagons subjected to stress σ (Sherwood and Hamilton 1991, 1994). Here:

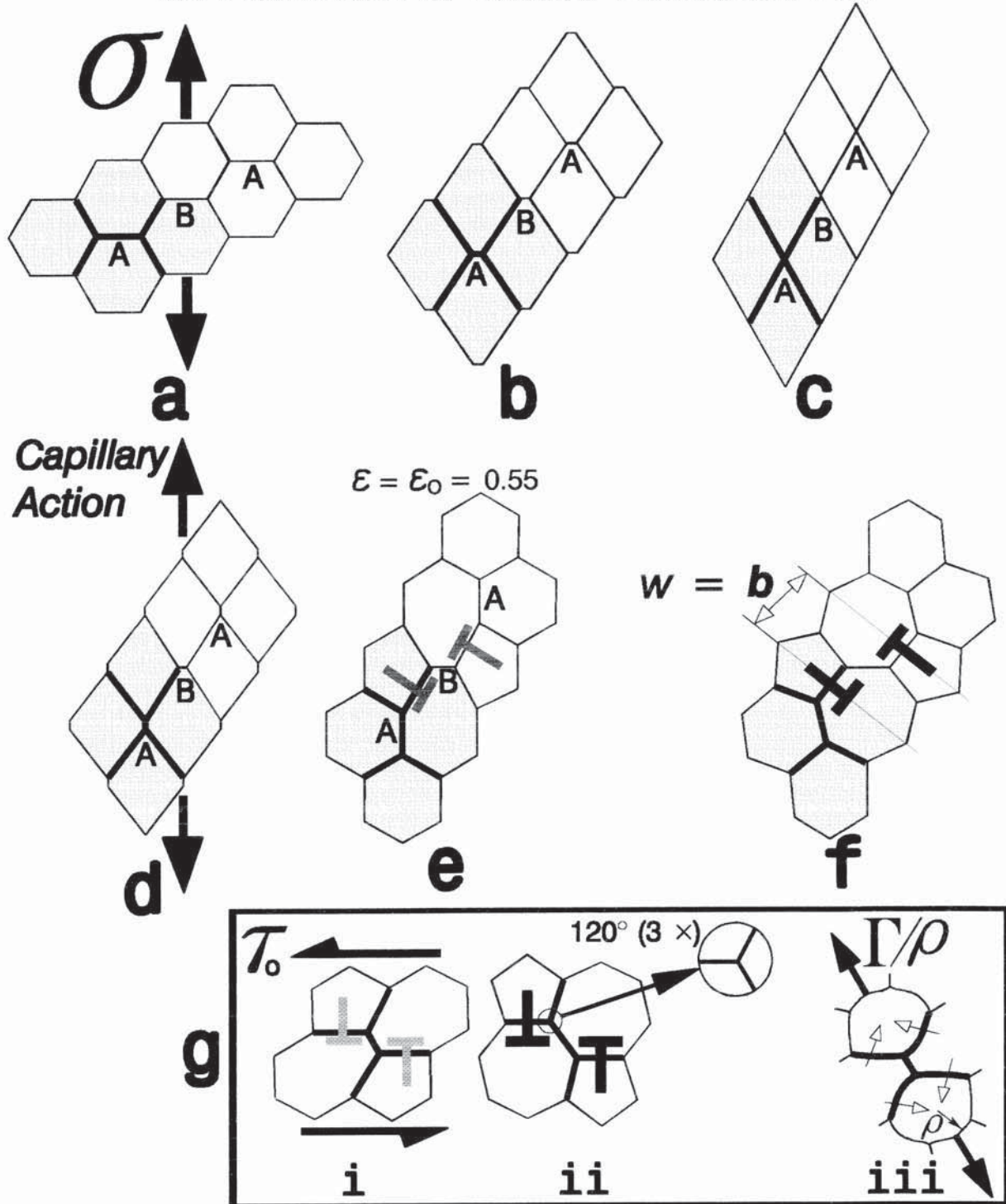
**All cells begin the neighbor switching reaction at the same time but one
cells group lags behind the others as the reaction finishes.**



Contrast the reaction here with that displayed by Figure 21c. Two groups of cells are shown, shaded and un-shaded. And there are two types of boundary, 'A' and 'B': type 'A' are internal to each group while type 'B' is shared between two groups. **a)** Initial configuration. **b)** Intermediate configuration resulting from grain boundary sliding/migration. **c)** The unstable intermediate configuration. **d)** The node 'B' does not undergo migration for neighbor switching while surrounding nodes 'A' do, perhaps, for example, because of a slight variation in edge lengths or, small misorientation angle between the separating cells at node 'B' (J. J. Hoyt 1991, personal communication). **e)** The prior *neighbor switching "accident"* nucleates a pair of 5-7 combinations. **f)** Defects from the nucleus separate a distance $w = b$ apart, as shown in box 'g'. **g)** *Capillary action* = $\Gamma/\varrho \approx \Gamma/2d$ provides the resolved "stress," τ_s , $\tau_s \approx \frac{1}{2}[\Gamma/2d] = \Gamma/d$ that separates the dislocations. **i.** The nucleus is subjected to "stress" τ_s from the boundary curvature shown by configuration iii. **ii.** The final state, a pair of cellular dislocations. Triple points satisfy surface tension equilibrium with minimal boundary length, *i.e.* boundaries are curved (not shown). **iii.** Bold boundaries are concave towards the smaller 5-sided cell and move as shown from capillary action, $\Gamma/\varrho \approx \Gamma/2d$.

Figure 42 (Continued).

Neighbor Switching Accident Mechanism for Production of Cellular Dislocation Pair



Cellular Dislocations from Cellular Disclinations

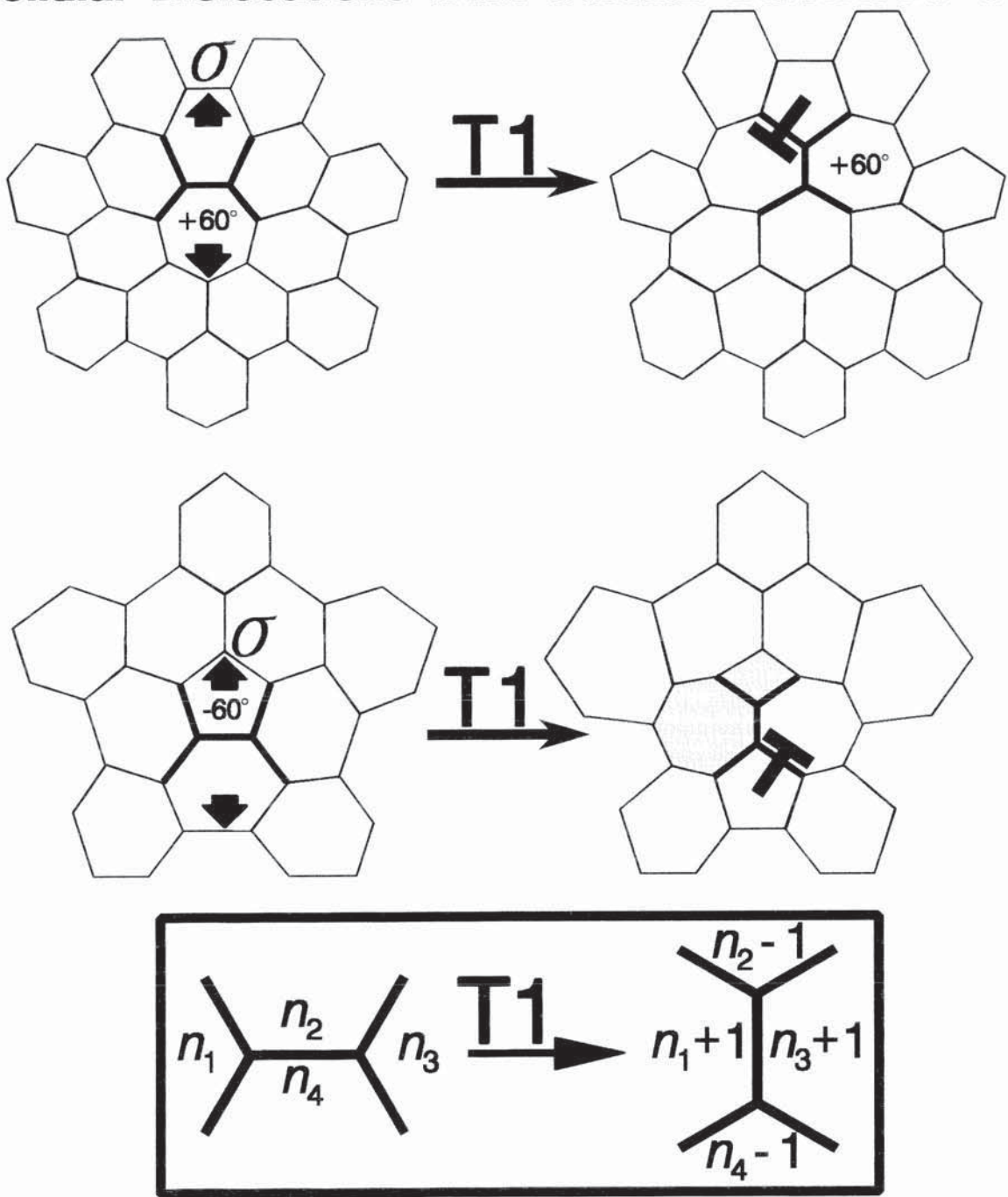


Figure 43. Dislocations are produced from disclinations per the topological rule (bottom).

Here, grain boundary sliding/migration causes $T1$ reactions only at defects.

Figure 44. *Cellular Dislocation Annihilation* (Sherwood and Hamilton 1994). **a)** A pair of cellular dislocations annihilate by neighbor switching per the topological rule. Here, dihedral angles ϕ are $\phi < 120^\circ$, but capillary action produces a "driving force" for neighbor switching only for $\phi > 120^\circ$ (Fortes and Ferro 1985); thus, the dislocation pair is actually stable. Parts 'b' and 'c' provide mechanisms for grain boundary migration during annealing and superplastic deformation, respectively, to produce cellular dislocation annihilation.

b) Annealing: Since bold cell edges have $\phi < 120^\circ$, before neighbor switching can begin, a thermal fluctuation must provide enough energy for grain boundary migration to increase ϕ . Capillary action then results in neighbor switching and annihilation of the cellular dislocations. **c) Superplastic Deformation:** The resolved stress $s\sigma$ acts on bold cell edges with sufficient magnitude for sliding/migration to result in neighbor switching and defect annihilation.

Figure 44 (Continued).

Cellular Dislocation Annihilation

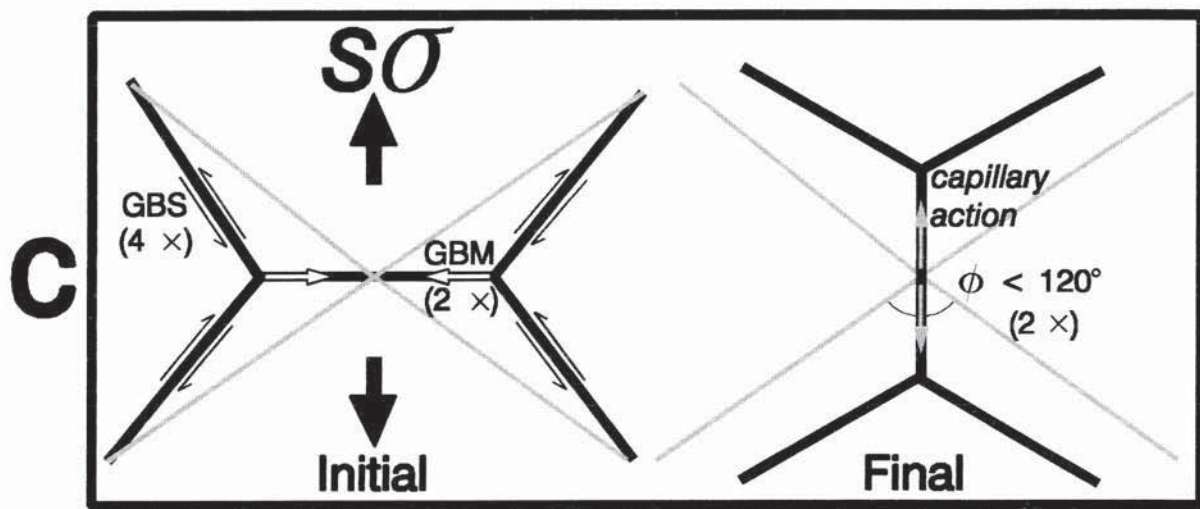
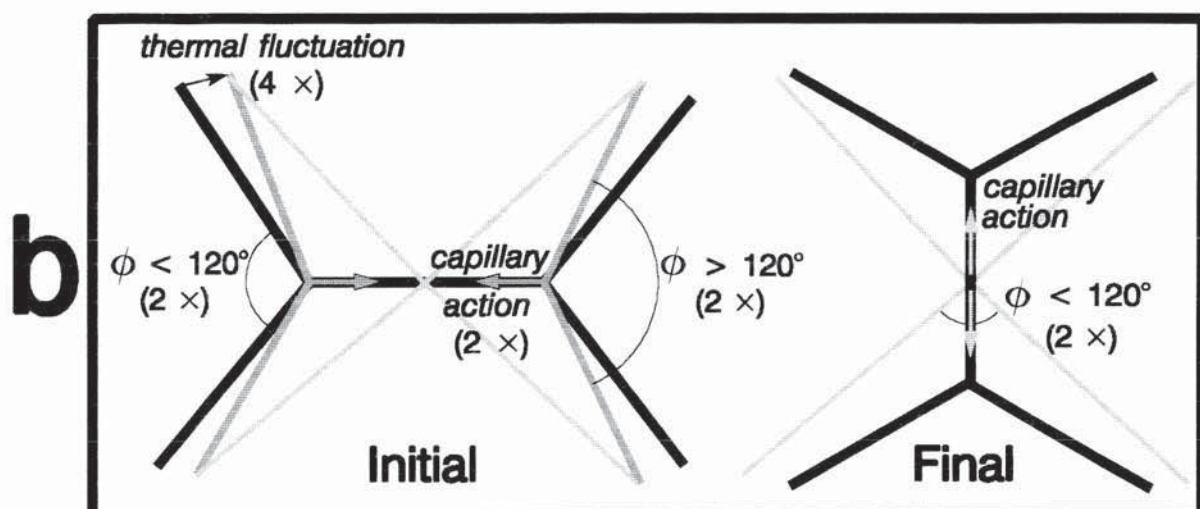
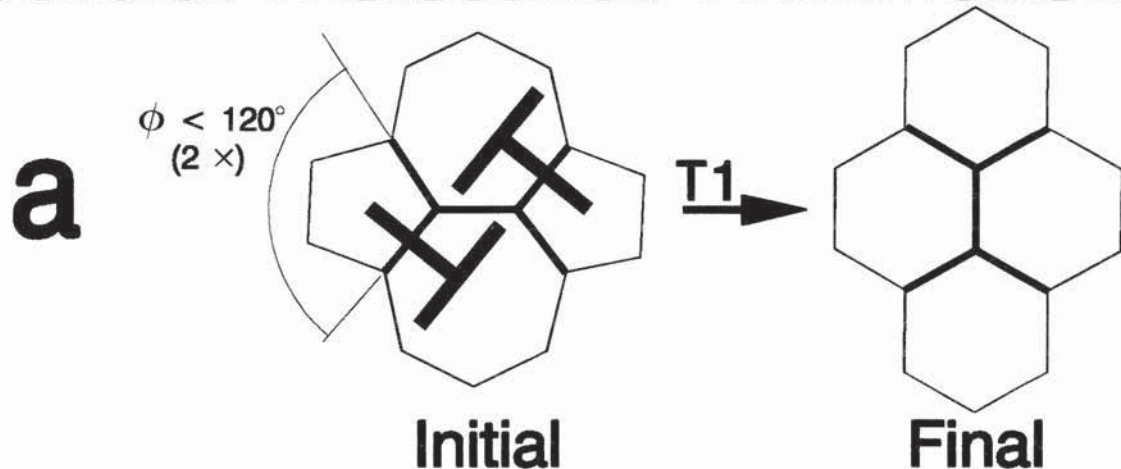


Figure 45. Stress-Driven Cellular Dislocation Climb (Sato *et al.* 1990). The "driving force" for grain boundary migration is attributed to "*lattice damage*" (Wilkinson and Cáceres 1984), or *triple-point strain concentration* (Ishida *et al.* 1965) from grain boundary sliding: migration is towards regions adjacent to triple-points where sliding is impeded (Ishida *et al.* 1965), resulting in neighbor switching and cell disappearance. Sliding and migration sequences for neighbor switching are after Ashby and Verrall (1973) and Ishida *et al.* (1965) (see their Fig. 8b and Fig. 10b). **a)** The first neighbor switching (T1) reaction: Cell boundaries shown in bold respond to the applied stress σ by sliding. Triple point convergence, configurations i - iv, migration occurs through areas "damaged" by sliding; triple-point separation, configurations v - vi, migration occurs through remaining "damaged" areas. **b)** The second neighbor switching reaction: Cell boundaries shown in bold (correcting the error in Fig. 3c from Sherwood and Hamilton (1992)) respond to the resolved stress, $\tau \approx \frac{1}{2}\sigma$, by sliding. Triple point convergence, configurations i - iv, migration occurs through areas "damaged" by sliding; triple-point separation, configurations v - vi, migration occurs through remaining "damaged" areas. **c)** Cell disappearance (T2) reaction: configuration *i* \rightarrow configuration *ii* when cell number 3 disappears, and the cellular dislocation reappears translated from its original position. 3-sided cells are unstable, capillary action can therefore complete stress-driven cellular dislocation climb. If, however, the applied stress again induces boundary sliding at the 3-sided cell, resulting in "lattice damage," boundary migration and cell disappearance are "accelerated," configuration *iii*. Ishida *et al.* (1965) suggest this migration sequence as a response to triple-point strain concentration from grain boundary sliding during creep deformation; see their Fig. 10a.

Figure 45 (Continued).

First T1 Reaction for Stress-Driven Cellular Dislocation Climb

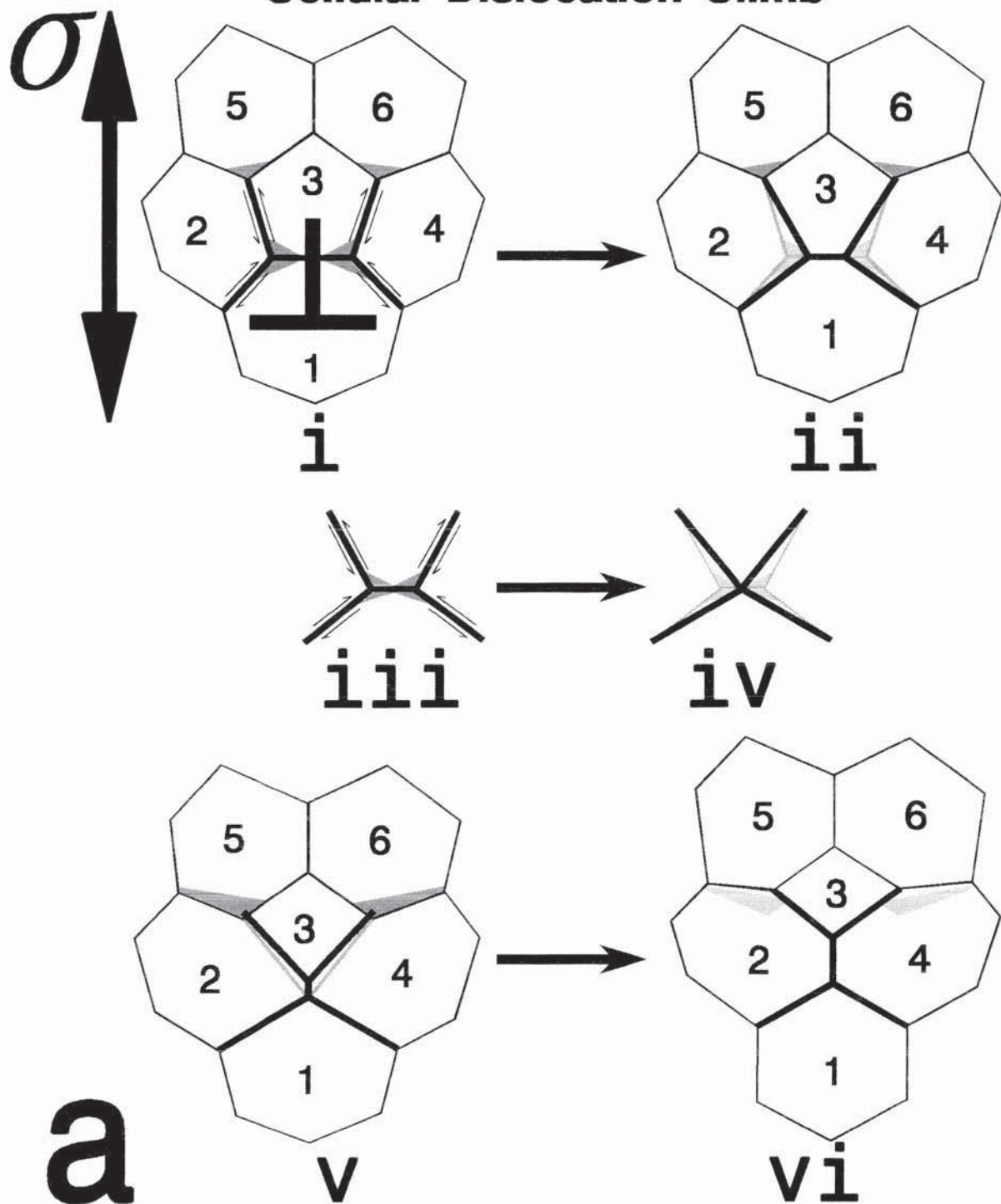


Figure 45 (Continued).

Second T1 Reaction for Stress-Driven Cellular Dislocation Climb

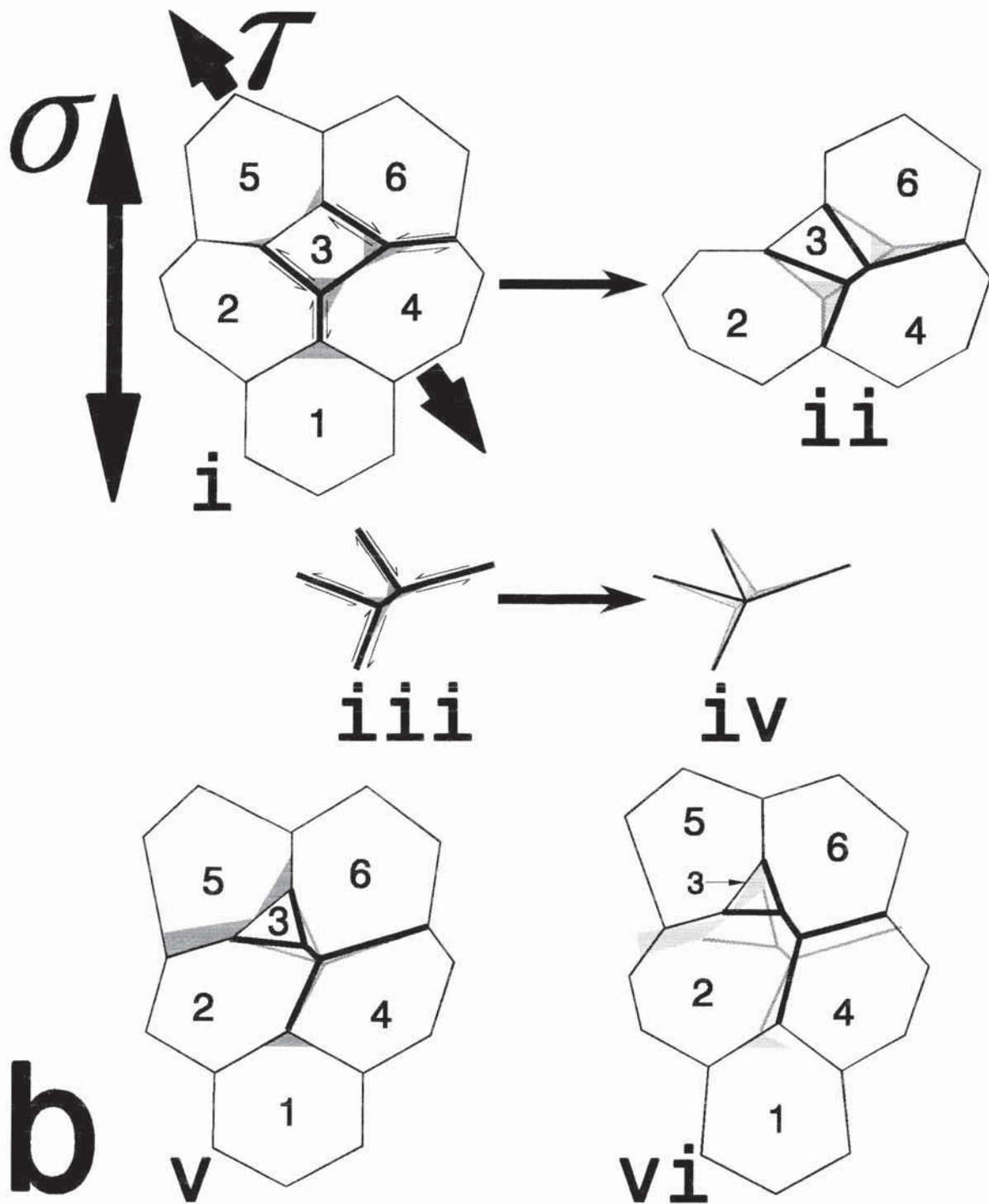


Figure 45 (Continued).

T2 Reaction for Stress-Driven Cellular Dislocation Climb

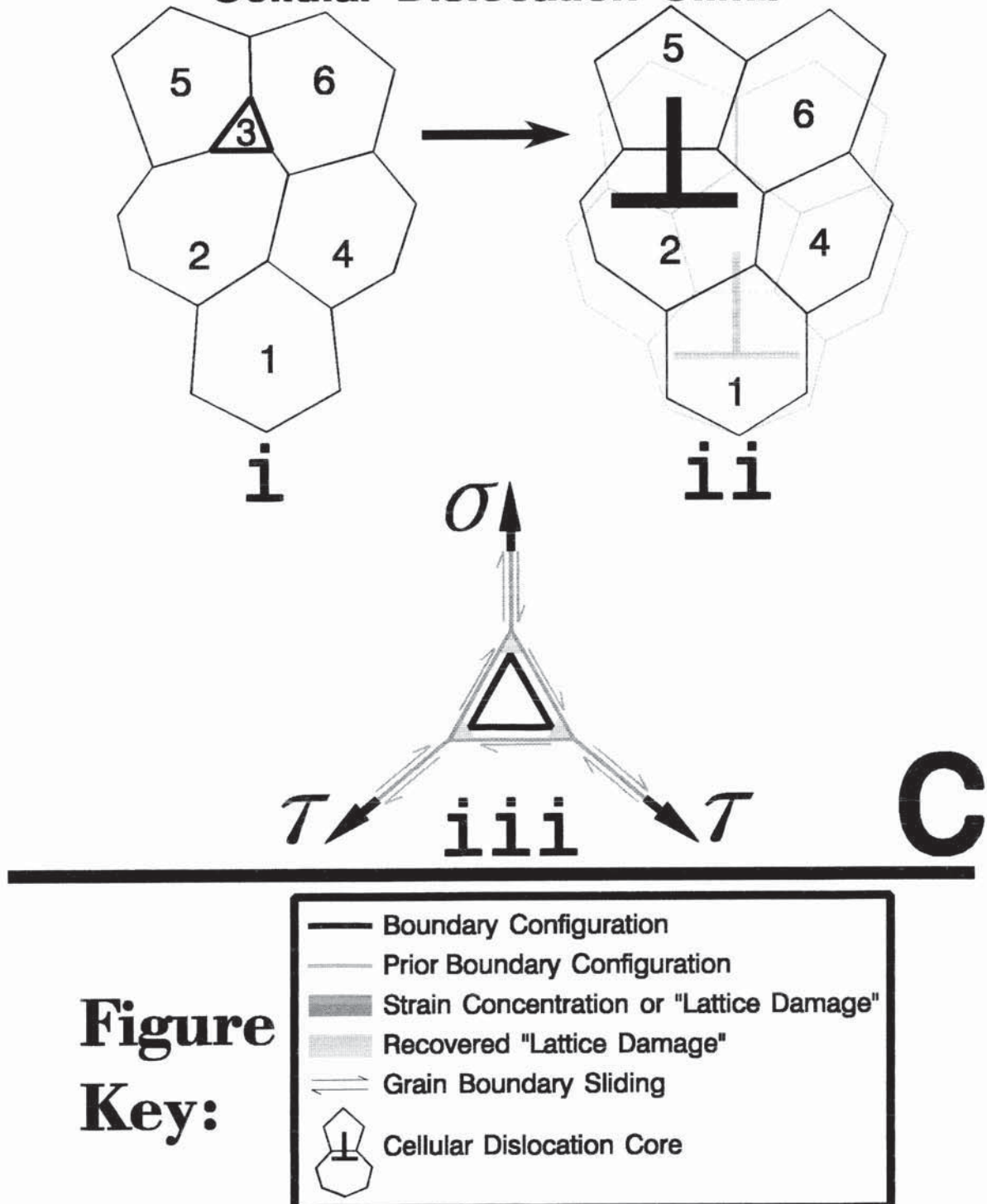


Figure 46. **a)** Model of superplastic flow via stress-driven cellular dislocation climb (Sherwood and Hamilton 1994)—a complexion. The array contains one dislocation for every four cells, $X_d(\varepsilon = 0) = 1/2$. Superplastic flow results from the elementary reactions required for climb. Initial state: 96 cells and 24 dislocations. Final state: 72 cells and 24 dislocations, $X_d = 2/3$, $d/d_0 = 1.15$, $\varepsilon \approx 0.5$. Note that the array must be wrapped into a tube in order to see six dislocations. **b)** Stress-driven cellular dislocation climb is analogous to Hillert's (1965) grain growth "reaction:" here, the applied stress, appropriately resolved, supplants capillary action for the elementary reactions shown by Figure 39. **i.** The initial state. The resolved stress $\mathcal{T} = s\sigma \approx 1/2\sigma$ causes grain boundary sliding/migration in the bold cell edges and the first T1 reaction. **ii.** The final state. The dislocation translates in the direction of the applied stress. **iii.** Analysis of "unit cells" shown on 'a' and 'b': the unit "cell" is strained by an amount $\varepsilon_c = 0.7$.

Figure 46 (Continued).

Superplastic Flow from Cellular Dislocation Climb

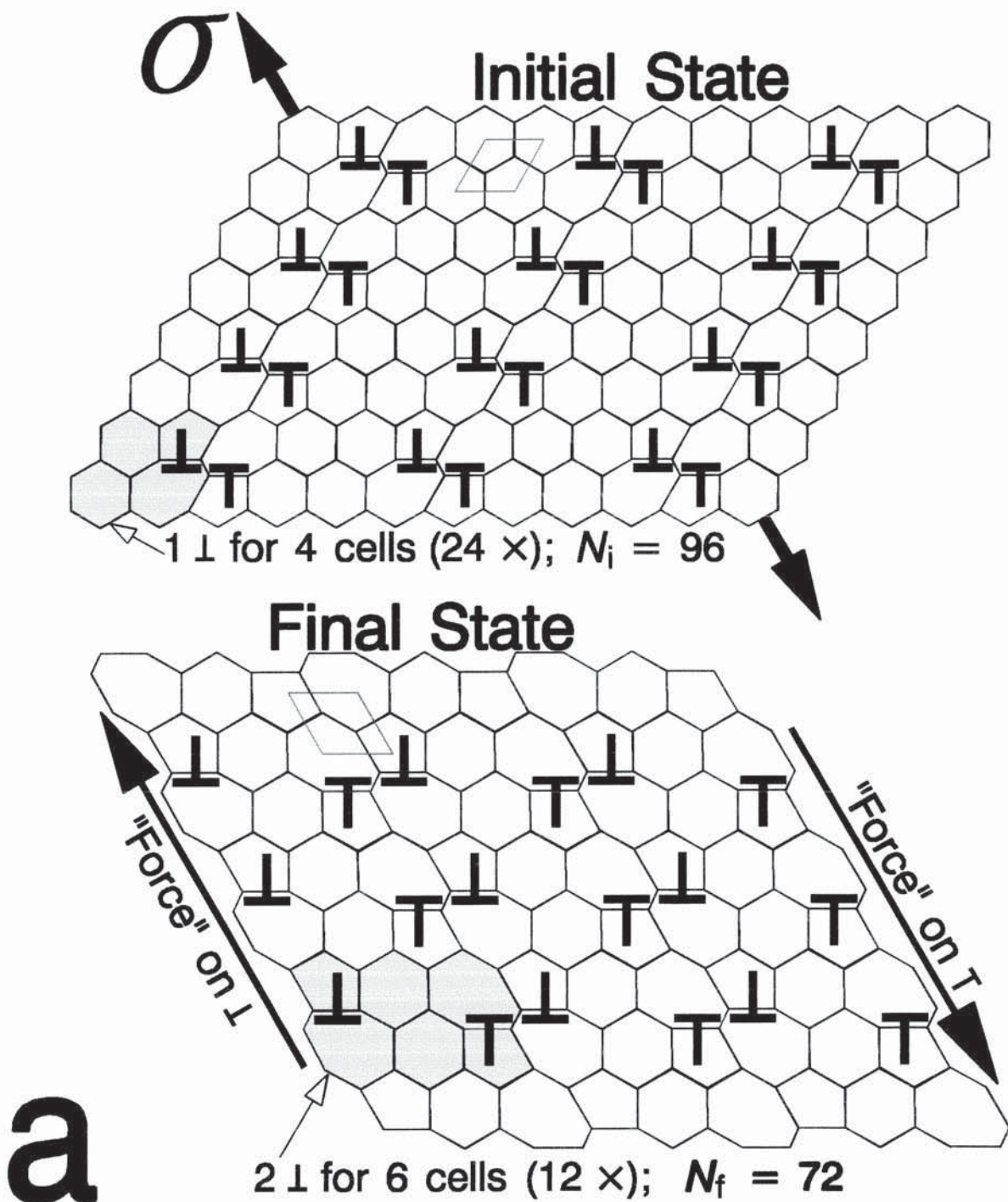


Figure 46 (Continued).

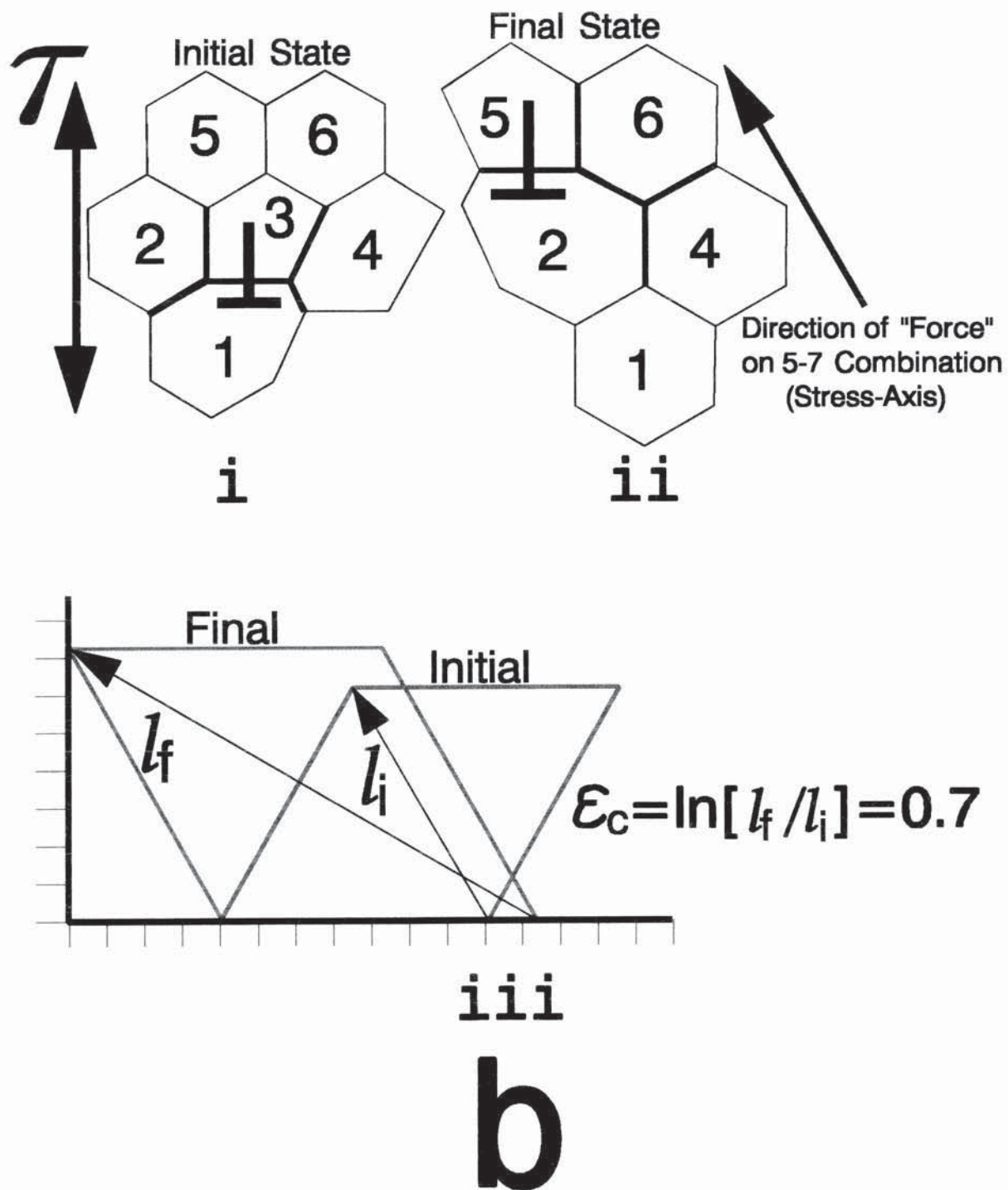


Figure 47. Grain growth of a Sn-1% Bi alloy (Clark and Alden 1973) annealed and deformed at 20 °C is predicted with equation (27) (Sherwood and Hamilton 1994). For this single phase material the initial grain size is $d_0 = 1.8 \mu\text{m}$. Clark and Alden reported $a = 0.067 \mu\text{m}/\text{min}^{1/2}$ for $a^2 = (4/3)M_B\Gamma X_d^0 = M_B\Gamma$, which obtains for $X_d^0 = 3/4$. For deformation-enhanced grain growth, $K = 6.80 \times 10^{-6}$, $\tau = 1.0 \text{ min}$, and $\kappa = 1$ are assumed; therefore, $K\tau = 6.8 \times 10^{-6} \text{ min}$, or $K\tau = 4.08 \times 10^{-4} \text{ s}$. The values K and τ for "excess" cellular dislocations differ from the values $k_1 = 4.1 \times 10^{-3}$ and $k_2 \equiv \tau^{-1} = 10^3/\text{min}$ that Clark and Alden reported for "excess" vacancies; but note that $\tau = 10^{-3} \text{ min}$ seems to be too short for "excess" cellular dislocations, since grain boundary migration is required for their annihilation. The longer value, $\tau = 1 \text{ min}$, improves the fit of the data at the highest strain rate, $\dot{\varepsilon} = 1 \text{ min}^{-1}$; otherwise, the correlation shown by this figure is the same as that displayed by Clark and Alden's Fig. 13.

Figure 47 (Continued).

Grain Growth of Sn-1% Bi at 20 °C

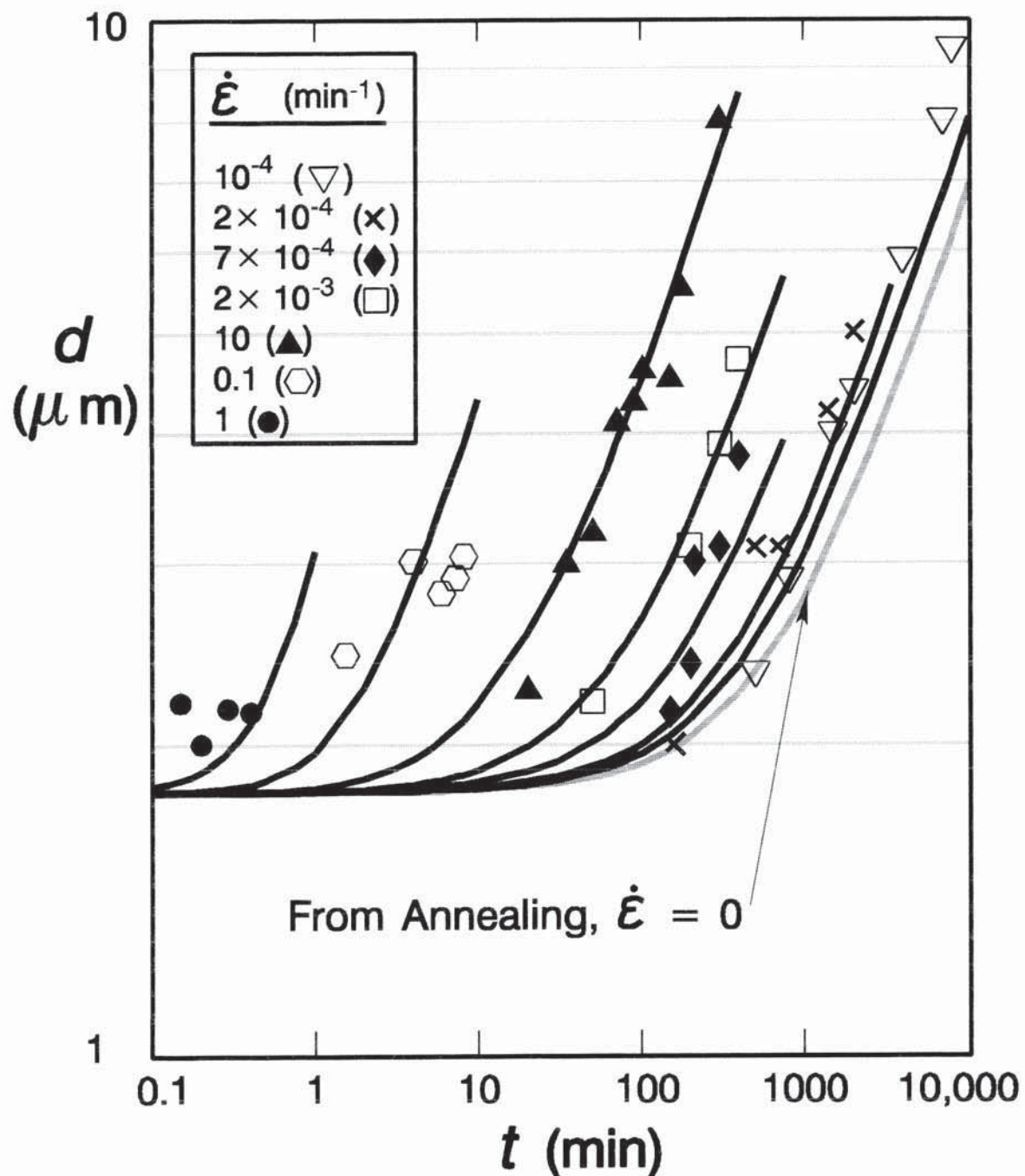


Figure 48. Illustration of grain growth from thermally-activated cellular dislocation climb model, equation (28), with 7475 Al data. **a)** 450 °C. **b)** 475 °C. **c)** 516 °C. **d)** The steady state, "excess" defect level, δX_d^{ss} ,

$$\delta X_d^{ss} = K\tau\kappa \dot{\varepsilon} = 20.2\dot{\varepsilon}^{0.67},$$

where $\dot{\varepsilon}$ is the imposed strain rate, and $\kappa\dot{\varepsilon} = \dot{\varepsilon}_{GBS}$ is the strain rate from grain boundary sliding/migration. The parameters K and τ have the following values:

$$K(450 \text{ } ^\circ\text{C}) = 3.25, K(475 \text{ } ^\circ\text{C}) = 6.17, \text{ and } K(516 \text{ } ^\circ\text{C}) = 16.2;$$

$$\tau(450 \text{ } ^\circ\text{C}) = 216 \text{ s}, \tau(475 \text{ } ^\circ\text{C}) = 96.9 \text{ s}, \text{ and } \tau(516 \text{ } ^\circ\text{C}) = 29.0 \text{ s.}$$

e) Behavior assumed for $\kappa = \kappa(\dot{\varepsilon}, T)$.

Figure 48 (Continued).

Grain Growth of 7475 Al at 450 °C
Thermally-Activated Cellular Dislocation Climb

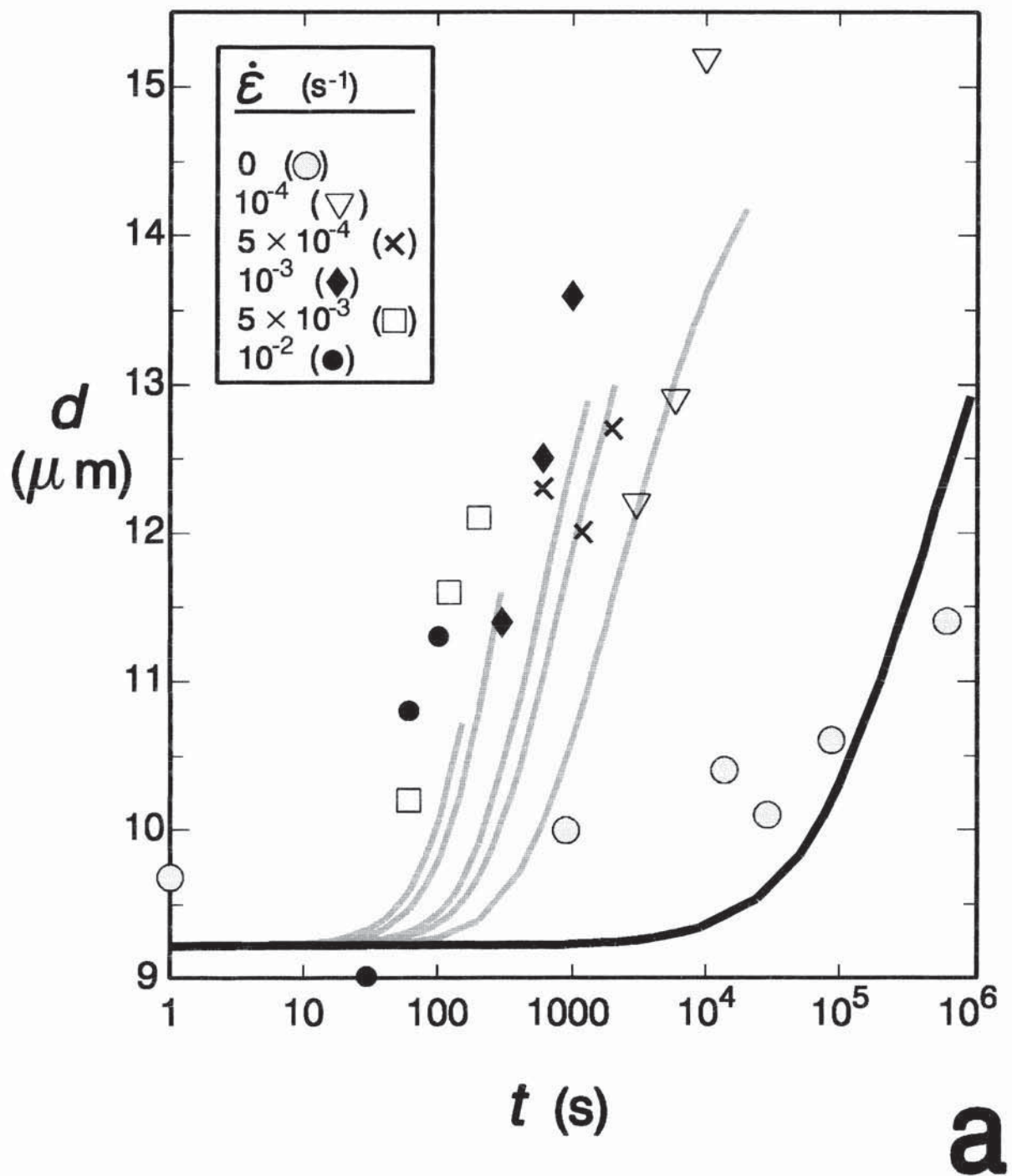


Figure 48 (Continued).

Grain Growth of 7475 Al at 475 °C
Thermally-Activated Cellular Dislocation Climb

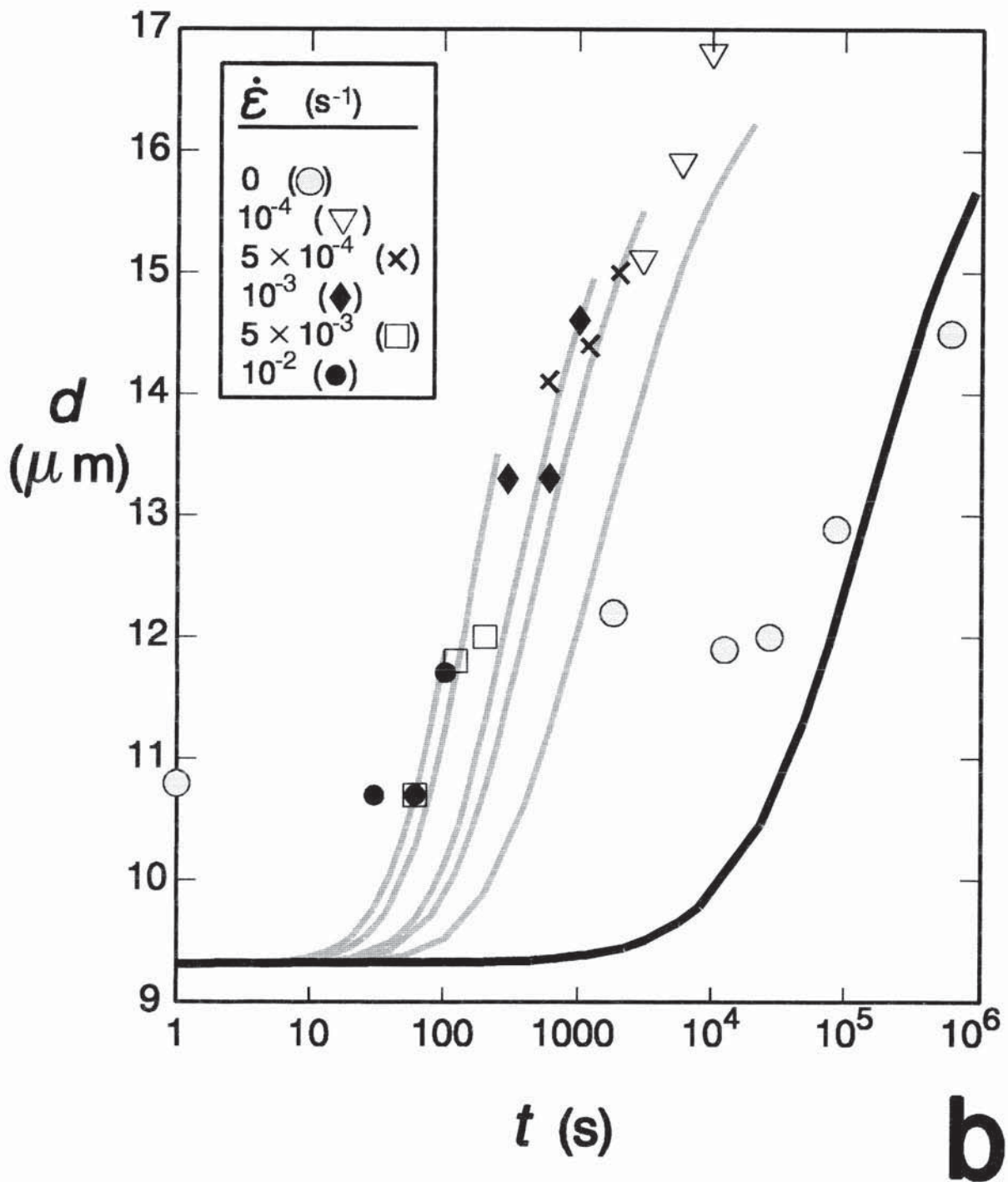


Figure 48 (Continued).

Grain Growth of 7475 Al at 516 °C
Thermally-Activated Cellular Dislocation Climb

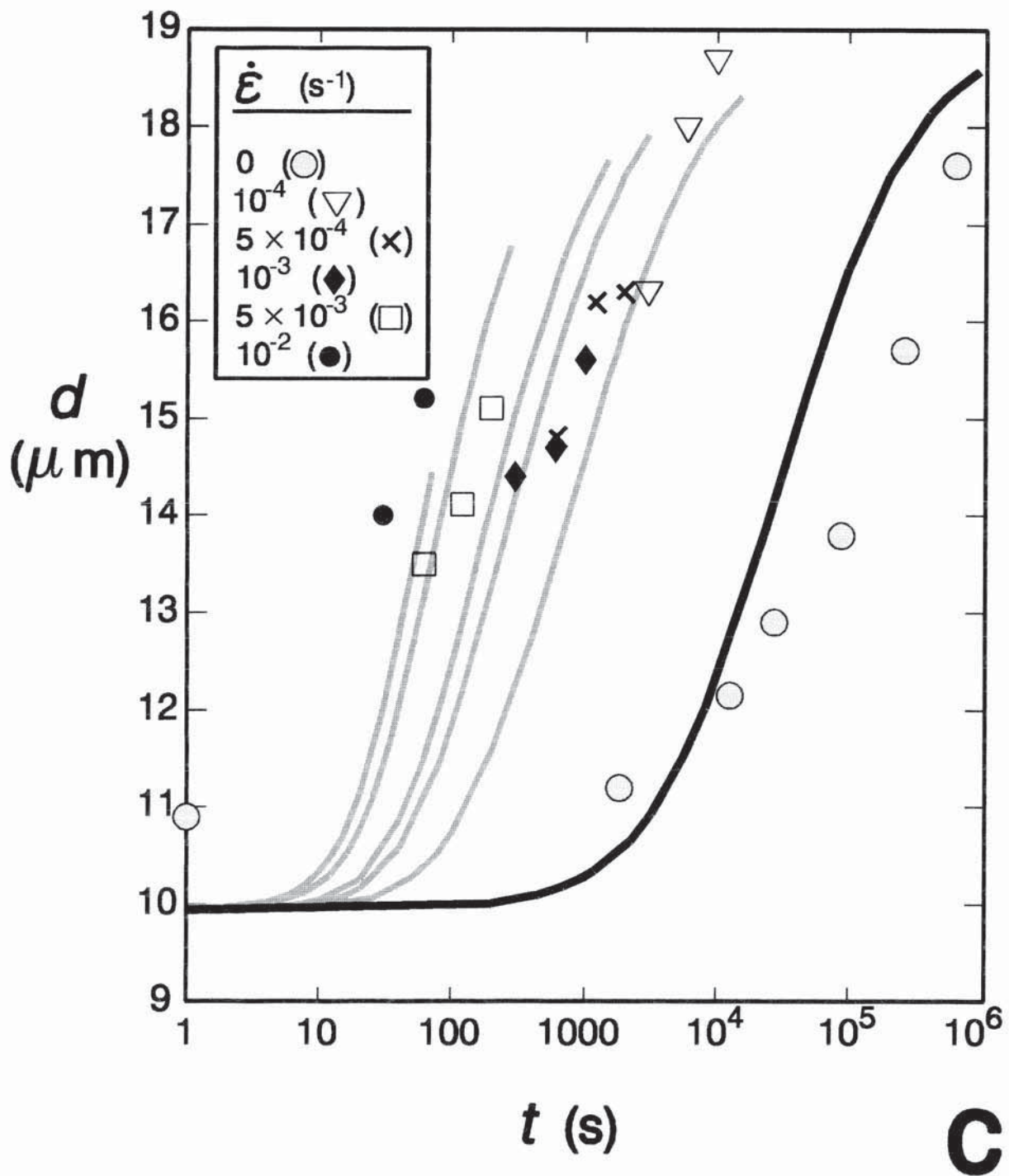


Figure 48 (Continued).

Assumed Level of Excess Defects Thermally-Activated Cellular Dislocation Climb

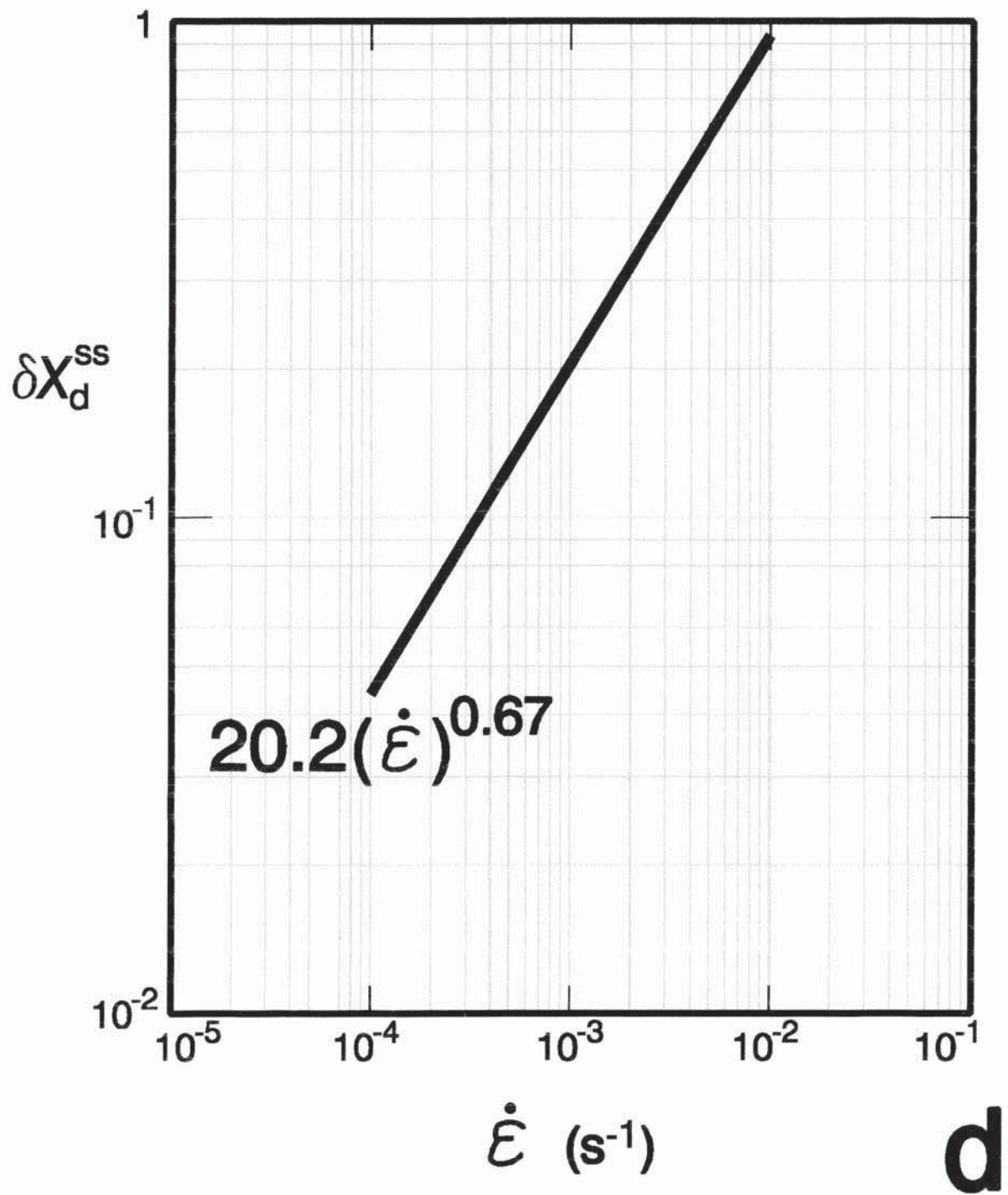


Figure 48 (Continued).

Assumed Behavior of GBS/GBM for 7475 Al Thermally-Activated Cellular Dislocation Climb

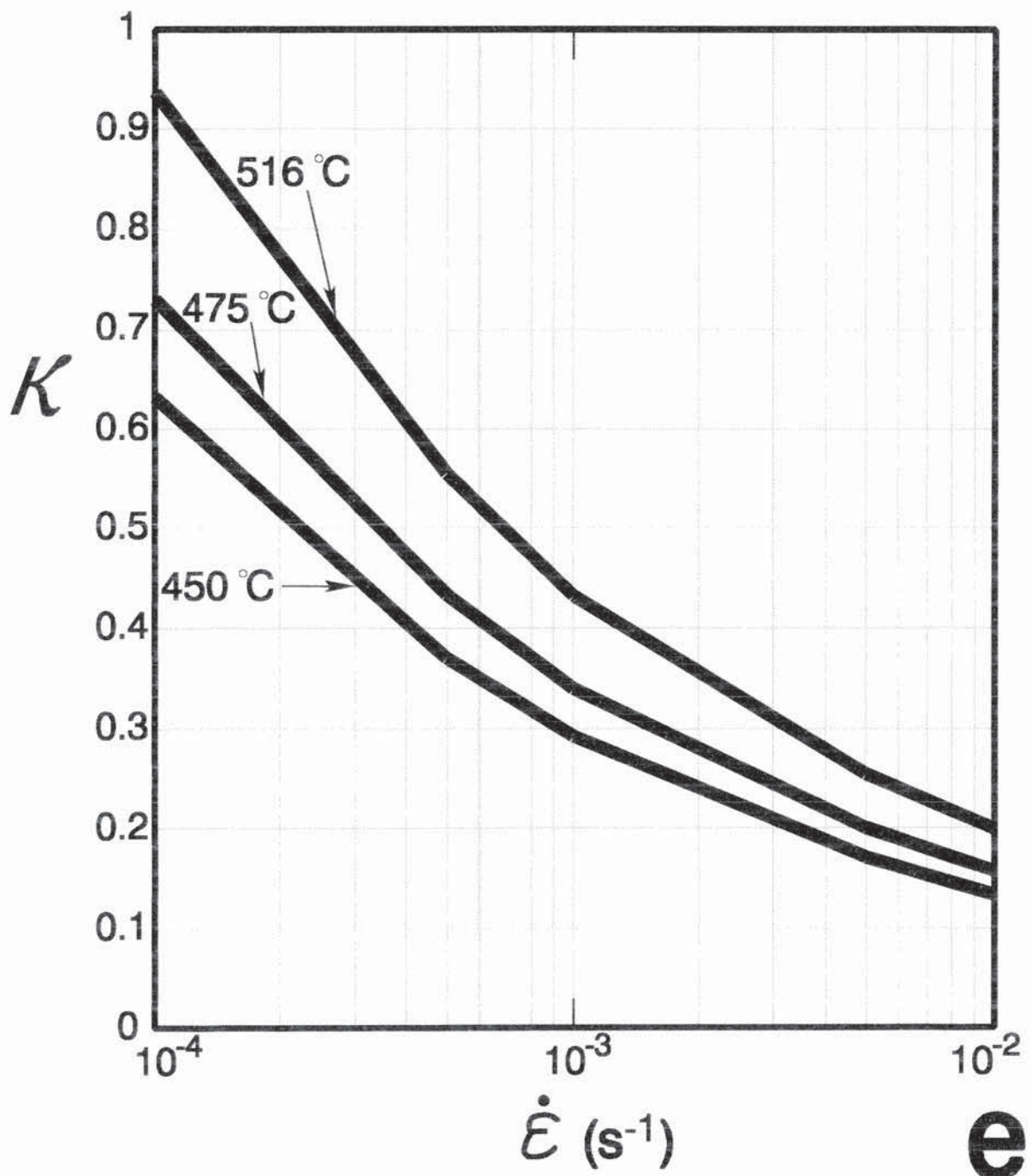


Figure 49. 7475 Al is a quasi-single phase material: grain boundary migration is inhibited by a dispersion of second phase particles. This particle distribution is effective at inhibiting grain growth: even for annealing temperatures above 516 °C the average grain size d only doubles for annealing periods of one week (Sherwood and Hamilton 1993). An interpretation of this observation is that while there are many grains in the microstructure with sufficient curvature for grain boundary migration, as shown by 'a', second phase particles pin the majority of these grains, so that only a few are actually mobile, as shown by part 'b'. As an illustration, let $X_d^0 = 1/1000$. Then only one cellular dislocation amongst two-thousand cells climbs (as in the grain growth "reaction" of Figure 39) through the microstructure at any given time. For an array of 2000 cells initially, a doubled grain size from annealing results in an array with 500 cells: $Nd^2 = \text{constant}$, where N denotes the number of cells in the array (Hillert 1965). For each unit of climb a cell disappears; so to eliminate 1500 cells, a dislocation has to climb a distance of roughly $1500d \approx 15000 \mu\text{m} = 1.5 \text{ cm}$. To do so in one week requires an average dislocation speed of $0.025 \mu\text{m/s}$.

a) Many cells are non-hexagonal and would be available for cellular dislocation climb as in Figure 39; but second phase particles pin all of the boundaries except for those belonging to the two shaded cells. **b)** Since hexagonal cells are immobile in a theory of grain boundary migration based on capillarity, the cellular array from part 'a' can be modelled as a hexagonal array with a single cellular dislocation. This dislocation can climb as in Figure 39.

Figure 49 (Continued).

Assumption for Thermally-Activated Cellular Dislocation Climb Model of Grain Growth as Applied to 7475 Al

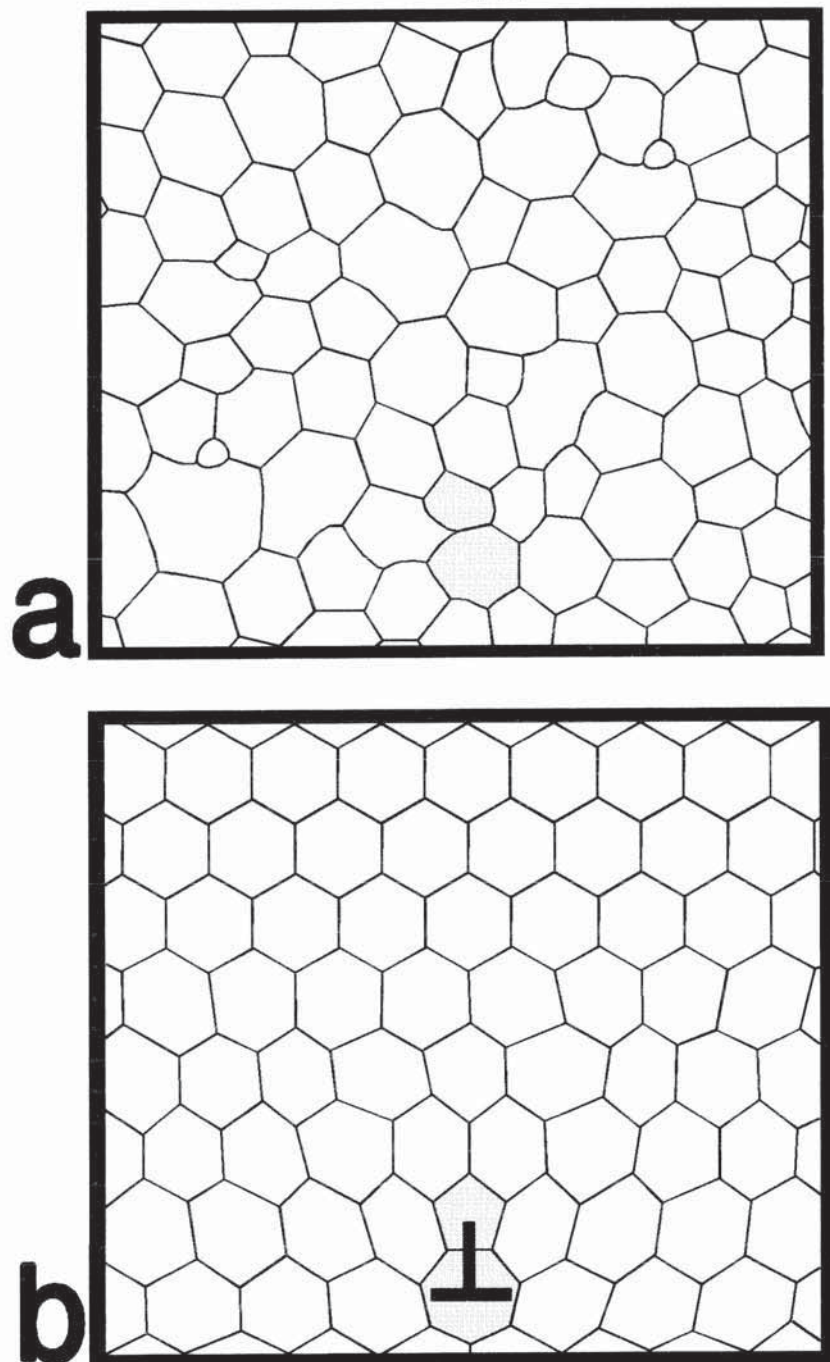


Figure 50. Illustration of deformation-enhanced grain growth from stress-driven cellular dislocation climb model, equation (30), with $\lambda = 0.6\kappa$, using 7475 Al data. In the as-received condition, 7475 Al has a grain size of $d_0 = 9.2 \mu\text{m}$. Initial grain sizes listed here, $d_0 = d(\varepsilon = 0)$, were determined from specimens subjected to the thermal cycle of the test. Curves for annealing are from an empirical fit of the data (Sherwood and Hamilton 1993).

a) 450°C , $d_0 = 9.3 \mu\text{m}$. **b)** 475°C , $d_0 = 10.7 \mu\text{m}$. **c)** 516°C , $d_0 = 10.6 \mu\text{m}$.

d) Behavior assumed for $\kappa = \kappa(\dot{\varepsilon}, T) \equiv \dot{\varepsilon}_{\text{GBS}}(T)/\dot{\varepsilon}$ to reproduce prior curves.

Figure 50 (Continued).

Grain Growth of 7475 Al at 450 °C Stress-Driven Cellular Dislocation Climb

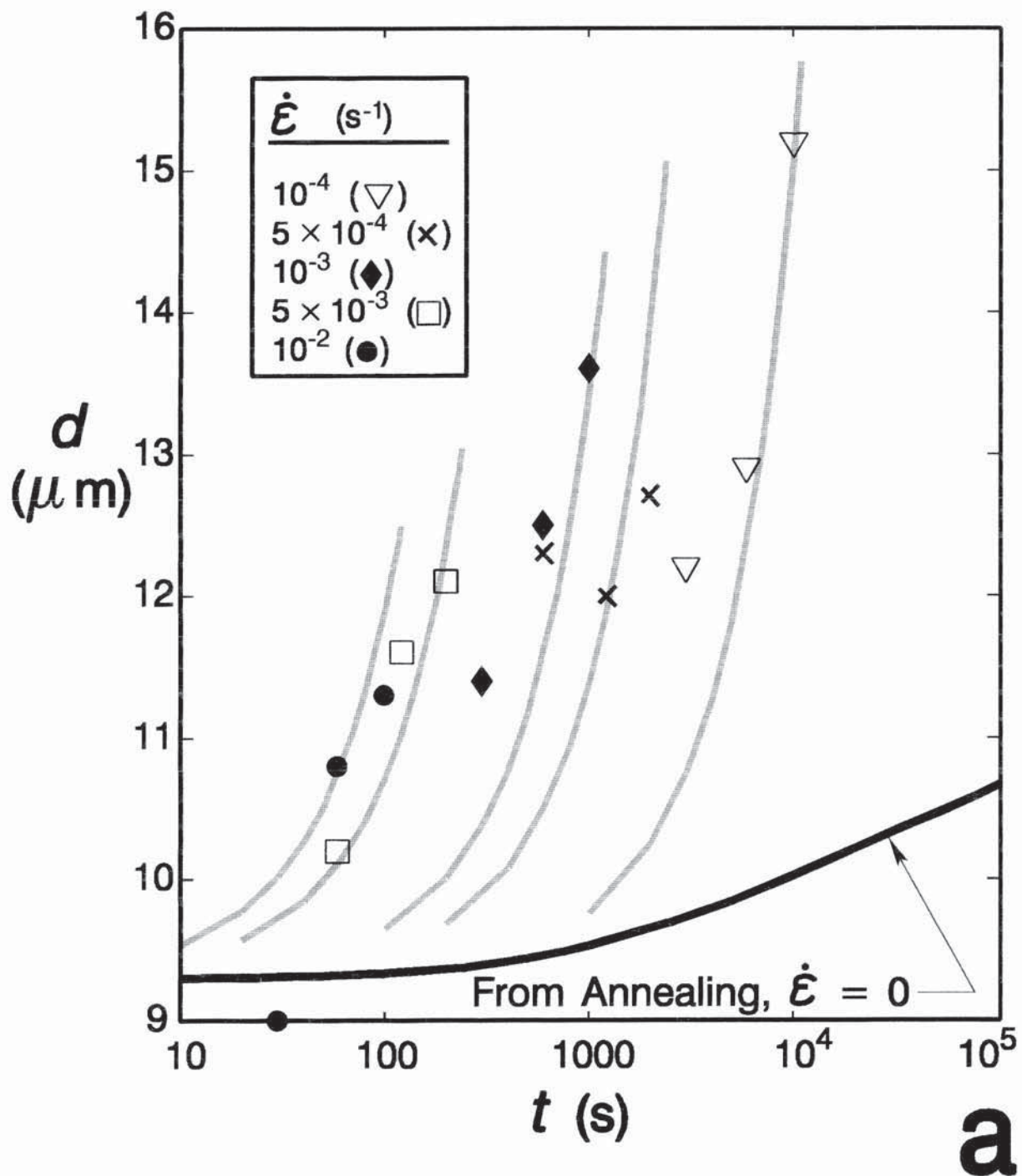


Figure 50 (Continued).

Grain Growth of 7475 Al at 475 °C Stress-Driven Cellular Dislocation Climb

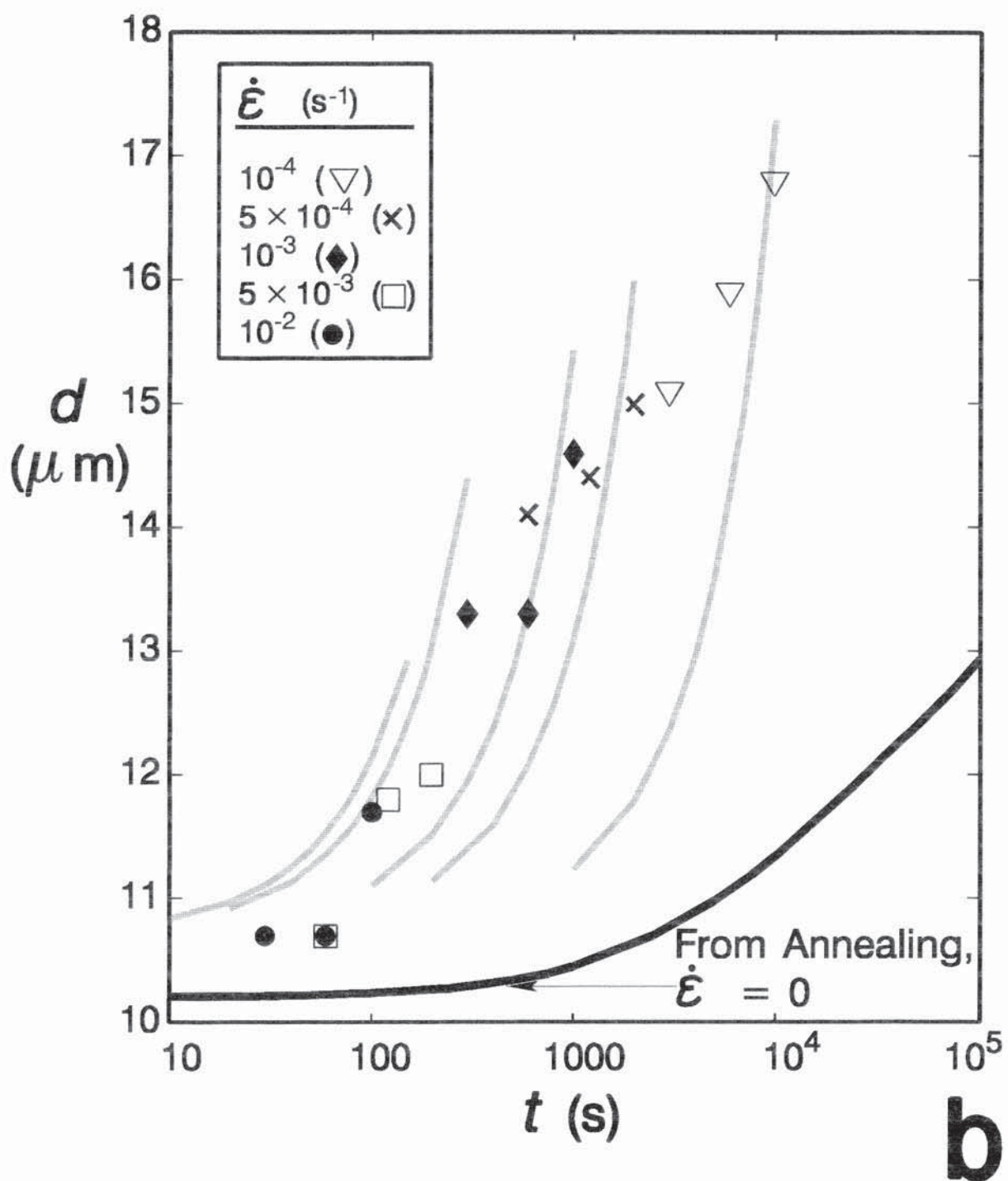


Figure 50 (Continued).

Grain Growth of 7475 Al at 516 °C Stress-Driven Cellular Dislocation Climb

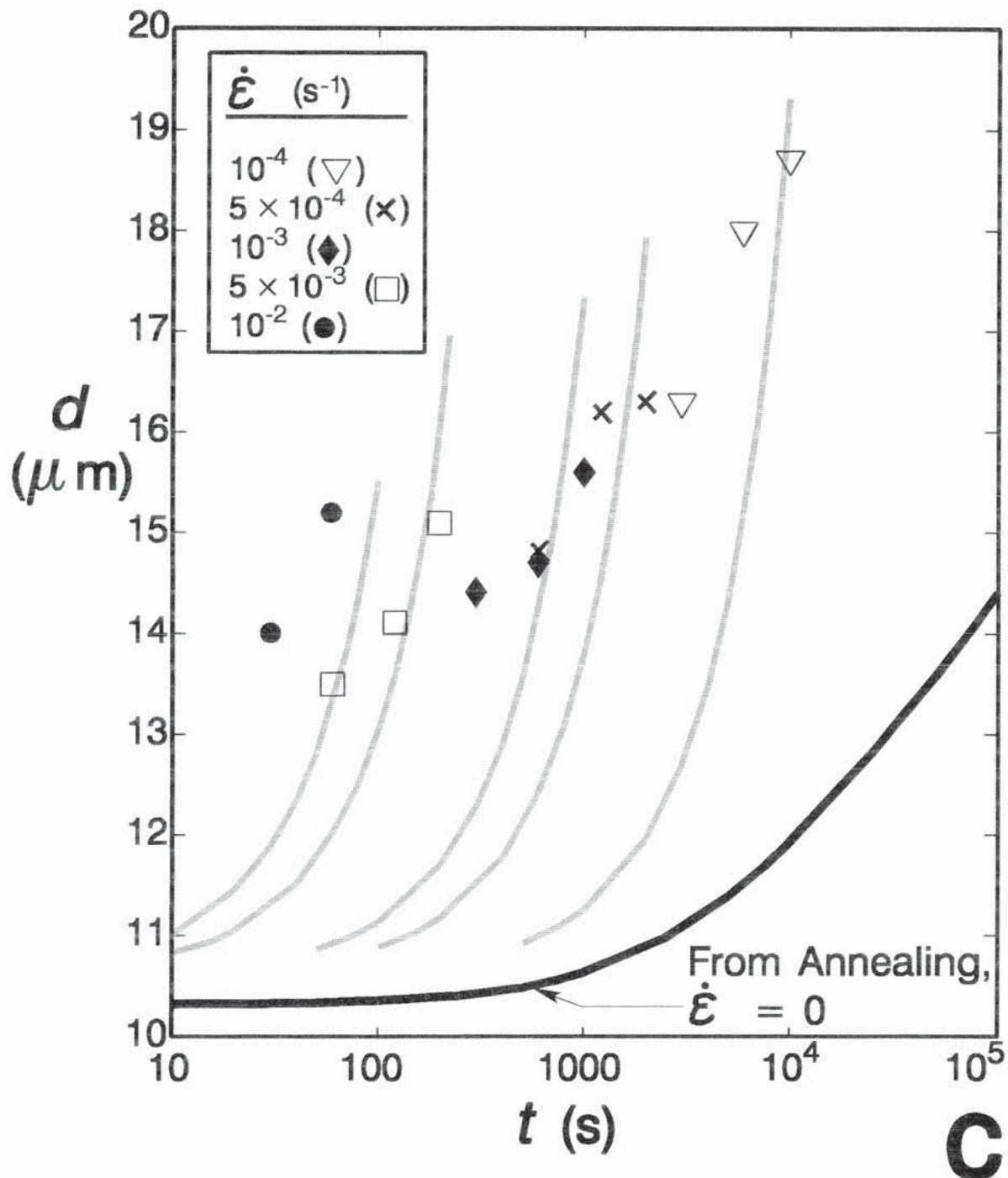


Figure 50 (Continued).

Assumed Behavior of GBS/GBM for 7475 Al Stress-Driven Cellular Dislocation Climb

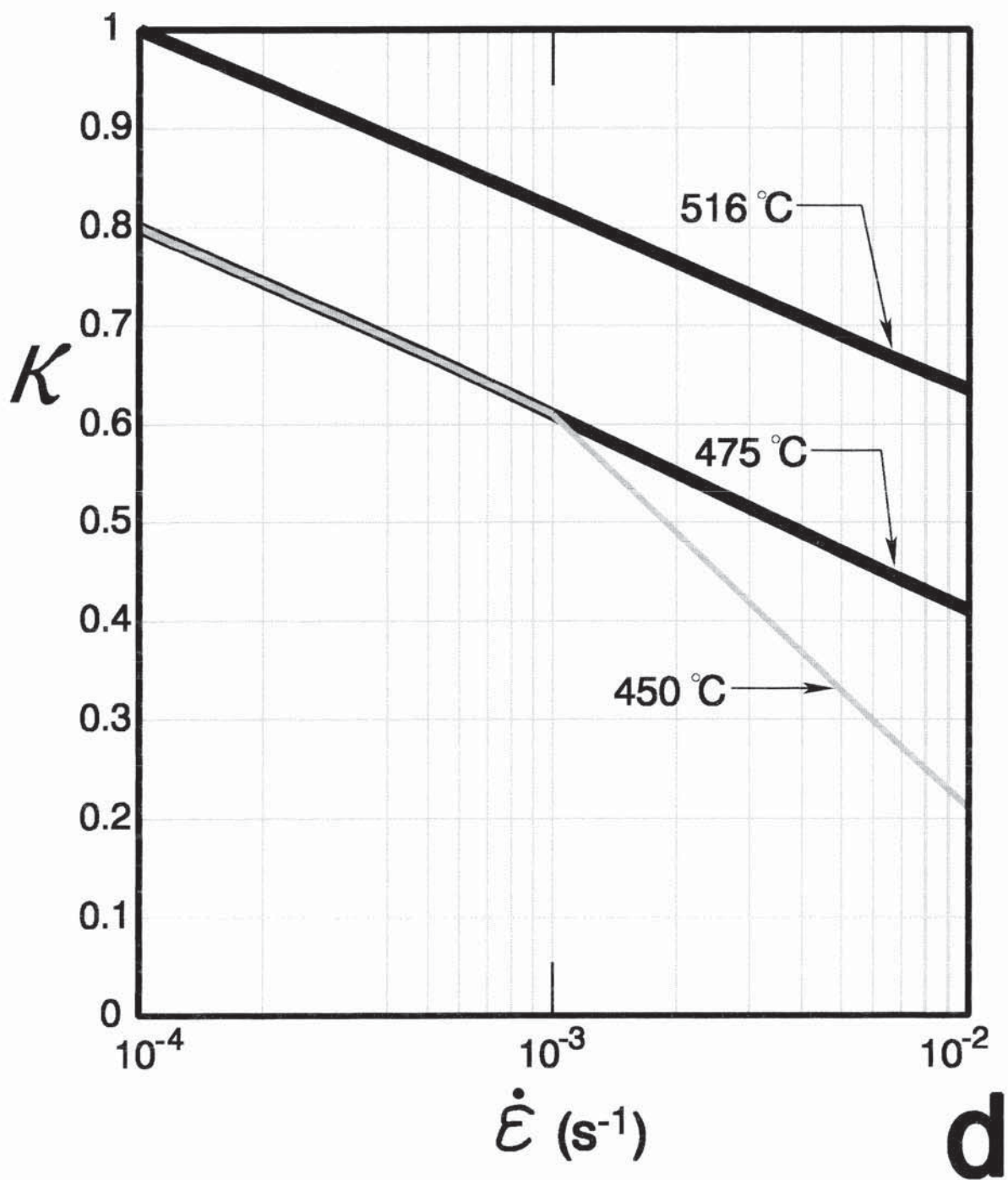


Figure 51. Application of equation (20) to Sn-1% Bi data from Clark and Alden (1973) and 7475 Al data from Hamilton *et al.* (1982).

$$\text{Sn-1% Bi: } A = 1.75 \times 10^8 \quad M_B(20^\circ\text{C}) = 4.48 \times 10^{-17} \text{ m}^4/\text{J-s};$$

$$\begin{aligned} \text{7475 Al: } A &= 2.50 \times 10^5 & M_B(450^\circ\text{C}) &= 1.62 \times 10^{-11} \text{ m}^4/\text{J-s}, \\ && M_B(475^\circ\text{C}) &= 2.66 \times 10^{-11} \text{ m}^4/\text{J-s}, \\ && M_B(516^\circ\text{C}) &= 5.64 \times 10^{-11} \text{ m}^4/\text{J-s}. \end{aligned}$$

a) $\dot{\varepsilon} = \dot{\varepsilon}(\sigma, T = 20^\circ\text{C})$ for Sn-1% Bi; $m = 0.4$ for lower strain rates. **b)** Behavior required for mobile cellular dislocation density, ρ , to generate prior curve:

$$\dot{\varepsilon} = 10^a \rho^b,$$

where $a = 3.17$ and $b = 3.09$ for lower strain rates, and $a = -0.6$ and $b = 1.25$ for higher strain rates. $\rho = 0.77X_d/d^2$, with

$$d = d(\varepsilon = 0.4, \dot{\varepsilon}) = 20, 14, 10, 6, 5.3, 4.2, 1.8, 3.0, 2.0, 2.0, 2.0, \text{ and } 2.0 \mu\text{m},$$

from low to high strain rates, taken from Clark and Alden's Fig.'s 4 and 5. **c)** $\dot{\varepsilon} = \dot{\varepsilon}(\sigma, T)$ for 7475 Al, $T = 516, 482, 427$ and 371°C ;

$$m(371^\circ\text{C}) = 0.3, m(427^\circ\text{C}) = 0.5, m(482^\circ\text{C}) = 0.7, \text{ and } m(516^\circ\text{C}) = 1,$$

all for lower strain rates. **d)** Behavior required of ρ to generate prior curves, $\rho = \rho(\dot{\varepsilon}, T)$.

e) $d = d(\dot{\varepsilon})$ assumed for 7475 Al to generate prior curves, for $\varepsilon \approx 0.2 - 0.3$, typical of strain rate jump tests.

Figure 51 (Continued).

Sn-1% Bi

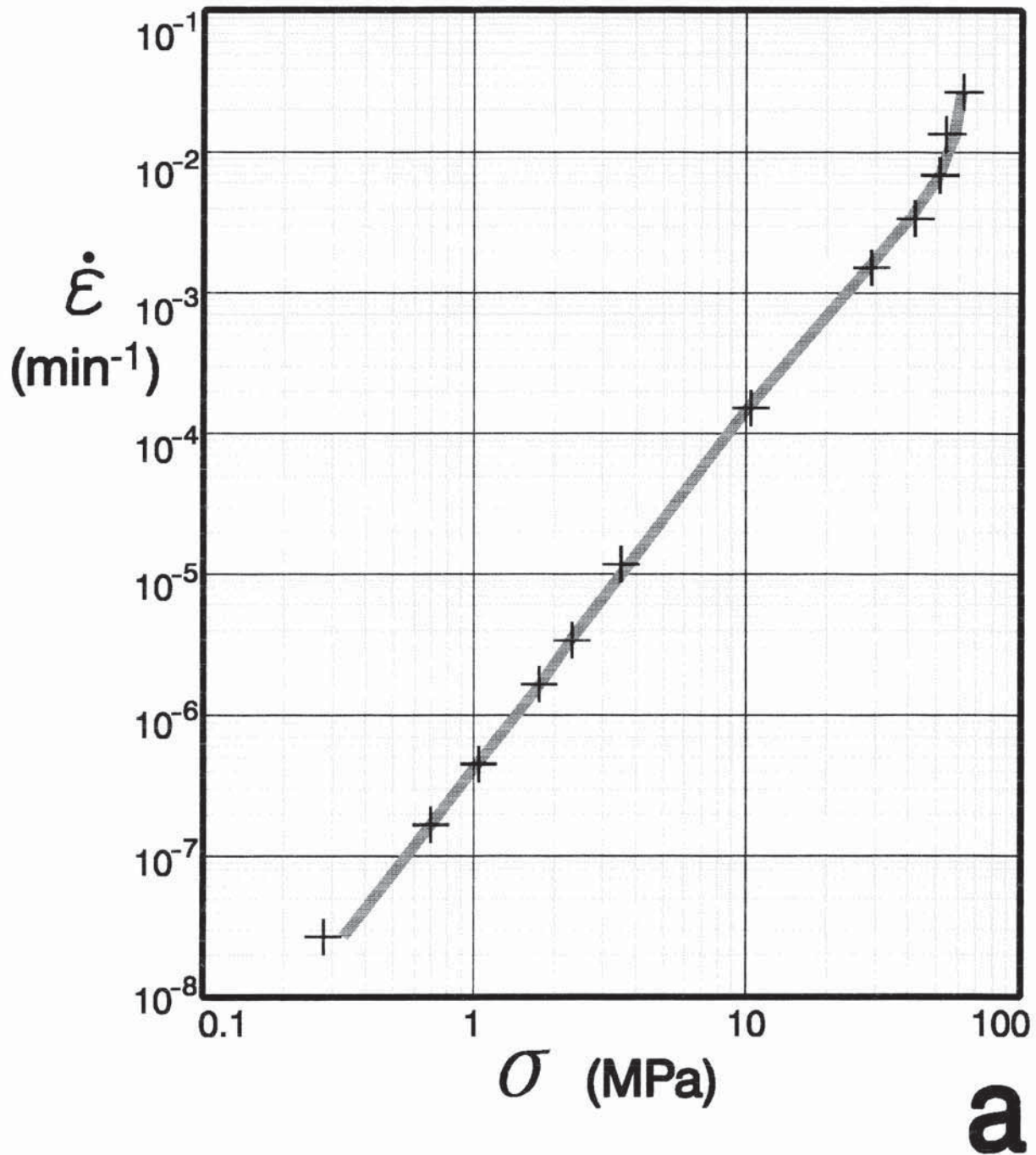


Figure 51 (Continued).

Mobile Cellular Dislocation Density Sn-1% Bi

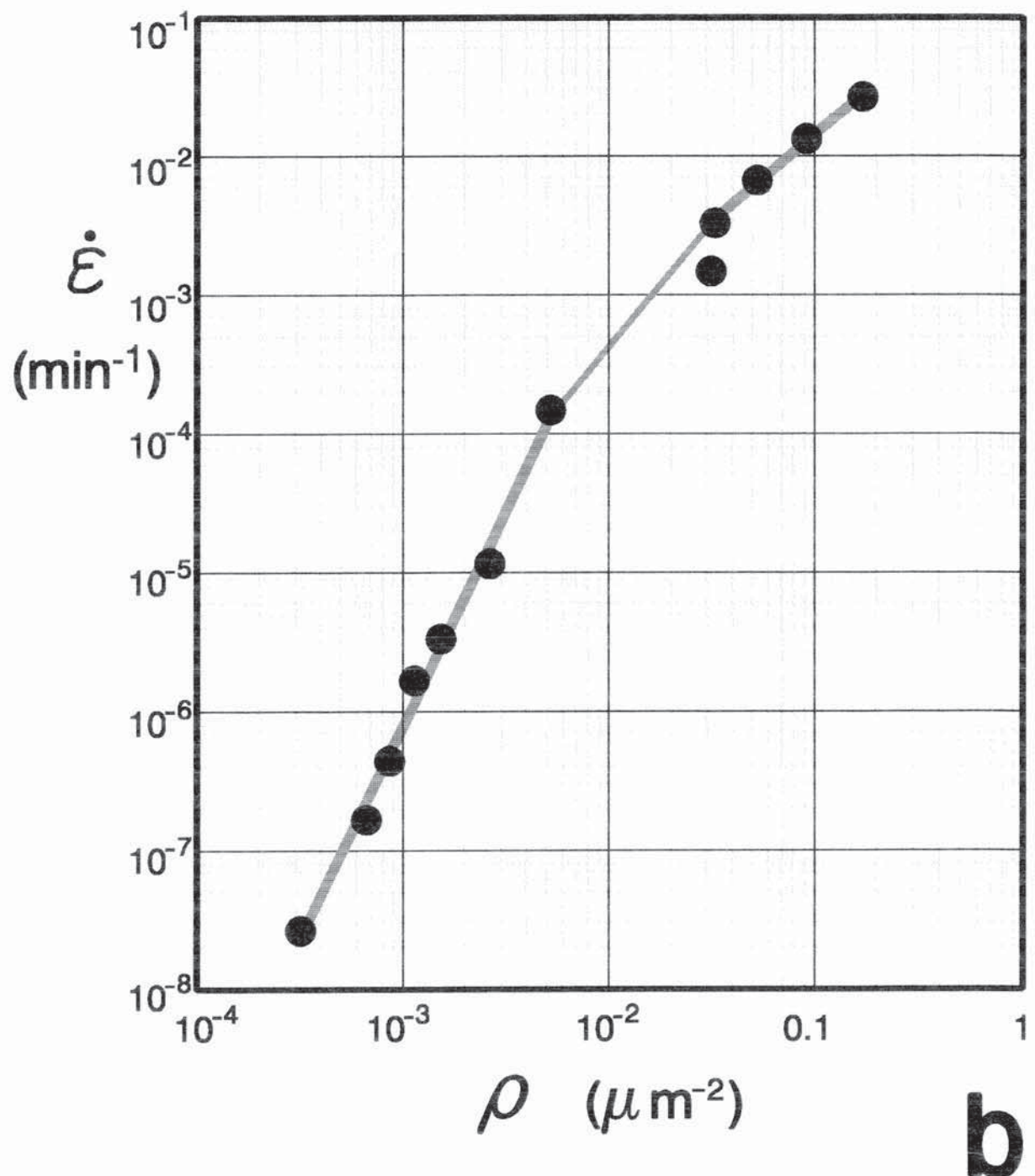


Figure 51 (Continued).

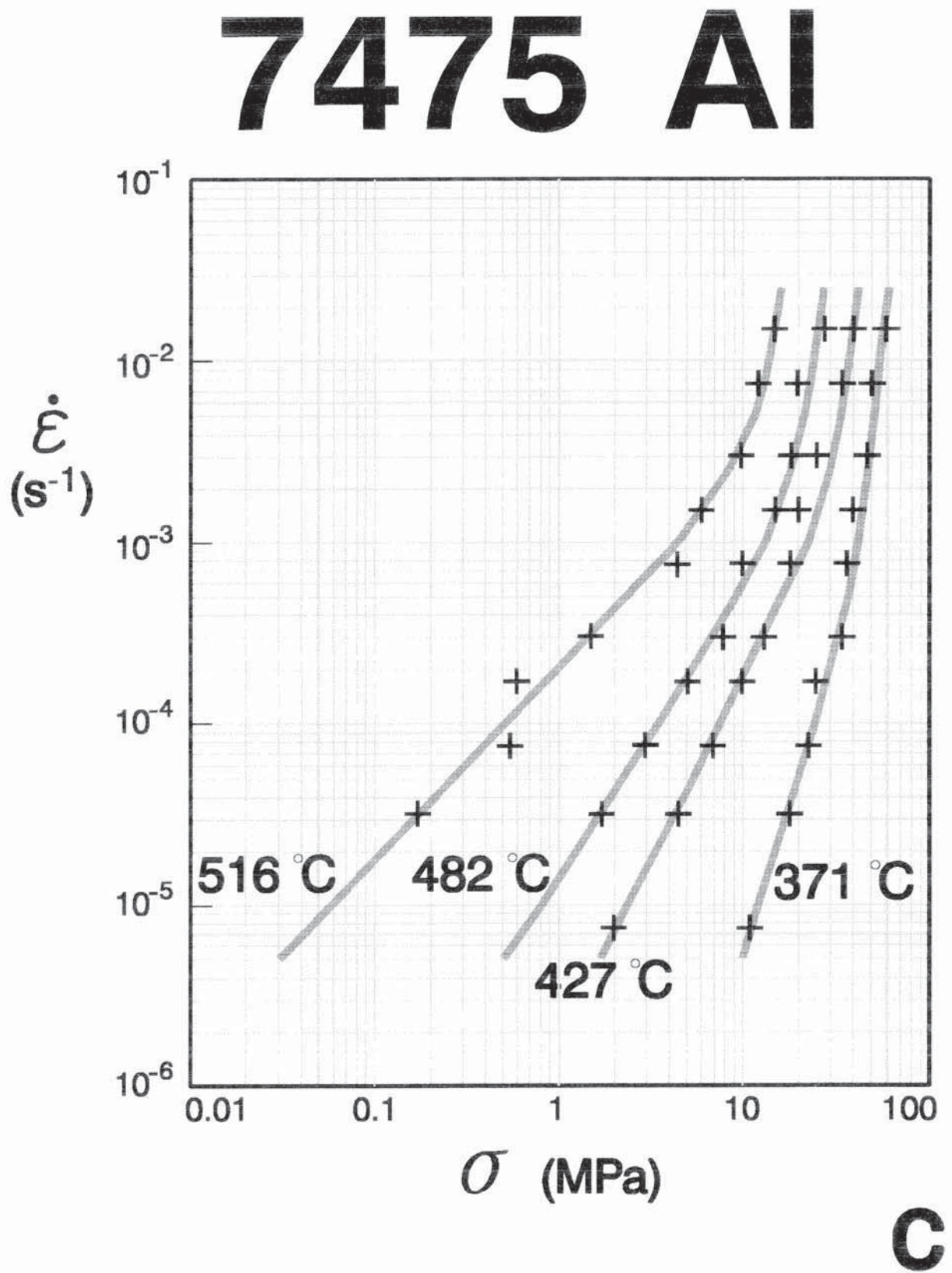


Figure 51 (Continued).

Mobile Cellular Dislocation Density 7475 Al

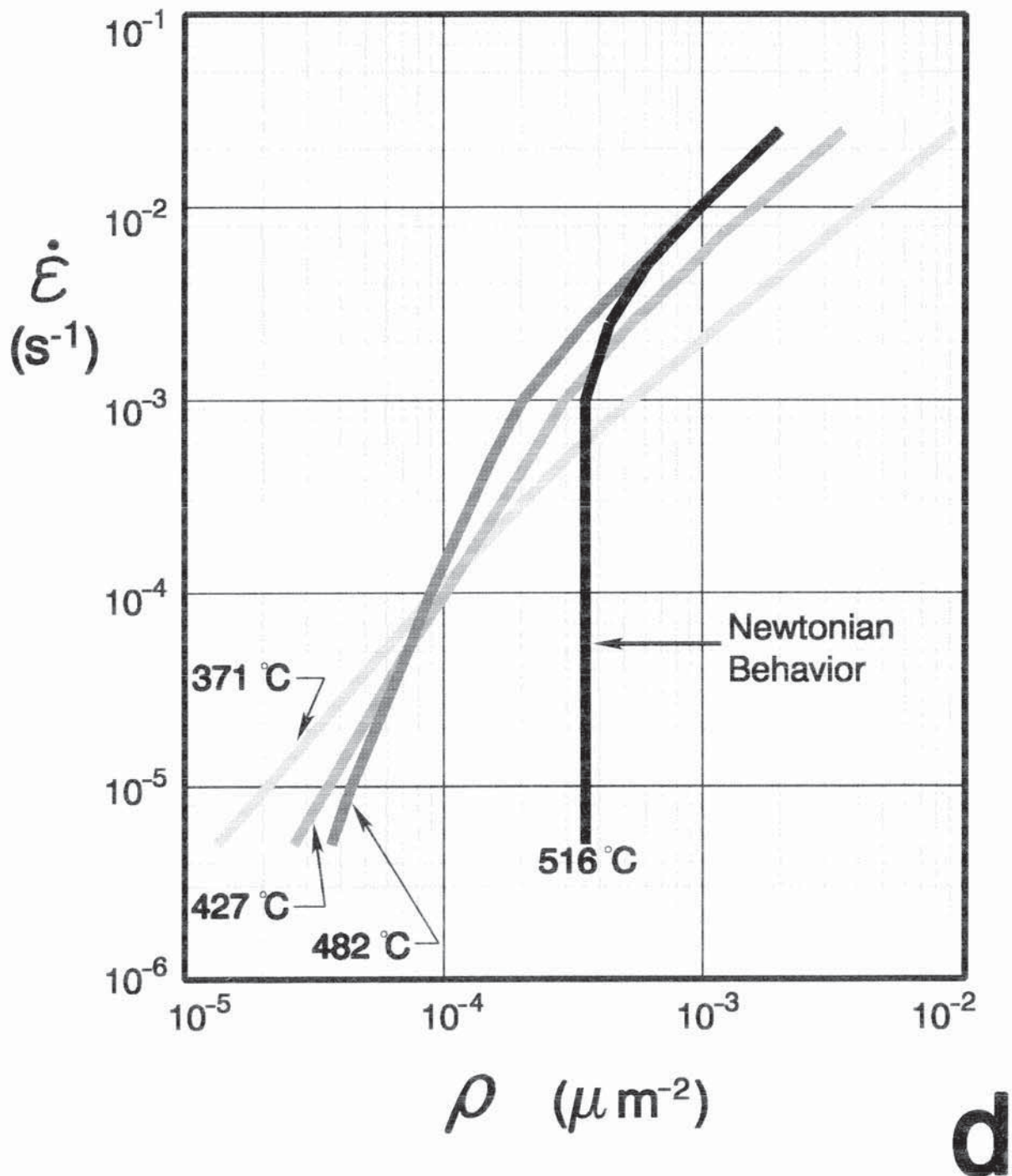


Figure 51 (Continued).

Assumed Behavior of 7475 Al Grain Growth Kinetics for Strain Rate Jump Testing

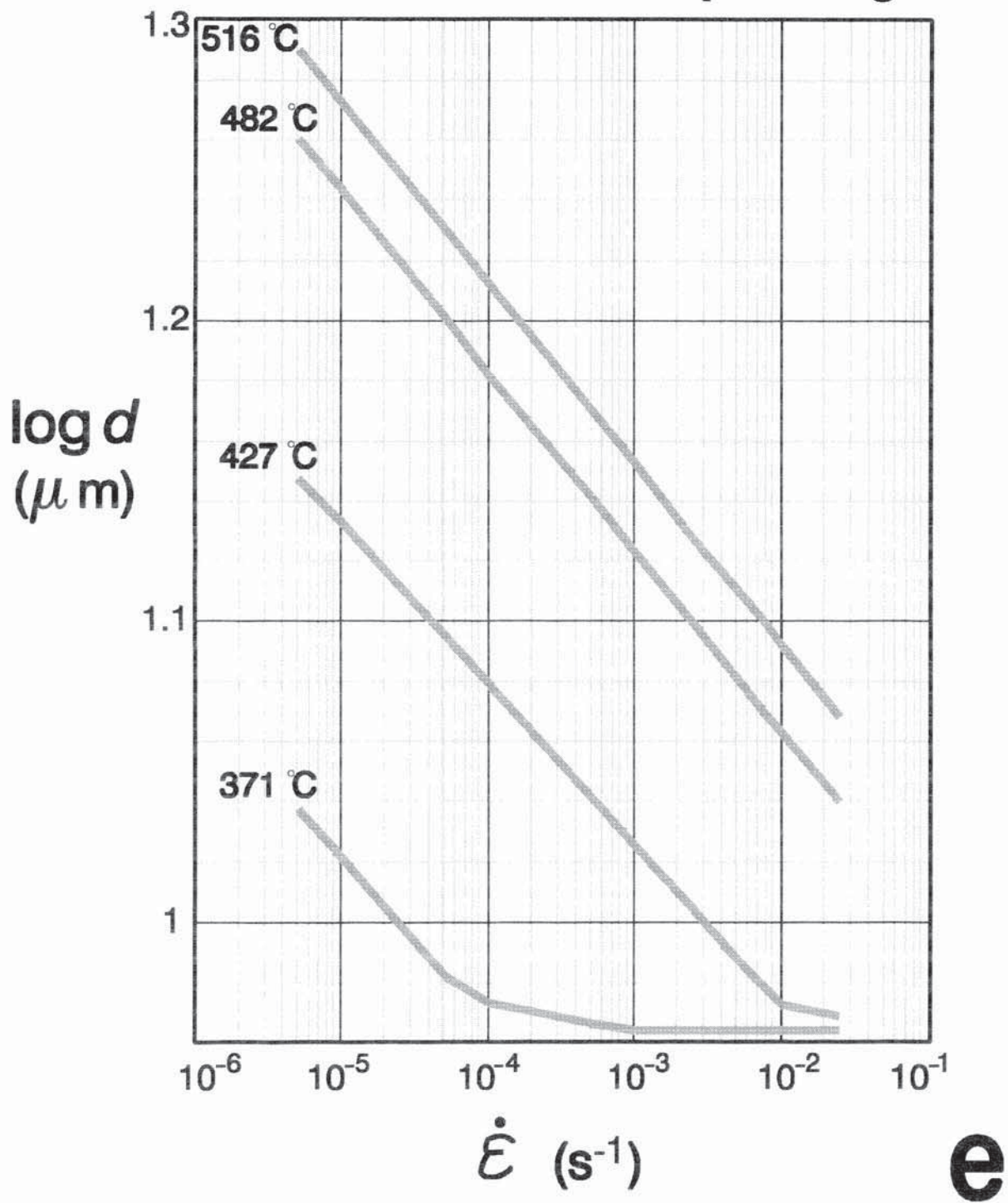


Figure 52. Application of equation (20) to 7475 Al stress-strain curves from Ghosh (1985),

for $\dot{\varepsilon} = 2 \times 10^{-4}/\text{s}$, and $T = 516$ and 482°C , with the 7475 Al grain growth data used in Figures 48 and 50. For $T = 516^\circ\text{C}$, d in equation (20) is given by the following average:

$$d(\dot{\varepsilon} = 2 \times 10^{-4}/\text{s}, 516^\circ\text{C}) \approx \frac{1}{2}[d(\dot{\varepsilon} = 10^{-4}/\text{s}, 516^\circ\text{C}) + d(\dot{\varepsilon} = 5 \times 10^{-4}/\text{s}, 516^\circ\text{C})].$$

And for $T = 482^\circ\text{C}$, d in equation (20) is given by the approximation

$$d(\dot{\varepsilon} = 2 \times 10^{-4}/\text{s}, 482^\circ\text{C}) \approx d(\dot{\varepsilon} = 10^{-4}/\text{s}, 475^\circ\text{C}).$$

Also for equation (20): M_b is given by equation (31), $A = 1.25 \times 10^5$, $X_d(516^\circ\text{C}) = 0.1$, and $X_d(482^\circ\text{C}) = 0.08$. The value for A here is one-half that assumed for 7475 Al in the prior figure. Heat-to-heat variations in this parameter are, however, likely to be easily justified (Arieli and Mukherjee 1982). Values for X_d are about the same as those for the 7475 Al of the prior figure; X_d denoting the fraction of defects moved by the stress σ .

Figure 52 (Continued).

Strain Hardening of 7475 Al from Deformation-Enhanced Grain Growth

